

POLITECNICO DI TORINO

Master's Degree Course in Petroleum and Mining Engineering

Master's degree Final Thesis

**The adhesion problem of the rock materials
to cutterhead and tools of roadheaders:
evaluation of its effect on the tools' wear**



Thesis Advisors

Prof. Cardu Marilena

Assoc. Prof. Ramazan Comakli (Nigde Omar Halisdemir University)

Candidate

Jahid Bayramov

A.A.2021/2022

Acknowledgments

First and foremost, I'd want to express my gratitude to my thesis advisors, Prof. Cardu Marilena and Assoc. Prof. Ramazan Comakli. I was extremely fortunate to have supervisors who genuinely cared about my work and responded to my concerns immediately.

I'd also want to thank Nigde Omar Halisdemir University and the Ankara University Geosciences Application and Research Center for allowing me to work in their laboratories. In particular, Assoc. Prof. Ramazan Comakli, engr. Abdullah Alani, and engr. Ruslan Ibrahimov were always helpful in answering any doubts I had about my research.

I would also like to thank each professor of Politecnico di Torino for the teachings and ideas they presented during the classes.

Finally, I'd like to express my gratitude to my classmates for their assistance and to all of my friends for providing me with some of my fondest memories.

Thank you.

CONTENTS

List of Figures	5
List of Tables	8
List of Abbreviations	9
1 Introduction	11
1.1 General.....	11
1.2 Project Background.....	12
1.3 Purpose and Scope of the Project	12
2 Literature Review	14
2.1 Boom-type Roadheaders	14
2.1.1 Classification of Boom-type Roadheaders.....	14
2.1.2 Cutting Tools.....	16
2.1.3 Performance Prediction of Roadheaders	17
2.1.4 Clogging of Roadheaders	17
2.2 Mineralogy and Texture of Pyroclastic Rocks.....	18
2.2.1 Formation and Composition of Pyroclastic Rocks	18
2.2.2 Texture of Pyroclastic Rocks	19
2.3 Atterberg Limits and Failure Mode of Pyroclastic Rocks.....	19
2.3.1 Atterberg Limits of Pyroclastic Rocks	19
2.3.2 Failure Envelopes for Pyroclastic Rocks.....	20
3 Previous Studies	22
3.1 Introduction	22
3.2 Adhesion and Adhesive Friction	22
3.3 Historical Studies	24
3.4 Recent Studies	28

4	Laboratory Studies	35
4.1	Physical and Mechanical Properties of Pyroclastic Rocks	35
4.1.1	Sample Preparation	35
4.1.2	Natural Unit Weight.....	36
4.1.3	Uniaxial Compressive Strength.....	37
4.1.4	Brazilian Tensile Strength	37
4.1.5	Ultrasonic Pulse Velocity of the Rocks	38
4.1.6	Cerchar Abrasivity Test.....	39
4.1.7	The Adhered Material on the Tip of Stylus and Rotating Steel Arm	42
4.2	Mineralogical and Petrographic Characterization.....	44
4.2.1	X-ray Diffraction.....	44
4.2.2	X-ray Fluorescence.....	45
4.2.3	Thin Section	48
5	Field Studies	50
5.1	Description of the Project.....	50
5.2	Geology of the Field.....	52
5.3	Roadheaders in Cold Storage Caverns.....	53
5.4	Field Performance Analysis of the Roadheaders.....	54
5.5	Field Cutter Consumption of the Roadheaders.....	56
6	Discussion and Conclusions	59
6.1	Summary	59
6.2	The Effects of Mechanical Properties and Adhesion on CAI	60
6.2.1.	The Effect of Mechanical Properties on CAI.....	60
6.2.2.	The Effect of Adhesion on CAI.....	61
6.3	The Effect of Mechanical Properties and Adhesion on Field Performance Parameters of Roadheaders	63
6.3.1.	The Effect of Mechanical Properties on Field Performance Parameters of Roadheaders	63
6.3.2.	The Effect of Adhesion on Field Performance Parameters of Roadheaders	64
6.4	Conclusions	66
	References	68
	APPENDIX A X-ray Diffraction	76
	APPENDIX B Field Performance Parameters of Roadheaders	82

List of Figures

Figure 2.1. Cutting action of roadheaders with; a) Ripping type (transverse) cutting head b) Milling type (axial) cutting head ⁸	14
Figure 2.2. Typical light (Mk-2A), medium (Mk-2B), and heavyweight (Mk-3) roadheaders ⁹	15
Figure 2.3 Cutting tools used on roadheaders: conical cutter (a) and radial cutter (b) ¹¹	16
Figure 2.4. Clean roadheader cutterhead (a) and after clay sticking (b) ¹⁶	18
Figure 2.5. Pyroclastic Rock Classification ¹⁸	19
Figure 2.6. The texture of pyroclastic rocks; Pictures (left) and macro photographs (right): a) pumices and scoriae; b) lithic fragments; c) phenocrystals ¹⁹	19
Figure 2.7. The relationship between effective mean stress and differential stress (“P – Q” plot). ²⁴	21
Figure 3.1. The shear surface at the metal-clay interface ²⁶	23
Figure 3.2. The internal shear surface within the clay ²⁶	23
Figure 3.3. Casagrande cup ²⁷	25
Figure 3.4. The modified lower half of the shear box for adhesion testing ³⁰	26
Figure 3.5. Relationship of water content and adhesion and cohesion: ranges of test results as given by Jancsecz (1991) ²⁶	27
Figure 3.6. The effect of water content on adhesion and cohesion of sample K122 ²⁶	27
Figure 3.7. Universal classification diagram for critical consistency changes regarding clogging and dispersing ³²	28
Figure 3.8. Results of roughness tests. above: for Speswhite below: for Boom clay. Contact time for both clays is 1 hour ³⁴	30
Figure 3.9. Influence of contact time on the adhesive shear strength. above: Speswhite below: Boom clay ³⁴	31
Figure 3.10. Consistency index as a function of the normal stress ³⁵	32

Figure 3.11. Cone Pull Out Testing Apparatus, developed by InProTunnel Working Group ³⁷	32
Figure 3.12. Pull energy over consistency (left) and Adherence over consistency (right) ³⁸	33
Figure 3.13. Draft of a classification scheme ³⁹	34
Figure 4.1. Specimens	35
Figure 4.2. Machine used for BTS sample preparation	36
Figure 4.3. Evaluating the weight of specimens by electronic precision balance	36
Figure 4.4. Hydraulic Press and specimen under analysis during the execution of the uniaxial compression test	37
Figure 4.5. The manual hydraulic press used for BTS experiments and specimen during the test for the determination of the indirect tensile strength	38
Figure 4.6. Determination of the ultrasonic velocity of the rocks by Pundit Lab (+)	39
Figure 4.7. Cerchar abrasivity test equipment	39
Figure 4.8. Specimens used for Cerchar abrasivity test.....	40
Figure 4.9. Scratching of stylus pin on rock surface across 10 mm and 50 mm.....	40
Figure 4.10. Minerals encountered by the tip of the stylus through its route	41
Figure 4.11. Measurement of tip flat wear by Microscope	41
Figure 4.12. The adhered material on the tip of the pin	42
Figure 4.13. Electronic precision balance	42
Figure 4.14. Result of XRD analyses for one sample.....	45
Figure 4.15. Thin-section images and mineralogical-petrographic analysis results of the rock samples.....	48
Figure 5.1. The location of project areas in the Cappadocia Region	50
Figure 5.2. General view of project areas.....	51
Figure 5.3. Plan view of dry CSC.....	51
Figure 5.4. Plan view of wet CSC.....	52
Figure 5.5. Vertical cross-section through the tuff sequence of the Cappadocia ⁴¹	53
Figure 5.6. General view of Paurat E134	54
Figure 5.7. The adhesion of formation on the cutterhead and gathering arm	54
Figure 5.8. Traveling mechanism	54
Figure 5.9. a) Excavating b) Mucking c) Trimming	55
Figure 5.10. Conical cutter	56
Figure 5.11. Worn steel body.....	56
Figure 5.12. Welded steel body	57
Figure 6.1. Relationship between UCS and BTS and CAI	60
Figure 6.2. Relationship between dry and wet CAIs.....	61

Figure 6.3. Difference of dry and wet CAI values	62
Figure 6.4. Difference between CAI (1 cm) and CAI (5 cm)	62
Figure 6.5. Correlation between UCS and field performance parameters of roadheaders	63
Figure 6.6. Correlation between BTS and field performance parameters of roadheaders	64
Figure 6.7. Correlation between CAI (1 cm, 5 cm) and field performance parameters of roadheaders	65
Figure 6.8. Correlation between CCR (wet) and Weight of Adhered Material on Pin of Stylus (CAI-5 cm)	65
Figure 6.9. Correlation between CCR (wet) and Weight of Adhered Material on Rotating Steel Arm	66

List of Tables

Table 2.1. Classification of Pyroclastic Rocks ¹⁸	18
Table 3.1. Results of Consolidated Undrained and Drained Direct Shear Box Tests & Steel Interface Shear Tests ³⁰	26
Table 3.2. Atterberg limits and water content at which testing took place ³⁴	29
Table 3.3. Physical characteristics of the tested clays ³⁸	33
Table 4.1. The results of rock mechanics experiment	43
Table 4.2. The results of XRF analyses	46
Table 4.3. The results of XRF analyses	47
Table 5.1. Machine specifications for Paurat E134 type Roadheader.....	53
Table 5.2. Field performance parameters of roadheaders for the Nar region	58

List of Abbreviations

σ_n	Normal Stress
τ	Shear Stress
τ_e	Effective Shear Stress
δ	Adhesive Friction Angle
ϕ	Internal Friction Angle
a	Adhesion
ASTM	American Society for Testing and Materials
BTS	Brazilian Tensile Strength
c	Cohesion
CAI	Cerchar Abrasivity Index
CCR	Cutter Consumption Rate
CM	The Weight of Adhered Material on the Tip of Stylus (CAI 5 cm, wet)
CSC	Cold Storage Cavern
CVC	Cappadocia Volcanic Complex
DAR	Daily Advance Rate
EPB	Earth Pressure Balance
EPBM	Earth Pressure Balance Machine
HRC	Rockwell Hardness
IC	Consistency Index
ICR	Instantaneous Cutting Rate
I_p	Plasticity Index
ISRM	International Society for Rock Mechanics
LL	Liquid Limit
MUT	Machine Utilization Factor

NCR	Net Cutting Rate
NE	North-East
P	Effective Mean Stress
PI	Potentially Sticky
Q	Peak Differential Stress
SE	Specific Energy
SW	South-West
TBM	Tunnel Boring Machine
UCS	Uniaxial Compressive Strength
UPE	Ultrasonic Pulse Echo
UPV	Ultrasonic Pulse Velocity
wmmb	Maximal Molecular Water Content
XRD	X-ray Diffraction
XRF	X-ray Fluorescence

Chapter 1

Introduction

1.1. General

Nowadays, excavation of tunnels and underground mines, including development and production is carried out by using mechanical equipment. One of the widely used mechanical excavators is roadheaders. The simple configuration of these machines makes them very mobile and therefore, they have the ability to perform different types and shapes of openings with various sizes. One of the main advantages of these machines is to have a favorable support installation due to the convenient face access. From an economical point of view, the capital cost of these machines is low compared to other mechanized tunneling machines.¹

Due to the friction between the cutter head of roadheaders and rock masses, one of the most common problems is clogging which affects the excavation process in a wide spectrum.² The sticking potential of the excavated materials to the cutting tools, especially on the body of the tools or conveying systems is mainly related to the interaction of tools with the interfaces/surfaces of the rocks. They can generate major issues including excessive energy consumption during roadheader advancement, breakdown or clogging of excavation tools, belt conveyors, or problems caused by the conditioned excavation material's lower shear resistance in reuse.³ The stagnancy of the tunnel driving, excessive leeway due to cleaning work, and reduced advance of the machines are the main issues that drive from the problems mentioned above. In addition, these problems can lead to hostilities between awarding authorities and executing companies. Thus, the sticking potential of the rock formations must be taken into account for the economy of a tunneling project.⁴

The minerals with high cohesive properties generally have high liquid limits and high plasticity index that leads to adhesion processes between the interface/surface of the minerals and the cutting tools. These adhesion processes are the main motives for the clogging of the cutting tools.^{5,6,7} Furthermore, the adhesion process between minerals and cutting tools increases due to the swelling effect driving from the contact between water and minerals when tunneling machines pass through the wet formations. There are several remedies on the market,

but not all of them have sufficient performance and this involves admitting that, clogging is one of the main issues in tunnel driving that can even lead to a complete standstill of tunnel driving.

1.2. Project background

Challenges and problems related to the sticking potential of rock formations entail the need for quantifying the adhesion properties by laboratory testing. This master thesis will be based on the traditional physical-mechanical test methods and as well as, the field studies carried out in the cold storage caverns in the Cappadocia region, Turkey, see Chapter 5.

The selected rocks for this thesis are pyroclastic, tuff rock formations obtained from the different regions of Cappadocia. The main focus besides the physio-mechanical properties and mineralogical and petrographic analyses is substantiated on the Cerchar Abrasivity Index and its effect on the adhesion of rock materials on cutting tools. Chapter 4 gives a further elaboration of these topics.

A thorough sample preparation involving drilling, slicing, cutting, and crushing of the selected rock material is performed, providing cores, cored cylinders, cubes, pieces, and milled dust. The laboratory test methods mentioned above and both mineralogical and rock mechanical test methods are carried out, in Chapter 4.

The test results will be then evaluated and presented, and comparisons between the different test methods and the sample types will be discussed to find correlations between them. Chapter 7 provides a detailed discussion of these evaluations and comparisons.

1.3. Purpose and scope of the project

The problem mentioned within the scope of this proposed project will be investigated for roadheaders, that used conical cutters, by evaluating the results of the laboratory studies and excavation field data together. In previous studies, similar problems were generally investigated for Tunnel Boring Machine (TBM) excavations, but there were not many studies on the roadheaders and this increases the originality of the project.

This study will be based on extensive laboratory work and field data, various rock mechanical tests and mineralogical analyses will be performed too. The scope of the MSc Project Task is:

- Classification of the main types of roadheaders and their cutting tools. Description of the main parameters for the performance prediction of roadheaders and the challenges that affect these parameters.
- Clogging potential of the pyroclastic rocks. Investigation of tuff formations and their mineralogical and textural composition. Failure envelopes and Atterberg limits for the formations containing clay minerals.
- Historical studies carried out by different authors. The effect of water content on the adhesion properties of rock formations.

- Recent techniques developed by different authors to evaluate adhesion properties such as plasticity, liquid limits of the formations containing clay minerals.
- Physical and mechanical tests, like density, Brazilian tensile strength (BTS), uniaxial compressive strength (UCS), Cerchar abrasivity index (CAI), as well as the X-ray Diffraction and X-ray Fluorescence petrographic analyses and thin section.
- Investigating performance parameters of roadheaders, including instantaneous cutting rate (ICR), daily advance rate (DAR), machine utilization factor (MUT), and field cutter consumption of roadheaders (CCR) in both dry and wet conditions.
- Evaluation and presentation of the sticking characteristics of the tested rocks. Discussion on the results of the tests and the field excavation performance parameters of roadheaders that affect the results.

The background information for the study is:

- The information provided by the supervisors
- Scientific articles and books related to the subject
- Technical information provided by the workers at Hoyuk Construction

Chapter 2

Literature Review

2.1. Boom-type Roadheaders

Boom-type roadheaders consist of a cutterhead in a conical shape that is covered by cutting tools. These cutting tools are generally tungsten carbide tipped that breaks rock as the cutter head rotates axially or transversely. An electric motor is used to drive the cutter head which performs either ripping (transverse type) or milling (inline or axial) cutting actions through the heavy-duty epicyclic or transverse gearbox. The cutter boom is bonded to a pedestal that allows unrestricted boom movement throughout a fixed maximum profile. Hydraulic cylinders are sized to provide a force sufficient to maintain the cutting head in contact with the face.

2.1.1. Classification of Boom-type Roadheaders

Roadheaders can be divided into two types: milling (axial) with the cutterhead rotating around the boom axis, and ripping (transverse) with the head rotating perpendicular to the boom axis (Figure 2.1).

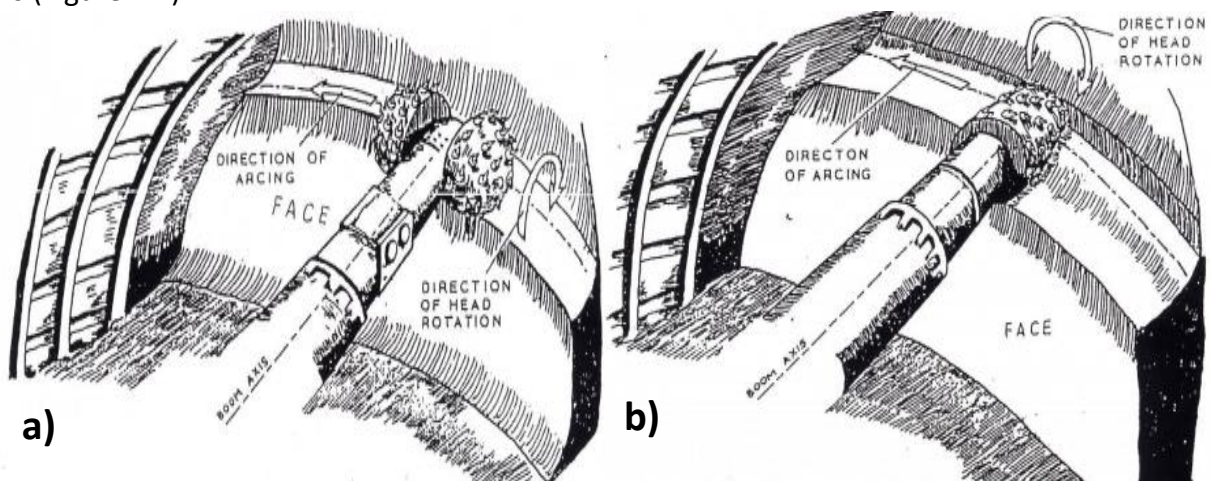
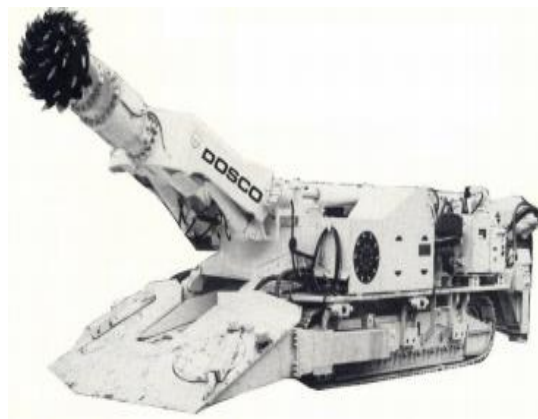


Figure 2.1. Cutting action of roadheaders with;
a) Ripping type (transverse) cutting head b) Milling type (axial) cutting head.⁸

Roadheaders are also classified according to their weights as small (30 ton), midsize (70 ton), and large (up to 120 ton) roadheaders. Dosco, one of the seven main roadheader manufacturers offers typical light (Mk-2A), medium (Mk-2B), and heavyweight (Mk-3) roadheaders. These machines operate with an installed cutting engine power of 80 kW up to 300 kW and maximum torque up to 2.5 times the running torque (Figure 2.2).



Dosco Mk – 2A



Dosco Mk – 2B



Dosco Mk – 3

Figure 2.2. Typical light (Mk-2A), medium (Mk-2B), and heavyweight (Mk-3) roadheaders.⁹

2.1.2. Cutting Tools

The most advanced bits for boom-type mechanical excavators' cutter heads are tungsten carbide tipped point attack bits that are efficient in terms of rock breakage. To reduce heat effects on the tip of the bits and to increase the stiffness of the tips, it is needed to modify the cobalt content of the tungsten carbide. Furthermore, to adopt more efficient cutting, the bit shape can be changed to avoid the excessive amount of dust and the heat generated during the cutting performance of the machine. However, the untimely loss of carbide could happen during the cutting. Recently, a new wear material with higher toughness and abrasive resistance has been made available by the steel industry for use in bit shakes. The higher quality of the matrix material is to prevent the acting forces on the carbide, thus, the new generation of the bits is supposed to have longer shanks and with less material around the carbide tip. Recent developments in layered carbides, shaped polycrystalline diamonds offer a breakthrough in technology that will allow more effective cutting. Without a doubt, there is a progressive increase in the use of these new cutters for the new roadheader designs and it will provide much more effective use of cutter head power.¹⁰

Conical cutters can cut rocks with a UCS of 100–120 MPa in most cases. A conical cutter consists of a circular shank, which performs rotating action in its tool holder, a conical body, and a conical tip made of hardened steel and tungsten carbide respectively at the top of the body. In comparison to radial cutters, their design allows them to wear down evenly, resulting in longer tool life. As a result, they are more prevalent than radial tools, particularly in the mining of harder ground. The larger tip diameters and shorter body lengths are preferred for relatively more difficult cutting conditions (Figure 2.3 (a)).¹¹

Rocks with the UCS of 40-60 MPa can be broken by radial cutters. In contrast to conical cutters, they have a rectangular shank that does not rotate in the tool holder but stays fixed. Their bodies are made of hardened steel and have a sharp tip made of tungsten carbide. They use lower cutter forces and specific energy (SE) to cut the rocks, resulting in less dust and fine particles. However, the radial cutters are very prone to blunting due to their very sharp tips and after a small amount of blunting, their cutter forces increase drastically (Figure 2.3 (b)).¹²

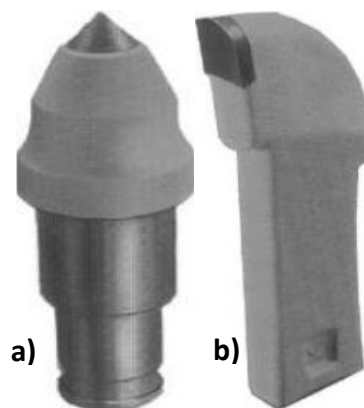


Figure 2.3. Cutting tools used on roadheaders: conical cutter (a) and radial cutter (b).¹¹

2.1.3. Performance Prediction of Roadheaders

To determine the mechanized excavation systems to be used in driving the tunnels, first of all, studies about the cuttability (excavability) of the rocks should be done. Depending on the physical, mechanical, and mass properties of the rocks, the cuttability of the rock formation varies in a great context. During the cutting action, cutting forces are evaluated to determine the rock's cuttability. Therefore, small and full size cutting analyses are carried out. The tunnel parameters (size, shape, gradient, etc.) should be considered when choosing the excavation system to be used. During this investigation, performance predictions (specific energy, cutting rate, etc.) of the machines can be estimated by using various methods.¹³

Correct machine selection, production rate, and bit cost estimation, which represent performance prediction, are the key factors for a successful roadheader application. The dictation in the successful application of roadheader technology to any mining operation is to develop accurate and reliable estimates for attainable production rates and the accompanying bit costs.

The main parameters of the performance prediction for different geological masses are bit consumption rates, instantaneous cutting rates, and machine utilization are controlled by several parameters, including rock parameters, ground conditions, machine specification, and operational parameters. Production rate during actual cutting time refers to the instantaneous cutting rate (ICR) (tons or m³/cutting hour). The number of picks changed per unit volume or weight of muck (picks / m³ or ton) is referred to as the pick consumption rate. The total time used for the excavation during the whole project is the machine utilization: it is called machine utilization factor and is represented as a percentage.¹⁴

The production capacity of a certain machine in a given rock mass and the ground condition is determined by a combination of the above-mentioned parameters. By modifying these parameters, the performance of the machine can be increased. However, the parameters such as rock and ground conditions, some operational parameters cannot be controlled. Thus, during a tunnel or drift excavation with specific requirements to the particular project, the only parameters that can be modified are the machine parameters. Typically, the first step is to assess the roadheader's viability and decide whether it can operate at an acceptable pace in a given environment. The subsequent step is to select the class and general specifications of the machine to be considered for the job among the machines available in the market. The last step is to match the current machine characteristics to the rock and ground conditions in hand to maximize its production rate. This can be performed by studying design parameters and practicing design optimization. Also, for the existing machines already working on the job site, it is always beneficial to conduct such a study to increase productivity and reduce excavation costs.¹⁵

2.1.4. Clogging of Roadheaders

In excavation operations, sometimes the effectiveness of the machine can be very low, and sometimes the machine may not be used because of problems relating to the uncontrollable parameters. One of the main uncontrollable parameters is the sticking potential of low-strength pyroclastic rock materials to the cutterhead of roadheaders.

Clogging of roadheaders can occur when excavating in agglomerate, clay, carbonate, silica and volcanic tuffs, and other pyroclastic rocks. To get better performance for roadheaders, water flow must be none or low. However, it is known that water might have adverse effects on the performance when excavating sticky clayey or low-strength pyroclastic formations. Sticking clay onto cutterheads might cause a stop in the excavation and requires a cleaning job (Figure 2.4).¹⁶

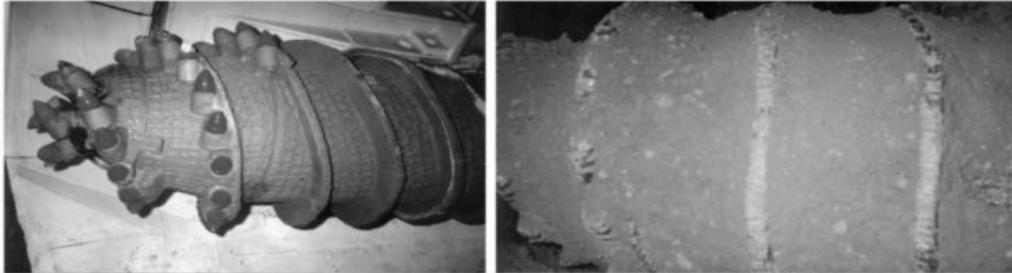


Figure 2.4. Clean roadheader cutterhead (a) and after clay sticking (b).¹⁶

To avoid this issue, after having opted for the choice of a roadheader in a specific tunnel, the appropriate machine should be selected, one that is compatible with the rock's adhesive qualities such as plasticity, liquid limit, and adhesive shear strength.

2.2. Minerology and Texture of Pyroclastic Rocks

2.2.1. Formation and Composition of Pyroclastic Rocks

Pyroclastic rocks are produced by volcanic eruptions due to endogenous forces. The material from the volcanic eruption is deposited before being by water or ice. Following deposition, the compacting process (lithification) occurs, resulting in rock/pyroclastic deposits. Pyroclastic deposits are primary volcano-clastic deposits composed of particles (pyroclasts) formed by an eruption and deposited by primary volcanic processes (fall, flow, surge).¹⁷ The explosive eruption process involved in the formation of pyroclastic deposits includes three main types: magmatic eruption, phreatic eruption, and phreatomagmatic eruption. These three types of eruptions are capable of producing abundant pyroclasts that range from fine ash (< 1/16 mm) to blocks several meters long. Classification of pyroclastic rocks is distinguished based on the size of pyroclastic rocks, and it can be seen in Table 2.1 and Figure 2.5.¹⁸

Table 2.1. Classification of Pyroclastic Rocks.¹⁸

Clast Size		Pyroclastic Fragments	Pumiceous Fragments
(mm)	(in.)		
>64	>2.6	Bomb, block	Lump pumice
64 - 4	0.16 - 2.16	Lapilli	Pumice
<4	<0.16	Ash	Pumicite

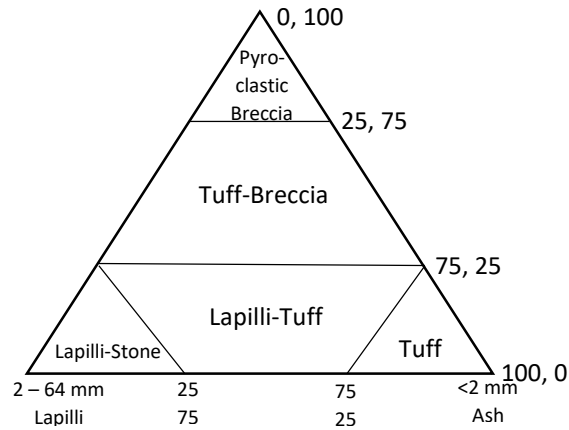


Figure 2.5. Pyroclastic Rock Classification.¹⁸

2.2.2. Texture of Pyroclastic Rocks

From a macroscopic point of view, pyroclastic rocks generally consist of clasts immersed in a grey aphanitic mass (Figure 2.6).

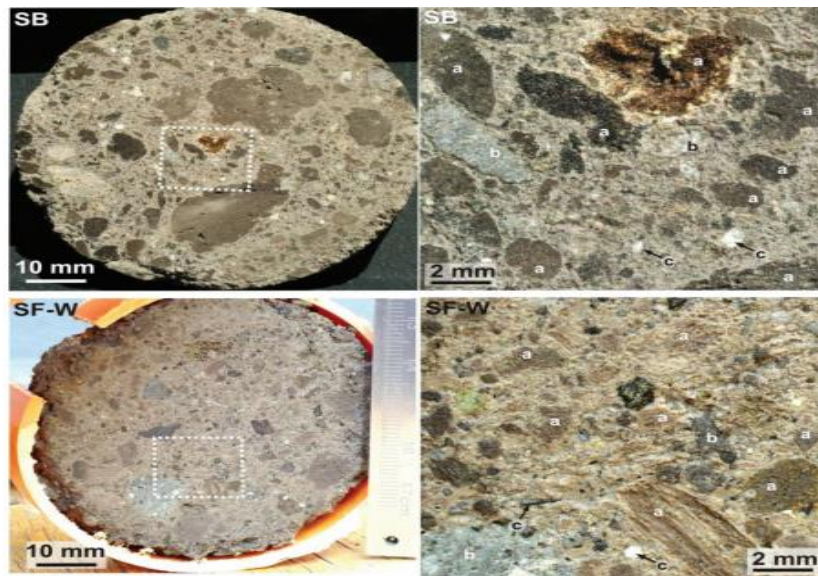


Figure 2.6. The texture of pyroclastic rocks; Pictures (left) and macro photographs (right): a) pumices and scoriae; b) lithic fragments; c) phenocrystals.¹⁹

The size of pumices and scoriae, the weakest and most numerous clasts, varies from a few millimeters to several centimeters, whereas lithic fragments rarely exceed 30 mm. Phenocrystals (sanidine, pyroxene, biotite, and analcimized leucite) are smaller in size.¹⁹

2.3. Atterberg Limits and Failure Mode of Pyroclastic Rocks

2.3.1. Atterberg Limits of Pyroclastic Rocks

The Atterberg limits are considered to be crucial and useful index properties that are used for the classification of fine-grained soils and are known to be important and useful indicators of

mechanical behavior, such as the shear strength, compressibility, and swelling potential.²⁰ Wet preparation and dry preparation (either air-dried or dried in an oven at a temperature not exceeding 60°C) are the two procedures used to prepare samples for Atterberg limit tests. The rock is pulverized to pass the No.40 U.S. sieve (sieve opening size is equal to 425 μm), hydrated with distilled water, and after the hydration process, the test is conducted. According to the result of the test, drying has been proven to induce considerable changes in Atterberg limits, particularly in weathered, residual, tropical/subtropical rocks containing certain minerals as halloysite or allophane, as well as organic content.²¹

A clay sample taken from New London, Connecticut, with an organic matter of 2.6%, is prepared to start from its in-situ moisture content to be tested to determine its liquid limit (LL) and plasticity index (Ip). Although it is estimated that liquid limit (LL) and plasticity index (Ip) is equal to 84% and 34%, after oven-drying, these values decreased to 51% and 9%, respectively. Hence, a difference of 33% in LL and 25% in Ip, and a ratio of $LL_{\text{oven-dried}}/LL_{\text{moist}}$ of 0.61 was observed. Other soil samples having $LL_{\text{oven-dried}}/LL_{\text{moist}}$ ratios of 0.71, 0.73, 0.85 having 2.5%, 2.0% and 0.0% organic content, respectively.²²

Increasing the particle size decreases the liquid limit. This is due to the drying process (oxidation) of organic soils which loses the water content in its pores, in an irreversible manner. Therefore, the cementation of the clay-size particles into larger aggregates occurs.

2.3.2. Failure Envelopes for Pyroclastic Rocks

Considering the actual mean stress P (“ $P - Q$ plots”) as a function in the comparison of brittle failure envelopes and compact yield caps on plots of differential stress at failure is one of the most suitable ways to compare the mechanical behavior of rocks. The brittle failure envelope is shown in the brittle regime due to the peak differential stress, Q , while in the ductile regime, the compact yield cap is depicted by the beginning of inelastic compaction, C^* . The creation of the last point in the yield cap is done by the plotting of the beginning of inelastic compaction under hydrostatic conditions, P^* , along the x-axis where differential stress is set to be zero. The “pre-failure” of the rock can be encountered if there is a presence of plotted differential stress inside the failure envelope or compact yield cap. If the condition of stress charts outside the failure envelope/compact yield cap, the rock is considered failed (or “yielded”). It could be plotted by a shear fracture or by inelastic compaction on the left and right sides respectively. As a result, the transition from brittle to the ductile regime has only occurred at the “top” of the cap.

The various pyroclastic rocks: two andesites from Volcan de Colima, dacite from Mt St Helens, trachyandesite from the Acores, and tuffs from Whakaari volcano and Alban Hills having the porosities in a range of 0.17-0.32 had been used to create the critical stress data (Figure 2.7). For trachyandesite, the dataset is also extended with new data from Volvic (porosity 0.21). The brittle failure and compact yield caps for pyroclastic rocks bear a resemblance to those for sedimentary rocks from a qualitative point of view: the increase of effective mean stress increases the Q , but decreases the minimum stress needed for C^* (Figure 2.7). The influence of porosity on the stress conditions necessary for the transition from the brittle to the ductile

regime and inelastic compaction is not only seen in sandstone and limestone, but also the pyroclastic rocks (Figure 2.7). Generally, these transitions occur when high stress is applied to the rocks with lower porosities. It's worth noting, that the dacite from Mt St Helens and the tuff from Alban Hills with completely different microstructures, which both have a porosity of 0.32 show similarity in their compact yield caps. Granular pyroclastic rocks and lava can be good examples of this phenomenon. However, although the compact yield cap for the rock with the highest porosity (rhyolite from Tarawera; porosity 0.39) is at the lowest stresses, the least porous rock (andesite C8 from Volcan de Colima; porosity 0.17) is not at the highest stress values. Considering the different volcanic rocks, the representation of brittle failure envelopes and compact yield caps is given in Figure 2.7. The yield caps for the tuff from Whakaari volcano (porosity 0.29), the other andesite from Volcan de Colima (porosity 0.24), the trachyandesite from the Achores (porosity 0.18), and the trachyandesite from Volvic (porosity 0.21) are all at higher stresses (Figure 2.7). Because of their different microstructures, it's difficult to pinpoint a specific reason or reason why these samples have yield caps at higher stresses than andesite C8 from Volcan de Colima, though the pore diameters or pore size range of these materials may provide some insight. For example, the average pore diameters of the tuff from Whakaari volcano (100 μm) and andesite LAH4 from Volcan de Colima (200 μm) are lower than that of andesite C8 (250 μm) and could explain the high stresses of their compact yield caps despite their higher porosities. To better understand the influence of pore size and shape on the transition from brittle to ductile behavior and the compact yield cap of volcanic rocks, yield caps for samples with vastly different pore sizes or pore shapes but similar porosities and other microstructural attributes are required.²⁴

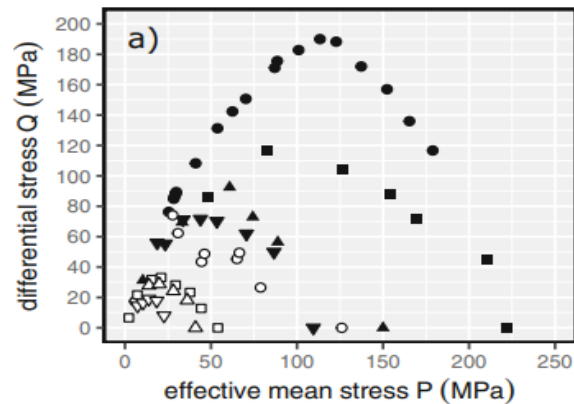


Figure 2.7. The relationship between effective mean stress and differential stress (“P – Q” plot).²⁴

Chapter 3

Previous Studies

3.1. Introduction

These phenomena have been investigated since 1838. The earliest construction industry research studies were published in the 1960s, and systematic study on rock material adhesion relevant to tunneling has been conducted since the late 1990s. Despite this, the interaction between the medium and the steel surface remains debatable. Many soil and rock adhesion test techniques and conditions were developed and investigated, but no widely accepted test method for assessing the adhesive properties of rock materials has been developed yet.²⁵

3.2. Adhesion and Adhesive Friction

3 cases can be described when there is a shearing of clay on the surface of metals:

Case 1. Shearing at the metal-clay interface. The Coulomb criteria can be used to define the shear resistance of the clay-metal contact surface. There are two parts to it: adhesion (resistance at zero normal stress; a) and friction (adhesive friction; defined by the angle). In Figure 3.1, it is seen that the Coulomb criterion between the normal stress (σ_n) and the shear stress (τ) is a linear relation.

Case 2. Shearing inside the clay itself. There is sticking of a little slice of clay onto metal due to the containment of shear within the clay and absence of displacement along the metal. As in case 1, the Coulomb criterion is used to define the internal shear resistance of the clay. The Coulomb criterion for case 2 is equal to $c + \sigma_n \tan\phi$, where c is the cohesiveness of the clay and ϕ is the internal friction angle (Figure 3.2).

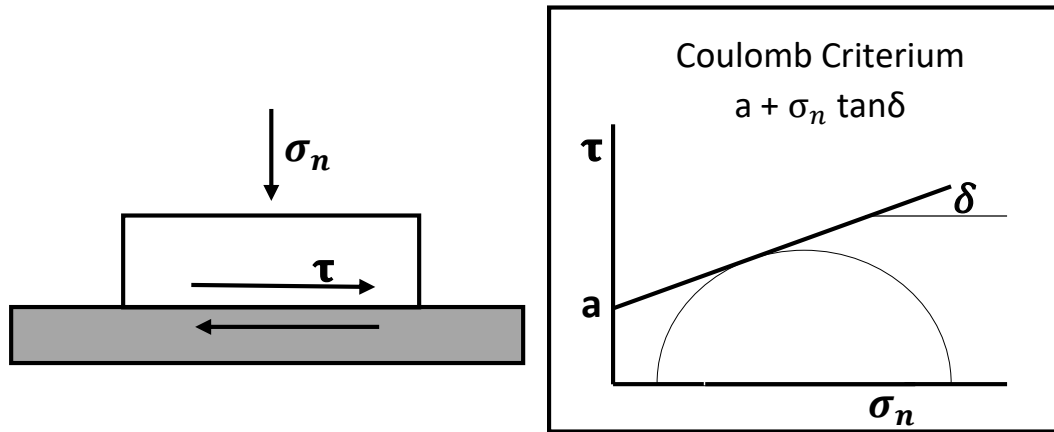


Figure 3.1. The shear surface at the metal-clay interface.

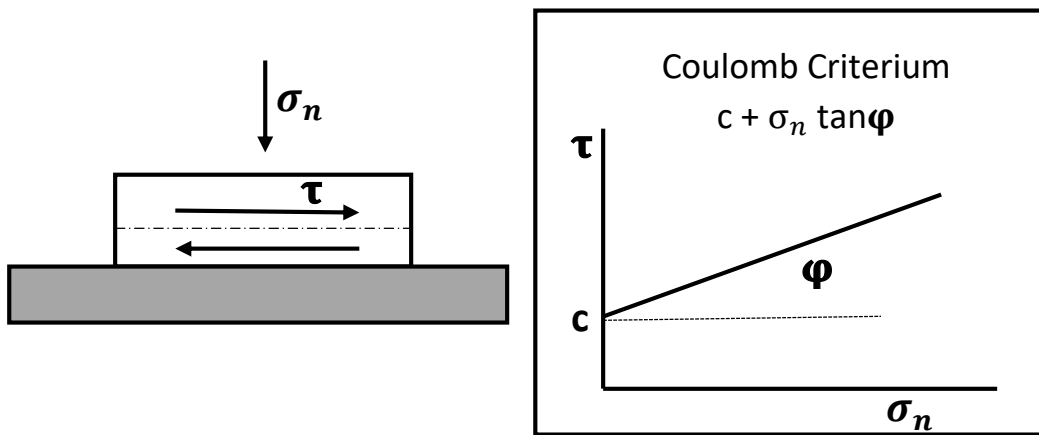


Figure 3.2. The internal shear surface within the clay.

The following procedures should be provided if there is a sticking:

$$\tau_e > c + \sigma_n \tan \phi \quad (3.1)$$

and

$$\tau_e < a + \sigma_n \tan \delta \quad (3.2)$$

i.e., if

$$\sigma_n < \frac{a-c}{\tan \phi - \tan \delta} \quad (3.3)$$

To determine whether sticking occurs, the following parameters should be available: adhesion (a), cohesion (c), adhesive friction angle (δ), internal friction angle (ϕ), and normal stress (σ_n).

Case 3. No shearing at metal-clay interface or within the clay. It is believed that the shearing of the clay occurs in all of the previous situations. Case 3 is seen, when it comes to clay cutting; in such case, the prior analysis can be applied to clay cutting by the tunnel boring machine's cutting wheel. However, circumstances of sticking without internal clay failure are observed in the mixing chamber of the tunnel boring machine and in the slurry line during the hydraulic transport of clay. The applied shear stress in these circumstances is less than the clay's internal and adhesive shear strengths. The following equations must be fulfilled for the occurrence of sticking:²⁶

$$\tau_e < c + \sigma_n \tan \phi \quad (3.4)$$

and

$$\tau_e < a + \sigma_n \tan \delta \quad (3.5)$$

3.3. Historical Studies

Seven restrictions governed the behavior of cohesive soils at varied water contents. The plastic behavior of the soil which is designated by the liquid and plastic limits and the shrinkage limit of soil is still widely used. Soil strength is often considered as a method of assessing the soil's liquid and plastic limitations. The liquid limit is primarily concerned with clay strength, but the plastic limit is concerned with the capillary suction at which the water phase stops to function as a continuous. Air ingress into the soil or heterogeneous cavitation of the pore water can both induce this.

According to Atterberg (1911), to determine the liquid limit of soils, it is fundamental to stroke enough for the creation of a groove in a clay bed. It is well known that the stability of slope depends on the strength of the soil. So, it is reasonable to infer that soil at the liquid limit has a fixed soil strength, which could theoretically be evaluated using more reproducible methods.

To find the plastic limit which is often referred to as a lower limit of plasticity, the following procedures should be applied: The mixture of clay paste and clay powders should be rolled into wires on a sheet of paper with fingers. The wires are rolled out again and again until they shatter into fragments. If the wires break into smaller pieces, it makes no difference if the fragments can be rolled out again when joined.²⁶

However, this method did not guarantee the same result if carried out by different operators. In 1932, a new design of the instrument was developed, which is currently known as the Casagrande cup (Figure 3.3) is still used to determine the liquid limit of clays, and it had been developed to eliminate the errors of the manual test.²⁷



Figure 3.3. Casagrande cup.²⁷

The Casagrande cup is made of a spherical cap attached to a device that employs a crank to activate a cam that elevates and then lowers the cap from the same height, creating a regulated shock against its base. Soil is deposited in the metal cup of the device, and a groove is cut through the middle with a 2 mm (0.079 in) wide standardized tool. At a pace of 120 blows per minute, the cup is repeatedly dropped 10 mm onto a hard rubber base, with the groove gradually closing due to the impact. The number of strikes necessary to close the groove is kept track of. The moisture content at which 25 drops of the cup cause the groove to shut across a distance of 12.7 mm is known as the liquid limit (0.50 in). To estimate the moisture content, the groove must be closed which required 25 blows. The test is performed at various moisture levels and results were recorded. ASTM standard test method D 4318.28 defines the liquid limit test. When testing tensile and shear adhesion in the laboratory, knowing the contact time between clay and steel is also critical.²⁸

Bonding between the clay and steel surfaces occurs over time, increasing the interface's adhesive shear strength. Consolidation occurs in the clay sample over time, pore water pressure changes, and the soil structure reacts to the increased stress.

At the so-called maximal molecular water content (w_{mmb}), which is the greatest quantity of water linked in the mineral skeleton by molecular forces, there is a maximum tensile adhesion for each normal stress. It consists of strongly bonded (adsorbed) water, capillary water, and a portion of weakly bonded water (osmosis water). The maximal molecular water content is a value that exists between the maximal hygroscopic moisture content and the plastic limit for each clay mineral under normal stress.²⁹

A set of modified shear box tests, similar to those described above, were performed in 1976 to assess the adhesion of various clays to a metal surface under shear under various confining pressures and compare with the clays' inherent shear strength. On specimens of kaolinite and illite clays, shear box and modified shear box adhesion tests were performed under unconsolidated undrained, consolidated undrained, and consolidated drained conditions. To perform the tests a 60 mm square shear box apparatus was used. The top face of the shear block, shown in Figure 3.4 was ground and polished before testing and the surface roughness in the direction of shear was measured before and after the tests, and the average roughness was found to be $0.18\mu\text{m}$ (0.00018mm).³⁰

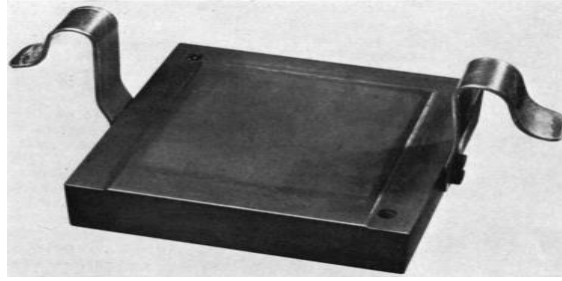


Figure 3.4. The modified lower half of shear box for adhesion testing.³⁰

Sample 1 of kaolinite was prepared from powder and the Sample 2 of illite was obtained from a supplier. Consolidation for the CU and CD tests were done under increasing loads as readings were taken to ensure at least 95% consolidation had taken place before shearing. The strain rate for the CD test was calculated using the Gibson and Henkel method. CU tests were performed at the highest speed of the instrument, which was 0.592 mm/min. A summary of the results from the CU and CD tests conducted by Littleton are shown in Table 3.1.³⁰

Table 3.1. Results of Consolidated Undrained and Drained Direct Shear Box Tests & Steel Interface Shear Tests.³⁰

Sample Test	PI	Peak Friction Angle	Peak Adhesive Friction Angle	Peak Cohesion (N/mm ²)	Residual Friction Angle	Residual Adhesive Friction Angle
S2-CU	33	15.0	-	0	12.5	10.5
S2-CD	33	20.0	18.2	0	14.0	11.5
S1-CU	53	14.8	-	0.009	-	-
S1-CD	53	19.5	17.5	0	14.5	11.5

Adhesion fluctuates with water content, with the greatest adhesion occurring somewhere between the clay's liquid and plastic limits (Figure 3.5). The author did not give any information about the clay's composition or data. The maximum adhesion value should be close to the plastic limit.

To investigate the influence of water content, the potters clay K122 was used. Shear box tests were performed at three different stress levels (25, 35, and 55 kPa). The shear rate was 0.5 mm/min. Adhesion (metal-clay) and shear strength tests (clay internal strength) were carried out. The adhesion was determined by linear regression. Figure 3.6 shows the variation of both adhesion and cohesion with the water content of the clay. The greatest adhesion is seen around the plastic limit in this case. It can be shown that cohesion is larger than adhesion for this clay and that cohesion falls exponentially with water concentration.²⁶

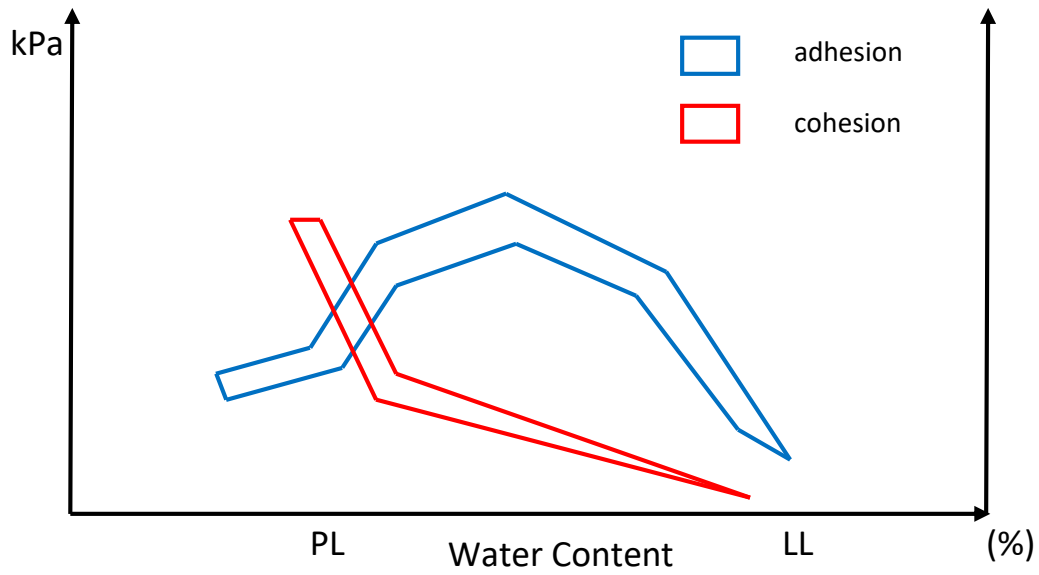


Figure 3.5. Relationship of water content and adhesion and cohesion: ranges of test results as given by Jancsecz (1991).²⁶

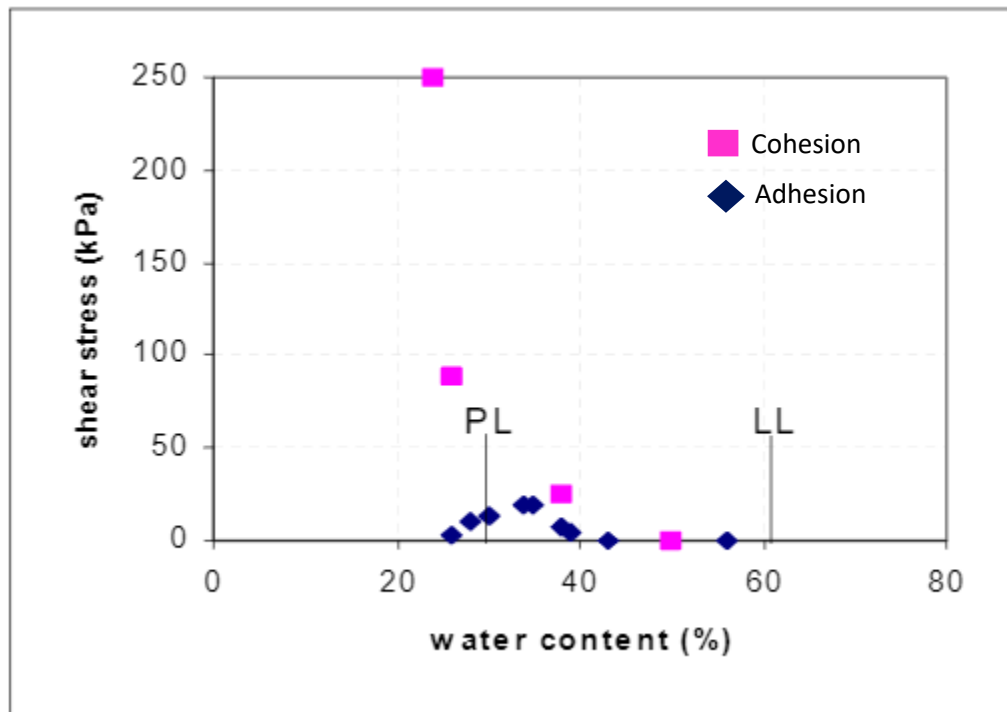


Figure 3.6. The effect of water content on adhesion and cohesion of sample K122.²⁶

3.4. Recent Studies

For tunnel drives in clayey soils, clogging issues have long been handled. Higher adhesion occurs with increased soil plasticity, or, as a result, a decreased activity index, and is regulated by the material's undrained shear resistance. There are four clogging mechanisms: adhesion, bridging, cohesion, and not dissolving. The most important element contributing to clogging among these four methods is particle adhesion to the metal surface, which can be characterized as tangential or normal adhesion. There is currently no defined way for assessing clogging potential in mechanized excavations.³¹

Clogging has been measured using a variety of empirical charts. The universal chart, also known as the Thewes chart, takes into account the plastic and liquid soil limits, as well as changes in water content and consistency index (IC), and correlates these with different clogging potential ranges, ranging from absent (lumps or fines dispersing) to strong clogging (Figure 3.7). For the creation of this graph, data from several projects with clogging incidents were gathered. However, in the case of mixed soils, one of the drawbacks of this relationship was that it did not account for variations in clay proportion. Also, the used data are from soils with maximum values for plasticity index around 70%, not being considered data from highly plastic soils.³²

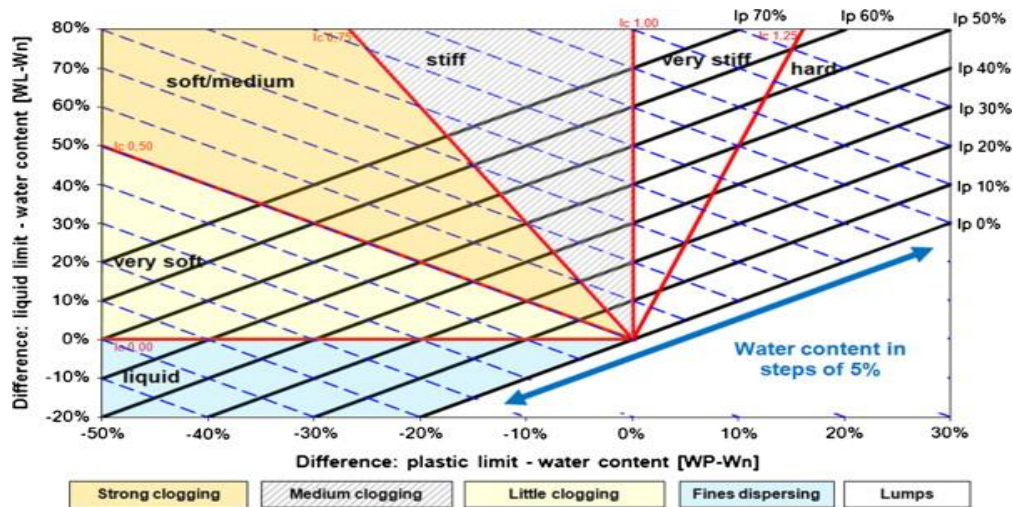


Figure 3.7. Universal classification diagram for critical consistency changes regarding clogging and dispersing.³²

Another approach for evaluating clogging is the direct examination of particle adherence to a metal surface, assessed using various laboratory instruments. In 2005, a research program has been carried out to classify clay formations in terms of their clogging potential for Earth pressure Balance Machine (EPBM) drives by testing the adhesion of clay on steel. This research was developed using real-world clogging investigations as well as laboratory testing with clay samples. A novel test has been devised to assess the adhesion of a soil sample to a steel piston as it is pulled vertically from the sample.

Several tunnel drives where adhering difficulties of various types and magnitudes occurred were studied during the program, and construction data and geological information

were collected. The machinery utilized in the case studies was not designed to excavate the clayey soils. In tunnel driving, especially at the excavation face, in stiff to hard swelling clays, the soil must first be conditioned using support techniques. Foams are usually introduced to the working chamber in such circumstances to lessen the effects of adhesion at the excavation face. He also noted that the mucking system, which generally comprises of a screw conveyor and muck skips on trains, is especially vulnerable to adhesion difficulties.

The Thewes chart is now commonly used in industry for predicting the potential for sticking clays to be an issue during the planning stages of a project’s development. The simplicity of the chart and the fact that it uses soil parameters that are commonly assessed at even the earliest stages of conceptual design make it a very useful tool for engineers and owners. Plasticity is a natural characteristic of clay formations that is linked to clay mineralogy and corresponds with clay activity (as previously demonstrated). The premise of the chart is that as the water content of a cohesive soil with a higher PI (potentially sticky) approaches the plasticity index ($I_c=1$) the stiffness and the likelihood of clogging issues increase.³³

In 2000, a test was conducted to gain a qualitative insight into the parameter that determine adhesive shear strength. The goal of the study was to clarify how clay mineral type, steel surface roughness, clay-steel contact time, and applied normal stress influenced the results. A direct shear box was utilized at a sliding speed of 0.1 mm/min.

Two clay powders, Speswhite, and the Boom clay were mixed with demineralized water. To obtain a good homogenous sample, a water content higher than the liquid limit was chosen (Table 3.2).

Table 3.2. Atterberg limits and water content at which testing took place.³⁴

	Plastic limit	Liquid limit	Water content
Speswhite	32%	62%	80%
Boom clay	24%	55%	70%

For obtaining the desired normal stress, the samples were gradually consolidated in an oedometer. The sample was taken from the oedometer, put into the shear box, and consolidated again at a little higher normal stress. The clay samples are taken into account to be typically consolidated clays. The clay sample was allowed to stick to the steel surface for a specified length of time, referred to as the contact time, before being sheared over it. This contact time includes the consolidation time.

When the adhesive shear strength is represented as a function of the normal stress, in the range of 0 to 50 kPa, it grows linearly for a given roughness and contact time. The amount of adhesion of a mineral is determined by its type. This is due to the different types of bonding, which can be formed between the different mineral types and the steel surface, as well as within the clay mass.³⁴

During the investigation, steel plates of different roughness were tested for both clays (Figure 3.6). For both clays the same trend is noticeable. Adhesive shear strength values are low at low roughness and rise as roughness increases. This is since when the roughness of the surface

increases, more internal deformation occurs, resulting in strain hardening. Shearing then takes place in mode two rather than mode one. According to Figure 3.8 for both clays, the critical steel roughness is between 2.4 and 4.7 μm . It's also worth noting that Speswhite's adhesion values are higher than those of the Boom clay. This is, apart from the difference in clay mineralogy, probably a result of a higher degree of deformation (strain hardening) of the Speswhite.³⁴

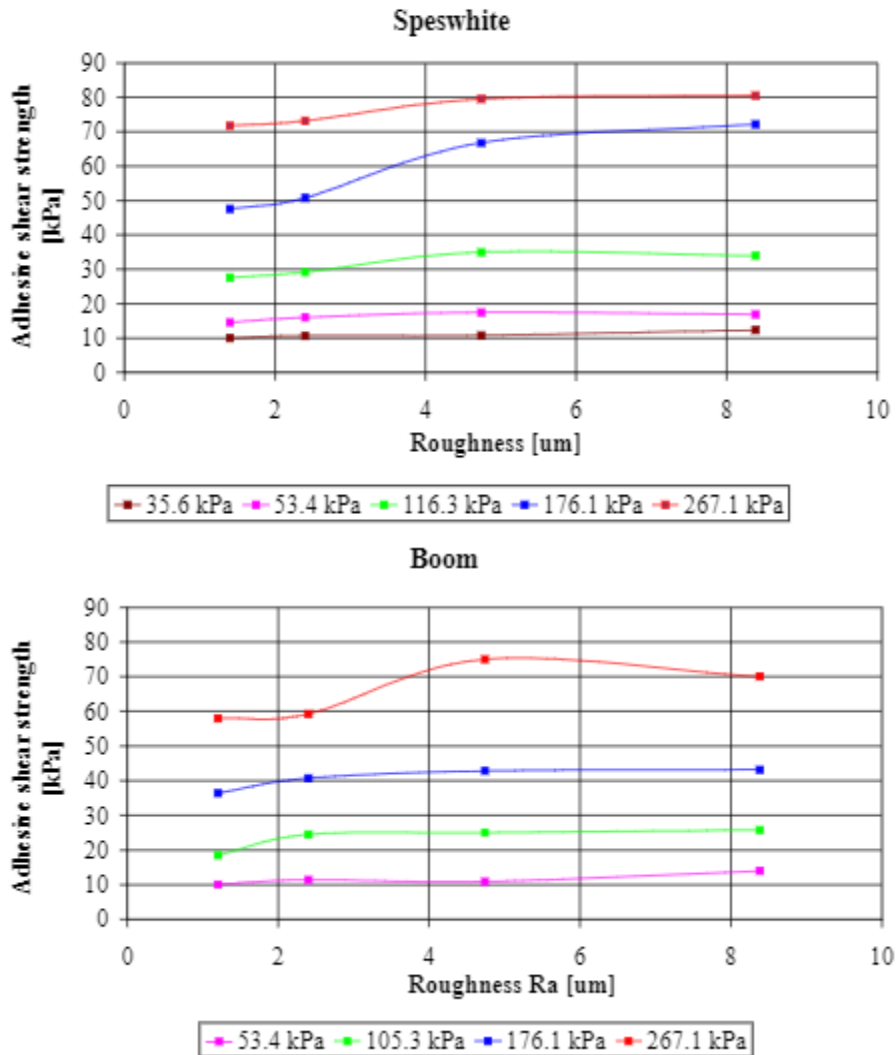


Figure 3.8. Results of roughness tests. above: for Speswhite below: for Boom clay. Contact time for both clays is 1 hour.³⁴

Figure 3.9 shows the results of a series of studies to determine the effect of contact duration on clay-to-steel adhesion. The steel plate with a roughness of 0.2 μm was selected to ensure that mode 1 was taking place. Contact times up to 10 times longer than the consolidation time were studied. When the contact duration is prolonged, there is an increase in adhesive shear strength. Both the Speswhite and the Boom clays show this behavior.

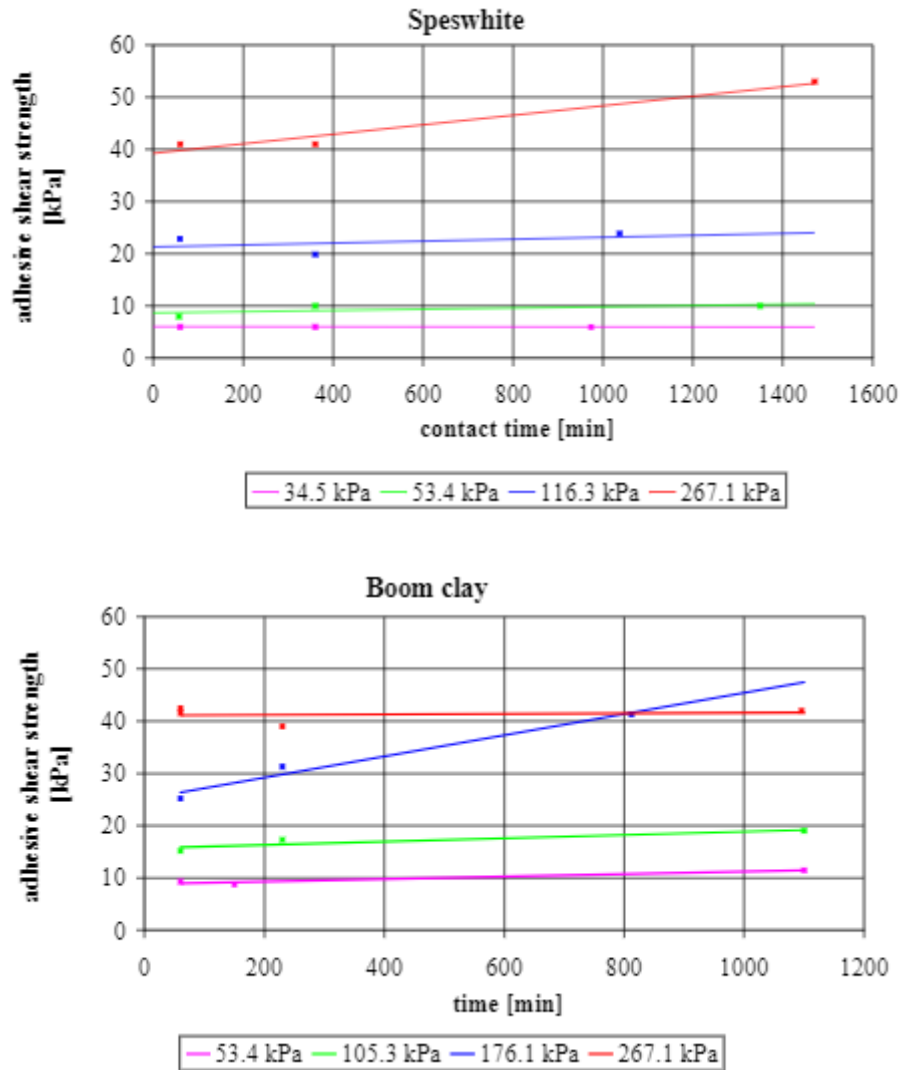


Figure 3.9. The effect of contact duration on clay-to-steel adhesion, the adhesive shear strength. above: Speswhite; below: Boom clay.³⁴

Before and after testing, the water content of each sample has been measured. In Figure 3.8, the consistency index is plotted as a function of the normal stress. The water content of both clays was over the plastic limit before and after shearing. As can be observed in Figure 3.10, the consistency index rises after sliding. When sliding a typically consolidated clay sample over a steel surface, an increase in adhesion potential might be predicted.³⁵

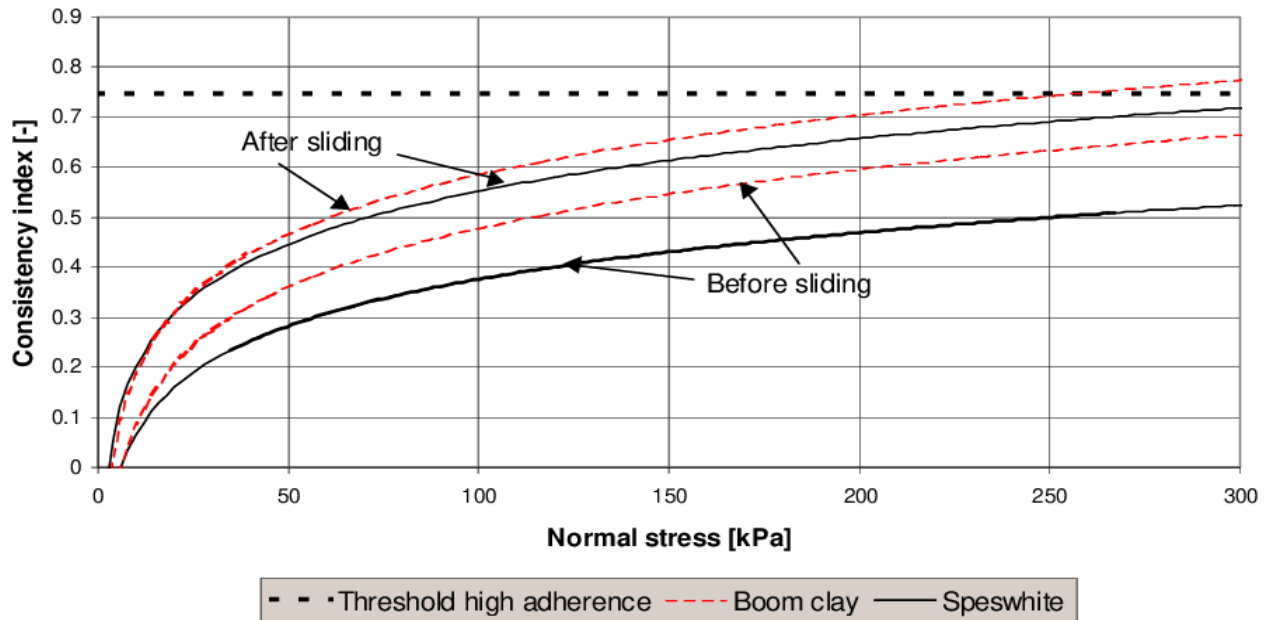


Figure 3.10. Consistency index as a function of the normal stress.³⁵

When water comes into contact with clogging-prone soil, a clogging risk is always indicated. As a result, one must discriminate between two scenarios. The first case involves a newly formed geological soil. As the strain on the soil increases over time, the density of the soils increases, lowering the water content and lowering the danger of clogging. In case 2, there are soils prone to clogging and water from a neighboring excavation geological formation present at the same time as the mechanical heading. When both are combined in the excavation chamber, a critical consistency may be achieved, resulting in clogging. Before excavation, the clog-prone soils were xeric. That means with high density and high consistency.³⁶

For a better identification and quantification of the mechanisms affecting the clogging behavior on a laboratory scale, the so-called “cone pull-out test” has been developed (Figure 3.11).³⁷

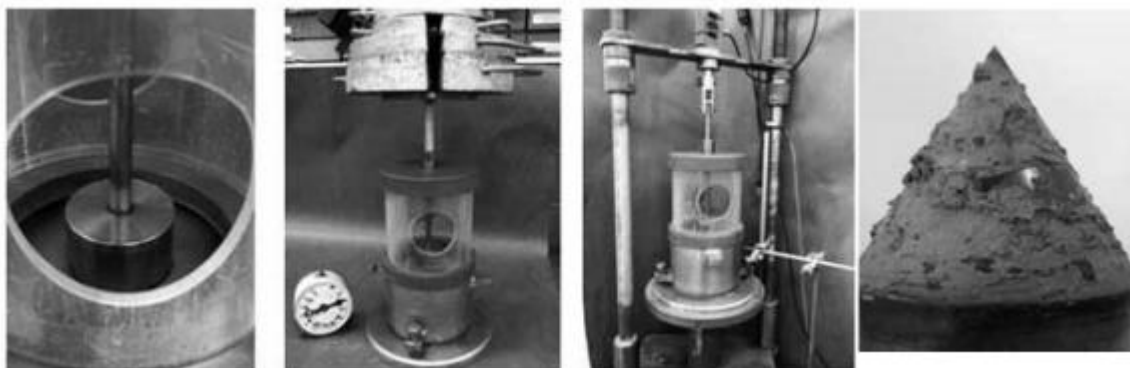


Figure 3.11. Cone Pull Out Testing Apparatus, developed by InProTunnel Working Group.³⁷

The sample material is compacted in a standard proctor device, a steel cone is inserted into a pre-drilled cone-shaped cavity and loaded for 10 minutes with an applied load magnitude

of 3.8 kN/m²-189 kN/m². The load is then taken off and the specimen is placed in a test stand where the cone is pulled out at a rate of 5 mm/min. The tensile forces and the displacements are recorded. Various clay types with different mineralogy and plasticity have been examined in a variety of tests with various cones and soil consistencies up to now. Table 3.3 shows the relevant properties of some selected clays.

Table 3.3. Physical characteristics of the tested clays.³⁸

Clay	13	14	15	16
Plasticity %	21	129	50	385
Liquid limit %	49	159	72	455
Loss on ign %	3.9	2.6	4.9	n.d
Fine content %	59	33	49	86
Smectite %	2	35	17.5	100
Kaolinite %	65	36	39	-
Illite %	12	7	20	-

The testing of four main clays was carried out: clay 13 and clay 16 from Germany and India, respectively, clay 14 and Clay 15 both from Belgium. In figure 3.10, (left) the curves of the pull energy over the consistency are shown for these four clays, whereas in Figure 3.12, (right) the corresponding adherences are plotted. The (quantitative) correlation of these curves is not always as excellent as it was in the early testing, but the (qualitative) shape is still somewhat identical. Nevertheless, from Figure 3.10, (right) a direct comparison of the four soils can be drawn. At a consistency of $I_c = 0.54$, Clay 14, the Ypresian Clay, has a distinctive steep development with a very extremely high adhesion (1150 g/m²). Clay 15, Boom Clay, and pure smectite (clay 16), with adherences of 275 g/m² and 350 g/m², exhibit more consistent curves. Finally, the highest value of 700 g/m² for Clay 13 from the Westerwald is in the middle, but the curve is a little irregular.³⁸

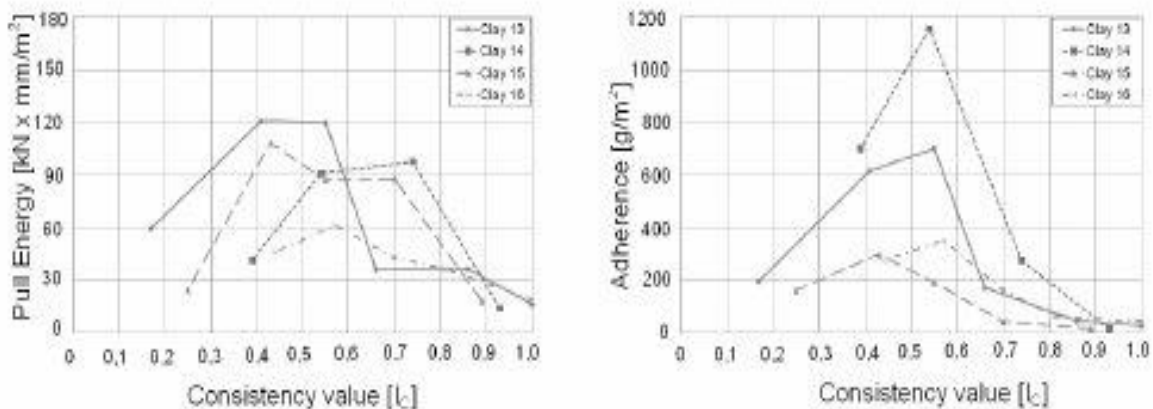


Figure 3.12. Pull energy over consistency (left) and Adherence over consistency (right).³⁸

A draft of a categorization strategy to measure the clogging potential of different fine-grained soils has been established based on the data acquired thus far (Figure 3.13). The

adherences found from cone pull-out tests are plotted over the consistency in the figure, which is split into three categories: high, medium, and low clogging potential. Clay 14 has a significant risk of clogging, which is immediately detectable. The fast increase in the curve up to the maximum of 1150 g/m² is a clear indicator that difficulties are on the way. Clay 13 will also cause a severe blockage with a maximum adhesion of 700 g/m². However, notable adherences must also be considered for the two other clays. In this context, it's worth noting that all of the clays described here were purposefully chosen as sticky clays. Other samples with adherences of less than 100 g/m² were tested and classified as "not prone to clogging." The high, medium, and low clogging potential ranges, on the other hand, are now arbitrarily defined. A verification using the Earth Pressure Balance (EPB) tunneling praxis is still required.³⁹

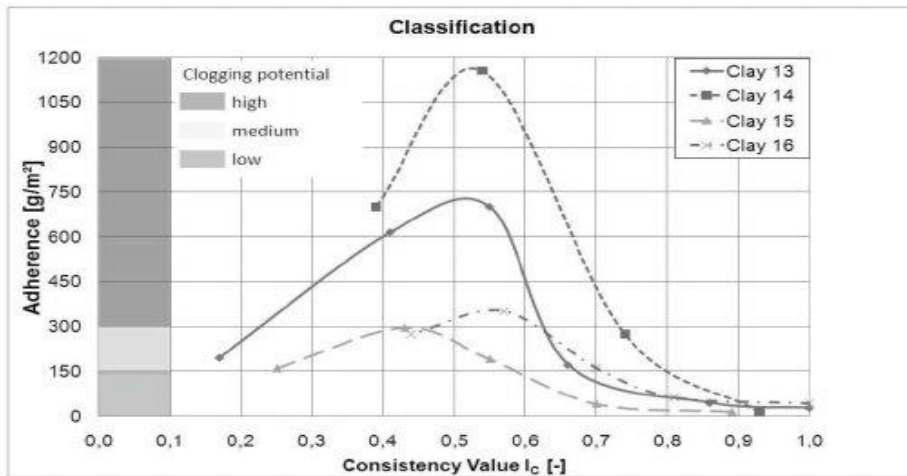


Figure 3.13. Draft of a classification scheme.³⁹

Chapter 4

Laboratory Studies

4.1. Physical and Mechanical Properties of Pyroclastic Rocks

Laboratory studies are carried out by using pyroclastic rocks that were obtained from cold storage caverns located in the Nevsehir and Niğde, Cappadocia region to investigate the adhesion problem of low-strength pyroclastic rocks and their effects on the cutter wear of roadheaders.

9 different pyroclastic rocks were utilized in this study (Figure 4.1). They are Zelve and Kavak ignimbrite units of the Urgup volcanic formation. Zelve ignimbrite is made of a single pyroclastic flow unit and comprises non-welded ignimbrite. These units are composed of pink ignimbrite and white pumice-fall basal deposits.



Figure 4.1. Specimens.

To understand their mechanical and physical behavior, various experiments were performed, including, natural unit weight, uniaxial compressive strength, Brazilian tensile strength, P wave velocity, Cerchar abrasivity index, and the weight of adhered material on the tool both in dry and wet conditions.

4.1.1. Sample Preparation

For laboratory testing, the collected rock blocks were cored perpendicular to the bedding planes by utilizing 54 mm core barrels. The rock specimens were prepared in accordance with the ASTM-D4543 and the physical and mechanical tests were performed according to ISRM (2007) standards. Samples for the BTS test is prepared using the device depicted in Figure 4.2.



Figure 4.2. Machine used for BTS sample preparation.

4.1.2. Natural Unit Weight

The density of rocks is estimated by the ratio between their weight and volume. The weight of the specimens is determined by an electronic precision balance (Figure 4.3).



Figure 4.3. Evaluating the weight of specimens by electronic precision balance.

The volume of the specimens is calculated with the diameter and the length of the samples by using a caliper. The natural weight of the specimens is determined by Equation 4.1 given below.

$$D = \frac{m}{V} \quad (4.1.)$$

where:

D = density of the rock

m = mass of the rock

V = volume of the rock

4.1.3. Uniaxial Compressive Strength

The uniaxial compressive strength (UCS) is the greatest axial compressive stress that a cylindrical specimen may expose shortly before failing. It's also known as a material's unconfined compressive strength because there is no impact on the sides of the specimen. To understand the compressive strength of rocks, laboratory tests were implemented by using NX cores (54 mm diameter) with a length to diameter ratio of 2 to 2.7. Hydraulic press (Figure 4.4) was used for the experiment and the loading rate of the machine was 0.2 kN/s. The tests were carried out both in dry and wet conditions due to investigate the effect of water saturation.



Figure 4.4. Hydraulic Press and specimen under analysis during the execution of the uniaxial compression test.

The compressive strength of the rocks can be estimated by the ratio between the force measured at the failure point and the area of the specimen.

$$\sigma_c = \frac{F}{A} \quad (4.2.)$$

where:

- σ_c = Compressive strength of the specimen
- F = Force measured at the failure point
- A = Area of the cylindrical specimen

4.1.4. Brazilian Tensile Strength

The tensile strength of rocks is one of the most important parameters affecting the deformability of the rock and the result of its breakage. The experiment is carried out to measure this tensile stress. NX cores with a length to a diameter between 0.44 and 0.54 are used for the laboratory test. By knowing the tensile stress of the rocks, the tensile strength of specimens is determined through the formula below. In Figure 4.5, the manual machine is shown for conducting the tests of BTS.

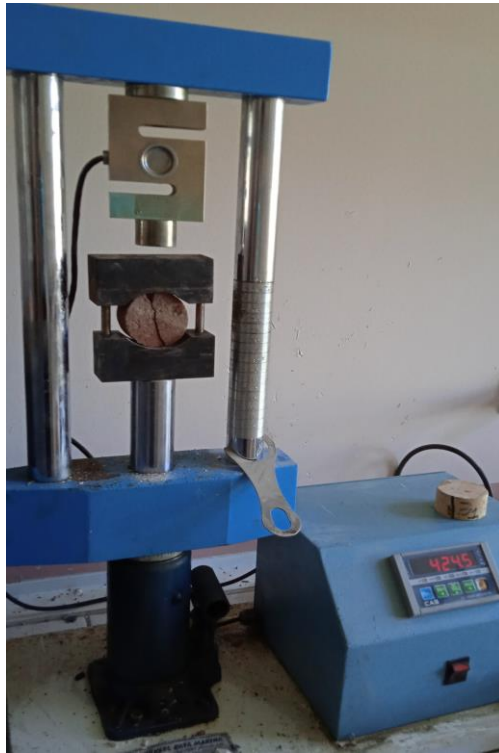


Figure 4.5. The manual hydraulic press used for the BTS experiment and specimen during the test for the determination of the indirect tensile strength.

$$\sigma_T = \frac{2 \cdot F}{\pi \cdot D \cdot t} \quad (4.3.)$$

Where;

- σ_T = tensile strength of the rock
- F = force measured at the failure point
- D = Diameter of the sample
- t = thickness of the sample

4.1.5. Ultrasonic pulse velocity of the rocks

Ultrasonic testing provides information on the strength and uniformity of the rocks. Ultrasonic pulse-echo (UPE) technology allows ultrasonic velocity (UPV) applications to be applied to objects with just one side of access. Pundit lab (+) was used to determine the ultrasonic velocity of the rock samples (Figure 4.6). The test was performed for both dry and saturated conditions on the samples used also for UCS testing.



Figure 4.6. Determination of the ultrasonic velocity of the rocks by Pundit Lab (+).

4.1.6. Cerchar Abrasivity Test

The test principle is based on a steel pin of defined geometry and hardness that scratches the surface of a rock sample over a distance of 10 mm under a static load of 70 N. The steel stylus has a Rockwell Hardness of HRC 55, a 90° conical tip and a diameter of 6 mm. According to the ASTM-D7625-10 and ISRM-SM, the speed of the scratching action is 10 mm/s. In our case, we also used a scratching distance of 50 mm, to evaluate the adhesion effect of the rock materials on the tip of the stylus. Cerchar abrasivity test equipment is shown in Figure 4.7.



Figure 4.7. Cerchar abrasivity test equipment.

The Cerchar tests were performed on dry and saturated, freshly broken rock surfaces from BTS and UCS test samples to evaluate CERCHAR Abrasivity Indices on field surface condition (Figure 4.8).



Figure 4.8. Rock specimens used for Cerchar abrasivity test.

The wear flat at the tip of the stylus is measured using the microscope. In this study, side view wear flat measurement methods of CERCHAR stylus were used to compute the CAI values. The rock sample was inserted into the apparatus and tightly fastened in place using a hard vice. To prevent any lateral movement, the device is fixed. The pin is jointed to the 7 kg dead load and is carefully lowered to the rock surface. The test was then carried out by relative displacement of the pin on the rock surface across 10 mm and 50 mm (Figure 4.9).

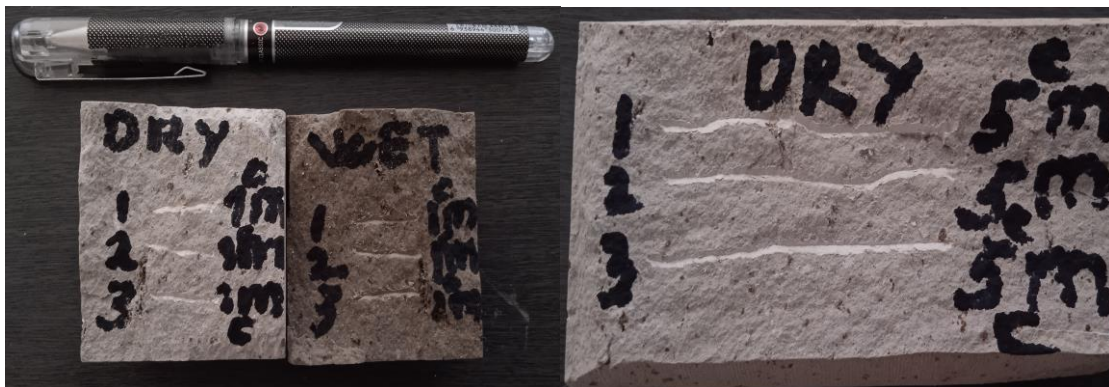


Figure 4.9. Scratching of stylus pin on rock surface across 10 mm and 50 mm.

In some rock samples, the tip of the pin encountered clay minerals through its route on the surface of the rock sample (Figure 4.10).

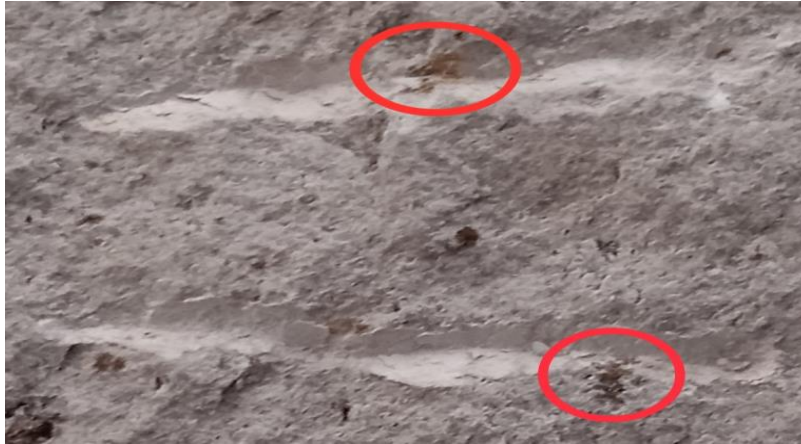


Figure 4.10. Minerals encountered by the tip of the stylus through its route.

After the test, the pin was carefully removed and the tip flat wear was measured by the microscope. In Figure 4.11, the measurement of the tip flat and the route of the tip on the surface of the rock samples is given.

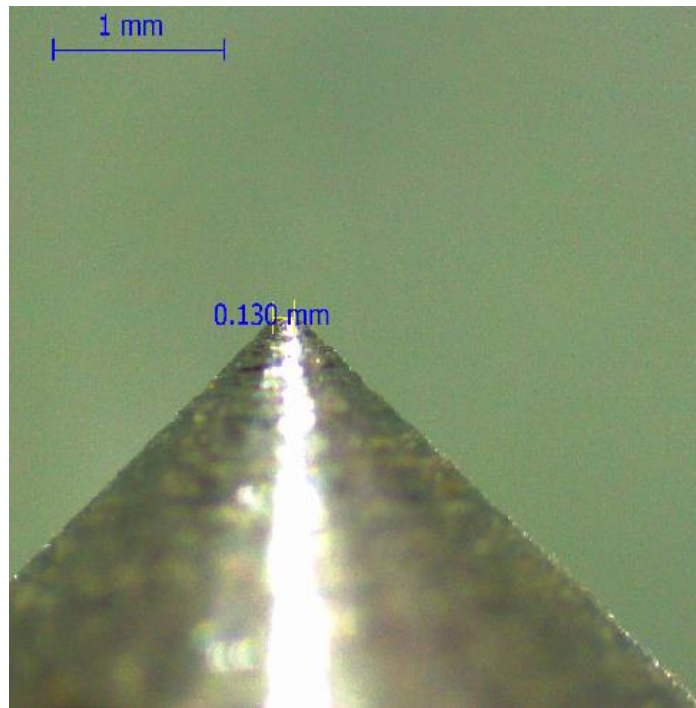


Figure 4.11. Measurement of tip flat wear by Microscope.

4.1.7. The Adhesed Material on the Tip of Stylus and Rotating Steel Arm

The test was performed both in dry and wet conditions. In dry condition, both in 1 cm and 5 cm scratching length, there was no existence of the adhered material on the conical tip of the pin. However, in saturated rock samples, a certain amount of material has adhered to the tip (Figure 4.12.).



Figure 4.12. The adhered material on the tip of the pin.

To better explain the possibility of the adhesion of rock materials on the steel surface, a new test was developed by using a rotating steel arm in the powdered rock material with 60 rpm (rounds per minute).

The adhered material in case of 1 cm scratching length can be neglected. The weight of adhered material in case of 5 cm scratching length on the pin of stylus and on the rotating steel arm was measured by the electronic precision balance (Figure 4.13).



Figure 4.13. Electronic precision balance.

The results of physical-mechanical laboratory experiments are given in Table 4.1.

Table 4.1. Rock mechanics experiments results.

Sample No	UCS (MPa)		BTS (MPa)		Density (g/cm ³)		Sonic Velocity (m/s)		CAI (1 cm)		CAI (5 cm)		Adhered Material (g)	Adhered Material (g)
	Dry	Wet	Dry	Wet	Dry	Wet	Dry	Wet	Dry	Wet	Dry	Wet	5 cm Scratching Length Wet	on Rotating Steel Wet
Sample 1	11.0	7.0	1.75	1.17	1.87	1.84	3158	3059.5	1.42	0.88	1.74	1.45	0.18	10.25
Sample 2	11.4	9.5	1.75	1.28	1.84	1.82	2012	1428	1.47	1.13	1.59	1.41	0.14	9.69
Sample 3	8.1	4.8	1.07	0.66	1.30	1.30	1671	844	1.13	0.63	1.33	1	0.10	8.64
Sample 4	12.4	8.5	1.67	1.06	1.57	1.55	1910	1467	1.4	1.05	1.73	1.5	0.13	10.56
Sample 5	12.8	9.6	3.61	3.11	1.30	1.30	2663.5	2362.5	1.9	1.41	2.2	1.91	0.25	16.25
Sample 6	14.1	9.1	2.25	1.20	1.58	1.56	1694	903	1.55	0.76	1.68	1.31	0.26	15.36
Sample 7	9.9	4.4	1.25	1.04	1.46	1.42	2462	1908	1.22	0.64	1.57	1.27	0.13	10.23
Sample 8	4.9	2.9	0.64	0.27	1.39	1.36	1786	1055	0.92	0.73	1.27	1.12	0.11	8.51
Sample 9	5.8	3.3	0.80	0.67	1.39	1.38	2021	1337	0.98	0.69	1.24	1.04	0.12	9.63

4.2. Mineralogical and Petrographic Characterization

Mineralogical and petrographic analyses are carried out by using X-ray Diffraction, X-ray Fluorescence, and thin section in Ankara University Geosciences Application and Research Center.

4.2.1. X-ray Diffraction

An X-ray tube, a sample holder, and an X-ray detector are the three fundamental components of an X-ray diffractometer. In a cathode ray tube, X-rays are formed by burning a filament to produce electrons, then providing a voltage to transmit electricity toward a target and hitting the target material with electrons. Characteristic X-ray spectra are created when electrons have enough energy to release inner shell electrons of the target material. These spectra are made up of various elements, the most prevalent of which are K_{α} and K_{β} . K_{α} is made up in part of $K_{\alpha 1}$ and $K_{\alpha 2}$. $K_{\alpha 1}$ has a slightly smaller wavelength than $K_{\alpha 2}$ and is twice as bright. The wavelengths are the function of the target material (Cu, Cr, Fe, Mo). Filtering, either using foils or crystal monochrometers, is necessary to get monochromatic X-rays for diffraction. Because the wavelengths of $K_{\alpha 1}$ and $K_{\alpha 2}$ are sufficiently similar, a weighted average of the two is employed. Copper is the most marketing aimed target material with K_{α} radiation of 1.5418\AA for single-crystal diffraction. As the X-rays reflect during the rotation of sample and detector, the intensity of reflections is recorded. A detector captures and analyses the X-ray signal, converting it to a count rate that is subsequently sent to a printer or computer monitor. An X-ray diffractometer's geometry is such that the sample spins at an angle θ in the direction of the collimated X-ray beam, while the X-ray detector is positioned on an arm that rotates at an angle of 2θ to capture the diffracted X-rays. A goniometer is an instrument that is used to maintain the angle and spin the sample. Data is captured at 2 angles ranging from 5° to 70° for common powder patterns, which are present in the X-ray scan. In this study, the target materials are copper and cobalt. Figure 4.14 shows the results of XRD studies for one sample, while Appendix A contains the results for the remaining specimens.

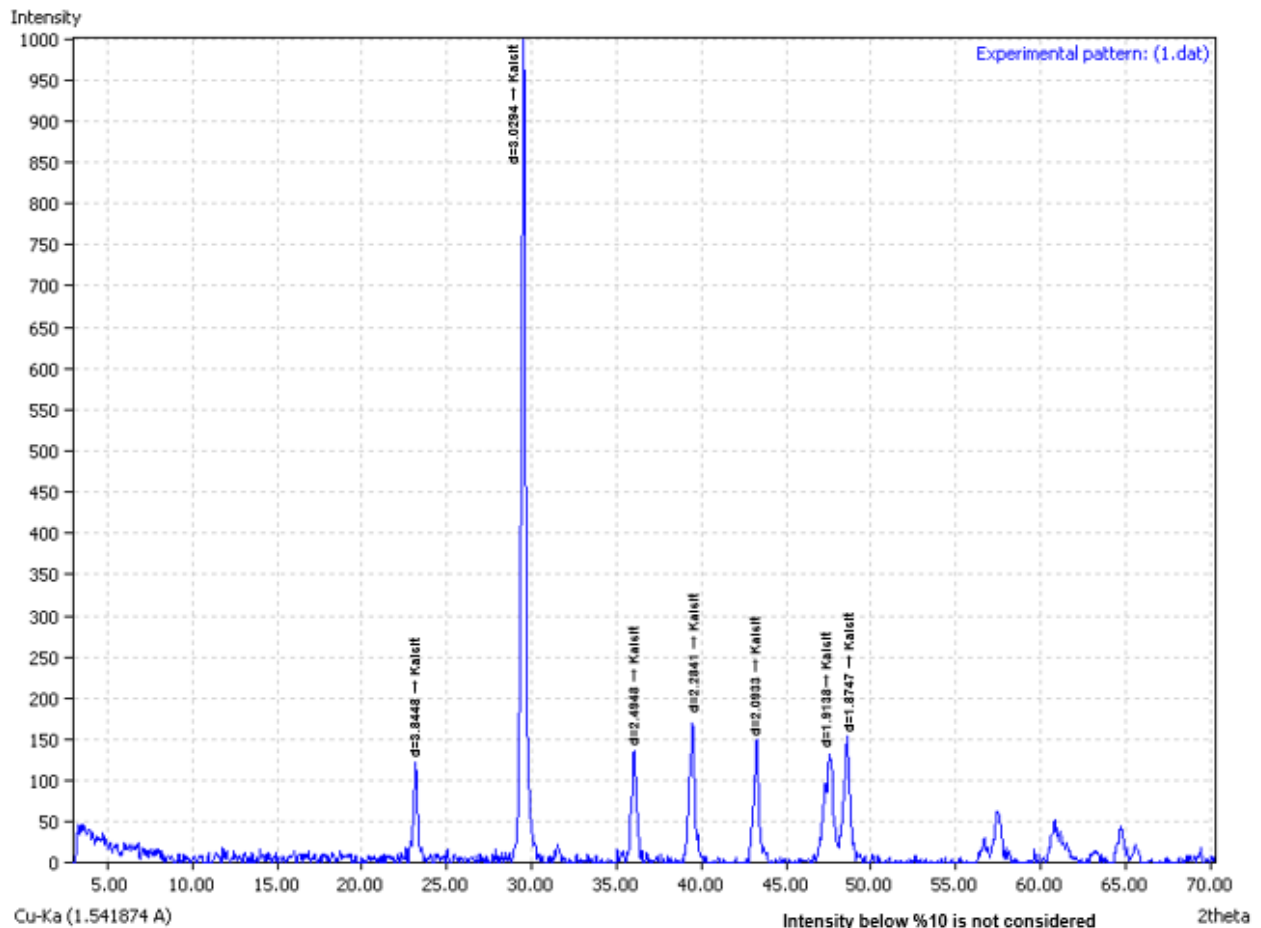


Figure 4.14. Result of XRD analyses for one sample.

4.2.2. X-ray Fluorescence

To determine the elemental content of the rocks, XRF (X-ray fluorescence) is used. XRF is an ideal technology for qualitative and quantitative investigation of material composition because each element in a sample creates a set of characteristic fluorescent X-rays ("a fingerprint") that is unique to that element. Tables 4.2 and 4.3 show the findings of XRF studies performed on 11 samples.

Table 4.2. XRF results.

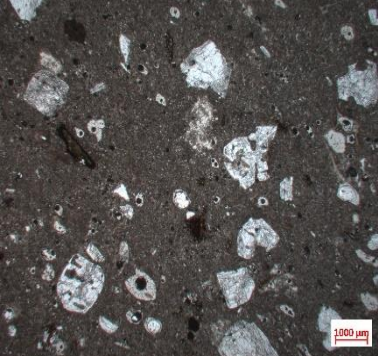
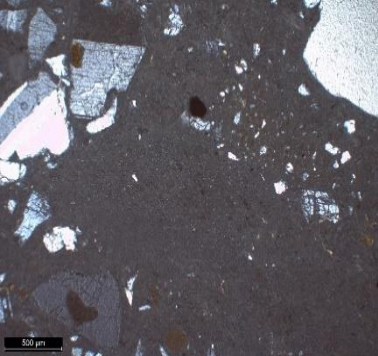
Element	Na2O	MgO	Al2O3	SiO2	P2O5	SO3	Cl	K2O	CaO	TiO2	V2O5	Cr2O3	MnO	Fe2O3	LOI	SUM
Dimension	%	%	%	%	%	%	%	%	%	%	%	%	%	%	%	%
Sample 1	0.045	0.186	0.2478	0.9547	0.0024	0.1131	0.0135	0.0677	55.78	0.0077	0.0012	0.00217	0.00781	0.0564	42.83	100.2705
Sample 2	4.11	1.527	13.81	61.45	0.2447	0.1844	0.0002	1.978	4.577	1.064	0.0142	0.001	0.1036	6.244	8.73	99.9281
Sample 3	5.27	0.29	12.93	76.29	0.01207	0.1883	0.01753	4.319	0.874	0.3245	0.0072	0.0008	0.02065	0.9175	3.72	99.91155
Sample 4	5.39	0.915	14.55	69.27	0.2235	0.21	0.0002	2.717	4.33	0.7858	0.0062	0.00096	0.0882	4.455	2.65	100.2019
Sample 5	3.62	1.148	13.72	66.64	0.1599	0.2265	0.08065	3.367	2.817	0.7106	0.0068	0.00094	0.0817	4.074	6.92	99.95309
Sample 6	5.08	0.235	13.45	74.54	0.0384	0.1876	0.00708	4.278	0.866	0.3072	0.0046	0.00117	0.061	1.823	4.66	100.4591
Sample 7	0.13	0.21	14.55	74.99	0.00667	0.205	0.0002	2.545	0.1505	0.1493	0.0054	0.00073	0.0348	1.125	6.59	100.5626
Sample 8	0.25	0.082	16.16	71.25	0.0333	0.9814	0.0002	0.4331	0.2273	0.186	0.0084	0.00219	0.00144	1.871	8.67	99.90633
Sample 9	0.16	0.014	15.68	72.27	0.00079	0.2648	0.0002	2.116	0.1232	0.1854	0.0095	0.00082	0.00173	0.4892	8.92	100.0756
Sample 10	0.037	0.242	14.74	73.2	0.00674	0.1924	0.0002	1.198	2.269	0.1727	0.0091	0.00078	0.0511	1.464	6.77	100.316
Sample 11	2.14	0.889	11.71	70.24	0.0502	0.1798	0.06785	4.035	2.3	0.2057	0.0109	0.00086	0.0661	1.974	8.92	100.6494

Table 4.3. XRF results.

Element	Dimension	Sample 1	Sample 2	Sample 3	Sample 4	Sample 5	Sample 6	Sample 7	Sample 8	Sample 9	Sample 10	Sample 11
Co	ppm	13	83.1	71.6	42.6	88.1	76.2	35.7	39.3	38.2	75	44.9
Ni	ppm	2.5	17.7	5.9	8.6	6.8	8.6	4.1	1.4	4.6	5.5	2.9
Cu	ppm	1	40.7	1	7.3	7	1.5	0.7	0.9	0.8	2.6	2.4
Zn	ppm	0.5	61.2	22.4	54.4	55.8	36.8	25.3	8.6	9.7	34.8	29.7
Ga	ppm	2.1	21	19.1	20.1	19.6	18.5	14.8	15.7	15.6	14.8	16.6
Ge	ppm	1.3	1.6	1.9	1.1	1.9	1.7	1.6	0.9	3.2	2.1	1.4
As	ppm	1.5	2.8	4.4	2.6	7.8	3.5	6.7	2.1	3.9	5.7	3.5
Se	ppm	0.4	0.6	1.3	0.7	0.9	1	0.5	0.5	0.6	0.4	0.6
Br	ppm	1.7	0.6	1.7	0.9	4.8	1.7	0.5	0.6	0.9	0.5	2.8
Rb	ppm	1.2	52.9	154.5	67.6	91.4	152.7	93.3	25.7	83.2	58.7	129.9
Sr	ppm	482.7	315.2	76.6	251.9	215.9	73.6	35.6	138.8	69.4	45.8	288.7
Y	ppm	0.5	28.2	18.5	38.8	33	46.3	12.8	11.1	11.8	19.2	10.6
Zr	ppm	7.3	252.8	339.7	336.4	325.7	338.1	91.1	99.9	96.4	107.5	123.1
Nb	ppm	3.4	13.6	21.5	15.9	17.1	20.2	14.4	13.3	13.5	12.1	12.6
Mo	ppm	2.8	6.4	5.3	3.6	3.1	4.3	2.3	1.6	2.1	2.3	3.1
Cd	ppm	0.9	0.8	0.7	0.8	0.7	0.8	0.6	0.6	0.7	0.6	0.7
In	ppm	0.9	0.8	0.7	0.8	0.7	0.7	0.6	0.6	0.7	0.7	0.7
Sn	ppm	0.8	1.7	0.4	2.2	3.2	0.8	0.8	0.6	0.8	0.8	0.4
Sb	ppm	0.9	0.5	0.8	0.9	0.8	0.8	0.8	4.9	6.2	3.3	0.8
Te	ppm	1.1	1.2	1.1	1.2	1.1	1.1	1.1	1	1.1	1.1	1.1
I	ppm	3.4	2.1	2	2	2	2	1.9	1.9	1.8	1.8	2.1
Cs	ppm	3.4	3.6	3.4	3.5	2.7	3.5	5.2	5	16.2	9.2	3.6
Ba	ppm	21	433.3	568.1	479.9	442.5	549.7	387.5	256.1	49	89.6	743.9
La	ppm	7.1	33.7	27.1	32.1	30.1	34.5	30.8	28.4	40.5	40.4	30.9
Ce	ppm	14.7	66.9	37.3	60.7	57	76.5	59.4	55.1	60.6	72.4	47.6
Hf	ppm	3	3.1	1.5	2	1.8	1.5	1.3	1.4	1.3	1.5	1.6
Ta	ppm	2.7	4	5.1	6.3	5.1	6.5	2.9	3.7	3.7	1.4	3
W	ppm	285.9	550.9	1056	681	1004	939.9	429.3	404.1	645.3	258.6	632.2
Hg	ppm	2.2	2.4	3	2.6	3.1	2.8	1.8	1.8	2.1	1.5	2.3
Ti	ppm	1.6	1.1	1	0.9	1.9	1.2	1.4	0.5	1.8	1	1
Pb	ppm	8.6	14.2	17.3	18	17.3	23.2	15.9	11.9	10.4	22.5	22.2
Bi	ppm	0.7	0.6	0.6	1.1	1.1	1.1	0.7	0.5	0.5	0.7	1.4
Th	ppm	0.5	12.3	27.2	16.9	17.4	28.8	22.9	23.1	24.2	23.4	20
U	ppm	10	8.1	6.9	12.5	9.5	7	7.6	6	6	5.8	6.9

4.2.3. Thin Section

Mineralogical and petrographic analyses were carried out to determine the percentage of abrasive minerals in the rock samples. The mineralogical and petrographic properties were determined as percentages from thin-section images collected by a camera mounted on a polarizing microscope. The results on the thin-section images, mineralogical and petrographic examinations of the rocks excavated by the roadheaders are given in Figure 4.15. As seen in the figure, the abrasive mineral contents of all the excavated rocks were close to each other, and all rocks presented clay alterations.

Sample Code	ROCK TYPE/NAME	Microphotograph (thin section)	Mineralogical Composition
AKTAŞ1	Magmatic Pyroclastic IGNIMBRITE		Matrix+shards (47%) Volcanic clast (8%) Rock fragments (15%) Quartz (13%) Plagioclase (12%) Biotite (3%) Opaque min. (2%)
AKTAŞ2	Magmatic Pyroclastic IGNIMBRITE		Matrix+shards (33%) Volcanic clast (13%) Quartz (17%) Rock fragments (15%) Plagioclase (14%) Biotite (5%) Opaque min. (3%)
KAYHAN1	Magmatic Pyroclastic IGNIMBRITE		Matrix+shards (32%) Volcanic clasts (16%) Quartz (19%) Rock fragments (12%) Plagioclase (12%) Biotite (5%) Opaque min. (4%)
KAVAK	Magmatic Pyroclastic IGNIMBRITE		Matrix+shards (25%) Volcanic clasts (21%) Quartz (17%) Rock fragments (16%) Plagioclase (14%) Biotite (6%) Opaque min. (1%)

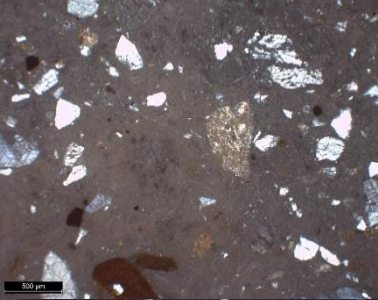
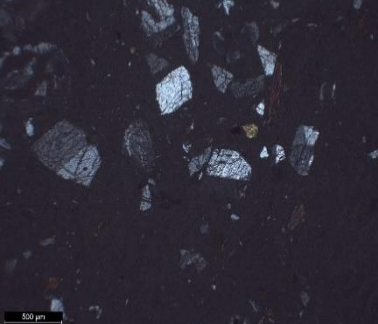
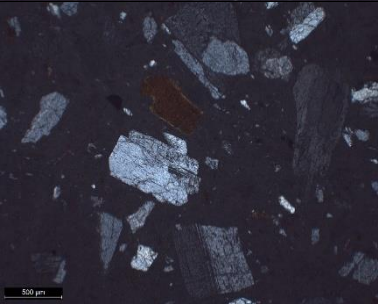
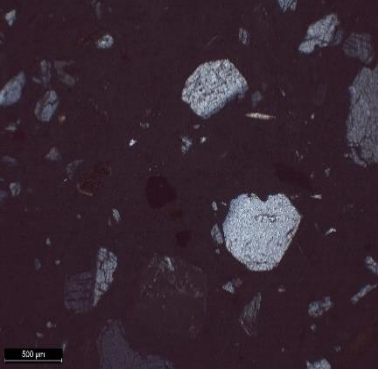
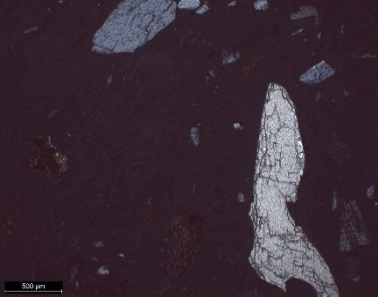
KAYHAN₂	Magmatic Pyroclastic IGNIMBRITE		Matrix+shards (26%) Volcanic clasts (14%) Plagioclase (19%) Quartz (15%) Rock fragments (14%) Biotite (9%) Amphibole (2%) Opaque min. (1%)
SULUSARAY	Magmatic Pyroclastic IGNIMBRITE		Matrix+shards (28%) Volcanic clasts (14%) Rock fragments (21%) Plagioclase (15%) Quartz (15%) Biotite (7%) Amphibole (2%) Opaque min. (1%)
HOYUK	Magmatic Pyroclastic IGNIMBRITE		Matrix+shards (30%) Volcanic clasts (14%) Plagioclase (14%) Quartz (13%) Rock fragments (21%) Biotite (5%) Amphibole (2%) Opaque min. (1%)
GUVENAL	Magmatic Pyroclastic IGNIMBRITE		Matrix+shards (39%) Volcanic clasts (12%) Rock fragments (16%) Plagioclase (13%) Quartz (11%) Amphibole (4%) Biotite (3%) Opaque min. (2%)
NAR	Magmatic Pyroclastic IGNIMBRITE		Matrix+shards (54%) Volcanic clasts (10%) Rock fragments (14%) Quartz (12%) Plagioclase (10%) Biotite (3%) Opaque min. (1%)

Figure 4.15. Thin-section images and mineralogical-petrographic analysis results of rock the sample.

Chapter 5

Field Studies

5.1. Description of the Project

Field studies are based on the performance of roadheaders at the excavation process of different cold storage caverns (CSC) located in the Cappadocia Region. These CSCs are close to Nigde and Nevsehir in Central Anatolia Region (Figure 5.1). In 15 km west of Nigde, Aktash CSCs are present while others are located in areas of Kayhan, Nar, Sulusaray, Kavak, and Hoyuk around Nevsehir.

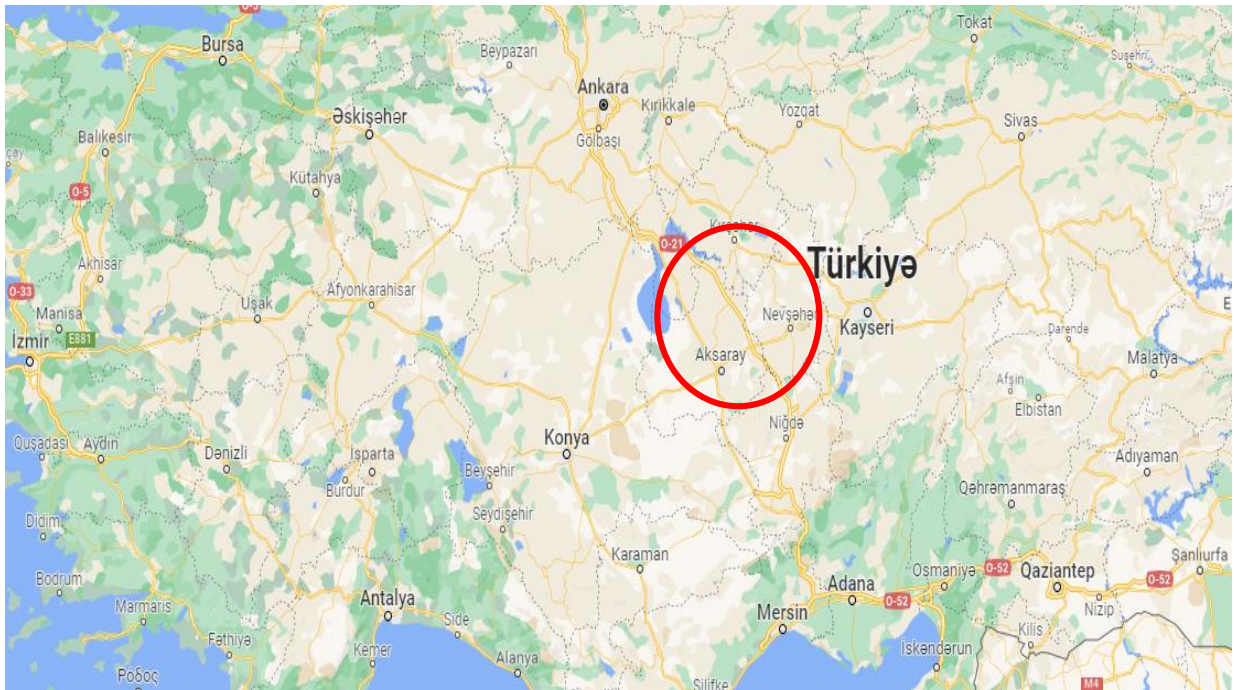


Figure 5.1. The location of project areas in the Cappadocia Region.

The field studies are carried out in different CSCs located in the different above-mentioned places in Cappadocia, in dry and wet conditions. The cold storage caverns built by Hoyuk Construction distinguish itself from other warehouses in the region with many features. The facility, which has a volume of approximately 45,000 m³, has all the natural advantages of underground warehousing, as well as state-of-the-art technology and fully computer-controlled ventilation/cooling units. The lodges, each of which is independent of

the other, with ventilation and cooling facilities; by hosting the above-ground technology underground, it provides economical, healthy, and natural storage. A general view of one of the project areas is given in Figure 5.2.



Figure 5.2. General view of project areas.

The design of the CSCs is usually based on the main gallery with multiple storage rooms on both sides (left and right). The main gallery of the dry Nar CSCs is a rectangular prism with a length, width, and height equal to 150 m, 6 m, and 7 m respectively. There are 24 different storage rooms for the dry CSC in Nar, each of them having 6.4 m in height and 6m in width with a length of 24 m on both sides of the main gallery. Figure 5.3. illustrates the general plan view of the main gallery and storage rooms of dry CSC with the sight from inside.



Figure 5.3. Plan view of dry CSC.

In the same way, wet CSCs in Nar, around Nevsehir consist of a main gallery and has 46 storage rooms. The length of the main gallery is longer than the main gallery of dry CSCs.

The dimension of the main gallery is 210 m in length and has 6.5 m in height and 6.3 m in width. Storage rooms have a length of 25 m, a width of 6 m, and a height of 4.3 m. In figure 5.4, the plan view of wet CSC is depicted.



Figure 5.4. Plan view of wet CSC.

5.2. Geology of the Fields

In this study, the cold storage caverns in the Cappadocia Region were taken into consideration, and these cold storage caverns were opened within the Neogene aged pyroclastic rocks in the Cappadocia Volcanic Complex (CVC). The Cappadocia Volcanic Complex has a width of 40-60 km and an extension of more than 250 km in the NE-SW direction.⁴² This region is bounded by the Taurus mountain belt in the south, the Kirsehir region in the north, and the Hasan Mountain and Erciyes Mountains in the east and west. The geology of the Cappadocia Region generally consists of pre-Neogene granitic rocks, Neogene sedimentary rocks, Neogene aged volcano-sedimentary, and Quaternary volcanic rocks. The Neogene-Quaternary volcano-sedimentary in the region is mainly composed of ignimbrites. The stratigraphy of the ignimbrites in the region classified as Kavak, Zelve, Sarımaden, Sofular, Cemilköy, Tahar, Gördeler, Kızılkaya, Valibaba and Kumtepe from the oldest to the youngest.⁴³

The volcanic units of Cappadocia are generally in off-white, gray, and pink colors and clastic, showing an alternation from fine-grained to coarse-grained, closed large and small pumice and obsidian lumps, locally sourced tuffs and tuffs interbedded with clay and marly clay beds of different duration and other in places. These cold storage caverns belong to the ignimbrite units of the Urgup volcanic formation which covers the Yeshilhisar formation, is widely exposed in the area. This formation consists of continental (fluvial to lacustrine) sediments interwoven with several pyroclastic sediments. The plateau of this nearly horizontal formation is at an altitude of 1100 – 1200 m near the Urgup.⁴⁰ The formation recently has been divided into 10 volcanic units due to the very marked lithological variability within the formation, both vertically and horizontally. The vertical part, which gives brief geological information about each member that passes through the Urgup formation, is shown in Figure 4.1.⁴¹

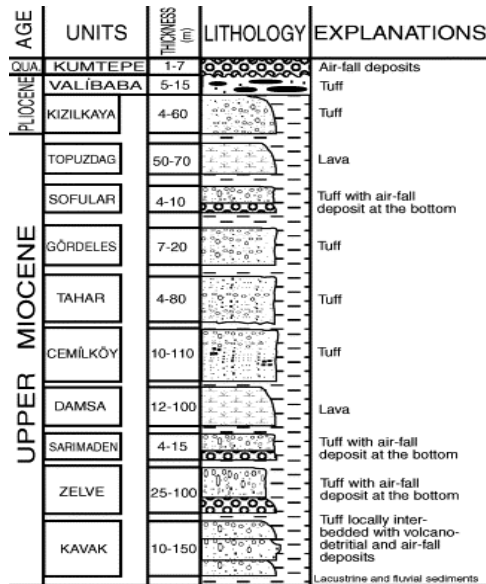


Figure 5.5. Vertical cross-section through the tuff sequence of the Cappadocia.⁴¹

5.3. Roadheaders in Cold Storage Caverns

Table 5.1 presents the machine specifications for the Paurat E134 type roadheader. The general view of the machine is depicted in Figure 5.6.

Table 5.1. Machine specifications for Paurat E134 type Roadheader.

Machine Chassis Dimensions	
Width	3700 mm
Height	2500 ± 500 mm
Length	8500 mm
Conveyor Belt	8500 mm
Machine Cutting Dimensions	
Width	4800 ± 500 mm
Height	7000 mm
Other Features	
Weight of the Machine	50 t
Cutting Power	200 kW
Hydraulic Power	40 kW
Tape Systems	60 kW
Total Power	300 kW
Voltage Source	380 V
Hydraulic System Pressure	65 Mpa



Figure 5.6. General View of Paurat E134.

5.4. Field Performance Analysis of Roadheaders

In the Cappadocia region, CSCs are generally excavated in low-strength homogenous pyroclastic formations. However, physical and mechanical properties of formations such as the structure of the discontinuities may vary. Especially, water content plays a huge role in the excavation performance of the roadheaders. Therefore, the excavation performance of two axial-type roadheaders (Paurat E134) with 55-ton weight is analyzed both in dry and wet cold storage caverns. Due to the stick properties of the formation, especially in wet CSC, there was an adhesion both on the cutterheads and the gathering arms of roadheaders. This phenomenon is depicted in Figure 5.7.



Figure 5.7. The adhesion of formation on the cutterhead and gathering arm.

Another problem generally is encountered in the traveling mechanism. So that, sometimes bigger blocks are stuck in the traveling system (Figure 5.8). To overcome this issue, the traveling system is rotated reversely. These problems cause a reduction in the average ICR.



Figure 5.8. Traveling mechanism.

The roadheaders' field performance data were continuously recorded for one week for each CSC excavation. The mean values of all recorded data were then estimated. Approximately, 4 rooms for dry and 3 rooms for wet CSCs could be excavated within a week. The recorded data cover the distribution of total working time and the daily advance rate (DAR - the advance rate of the excavation in a day as m/day). Furthermore, excavation, mucking, trimming the excavated surface, site surveying, machine breakdown maintenance, and breakages are considered as the operating times. Figure 5.9 depicts some of these operations.



Figure 5.9. a) Excavating b) Mucking c) Trimming.

Other performance parameters, such as machine utilization time and instantaneous cutting rate are calculated from the recorded field data by using Equation 5.1 and Equation 5.2. The mean performance parameters taken from the fields are given in Table 5.2.

$$MUT = \frac{Boring\ Time}{Shift\ Time} \quad (5.1)$$

$$ICR = \frac{Volume\ (Advance*Area)}{Boring\ Time} \quad (5.2)$$

Where;

- MUT= Machine utilization factor (%)
- Boring time= Time spent for excavation (hours)
- Shift time= Working time (24 hours)
- Field ICR= Instantaneous cutting rate (m^3 /h)
- Area= Area of the tunnel (m^2)

5.5. Field Cutter Consumption of Roadheaders

One of the most crucial parameters in mechanical excavation is the cutter consumption rate (CCR) of the roadheaders. Cutter consumption holds a big share in the excavation project budget. Due to the low-strength characteristic of tuff formations, CSCs were easily excavated by roadheaders. The conical cutters consist of a steel body and a tungsten carbide tip in the body (Figure 5.10).

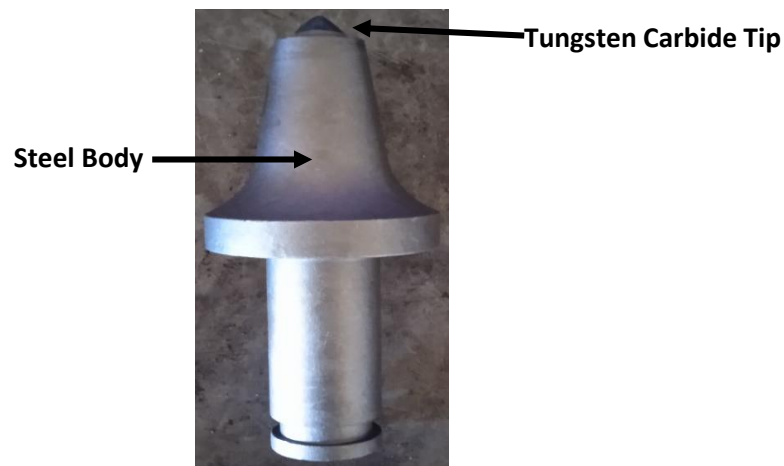


Figure 5.10. Conical cutter.

Although the steel body does not come in contact with the formation, it can wear easily compared to the tungsten carbide tip. However, cutter wear can increase due to several factors. It includes excavation in wet formations, an increase in the depth of cut due to the easy excavation in low-strength formations. Figure 5.11 depicts a worn steel body.



Figure 5.11. Worn steel body.

To reduce the project cost, the contractor company does not completely replace the cutters whose steel bodies are worn, but only welds the worn steel body. However, this process changes the original cutter design parameters, such as the tip angle, or clearance angle (Figure 5.12).



Figure 5.12. Welded steel body.

The main technical parameters of roadheaders and other parameters related to the Nar region are given in Table 5.2; as for the other regions, they are given in Appendix B.

Table 5.2. Field performance parameters of roadheaders for the Nar region.

Nar		Dry CSC	Wet CSC
Project Activity Dates	Starting		
	Ending		
Used Machine	Model / Weight (ton)	PAURAT E 134 55 TON	PAURAT E 134 55 TON
	Power (kW)	370	370
Daily Working Time (hour)		10	10
Daily Excavation Time (hour)		6	5.5
Machine Breakdown Maintenance (hour) per day		2	2.5
Lunch and Cofee Break (hour)		2	2
Daily Excavation Amount (m3)		576	258
Number of Main Corridors		1	1
Main Corridors Dimensions (m) Length / Width / Height		150.00 * 6.00 * 7.00	210.00 * 6.30 * 6.50
Number of Lodges		24	46
Lodge Dimensions (m) Length / Width / Height		24.00 * 6.00 * 6.40	25.00 * 6.00 * 4.30
Daily Chisel Consumption		15	10
Net Cutting Rate (m^3/d)		576	258
Daily Advance Rate (m/d)		15	10
Machine Utilization (%)		60	55
Instantaneous Cutting Rate (m^3/h)		96	46.9
Cutter Consumption (picks/ m^3)		0.026041667	0.03875969

Chapter 6

Discussion and Conclusions

6.1. Summary

Mineral extraction and construction operations in the mining and construction industries are typically done using either conventional (drilling and blasting, mechanical excavation by hammers, and so on) or mechanized excavation methods. One of the main drawbacks of mechanized excavation methods is tool consumption. These excavation methods make use of tools to attack the rock, causing the tools to wear out or deteriorate. Rapid wear of excavation tools used in mining and tunneling operations can raise tool consumption and expense significantly.⁴⁴

The host rock is wet in most situations, and in other cases, it is completely saturated with water. Furthermore, rock excavation is typically carried out in saturated rock in specific applications such as off-shore drilling, harbor building, dredging of hard formations, and construction of structures beneath bodies of water. Bits or other cutting instruments are utilized by all excavators for such applications to extract rocks in both dry and saturated conditions, which affects the bit wear rate, bit life, cutting pressures, and specific energy. Air-dried rock samples are typically used in laboratory testing to estimate the performance and production rate of these excavators. This can lead to an overestimation or underestimation of cutting forces and rock abrasivity, affecting the overall technical/operational viability of the proposed systems as well as the project's finances. A quick review of the literature (Broch 1979, Erguler and Ulusay 2009, Yilmaz 2010) on rock behavior (abrasiveness, cutting forces, specific energy and strength, and so on) reveals that rock behavior changes at different moisture contents, and that these changes may have an impact on the production rate and tool consumption of any excavation machine under saturated conditions.^{45, 46, 47, 51, 55, 57}

There are a lot of previous studies (Mammen 2009, Perera 2011, Poulsen 2014, Soni 2015) that looked at the effects of water saturation on the physical and mechanical characteristics of rocks. Many researchers have worked on the influence of water saturation on UCS and BTS values, showing that the compressive and tensile strengths of saturated rocks are much lower than those of air-dried samples in the vast majority of cases.^{56, 58, 59, 60}

In this chapter, we will focus on the effects of physio-mechanical and petrographic properties of the 9 rock samples collected from the different regions of Cappadocia on the Cerchar abrasivity index (CAI) and field performance parameters of roadheaders both in dry

and fully saturated conditions. The reason to analyze the effect of water is that, in the presence of water, the capacity of certain rock minerals to attach or stick to the metal components of a roadheader has the potential to have quantifiable effects on a project's schedule and budget.

6.2. The Effects of Mechanical Properties and Adhesion on CAI

6.2.1. The Effect of Mechanical Properties on CAI

The Cerchar abrasivity index (CAI) is commonly used in mining and tunneling operations to assess tool life and wear in various excavation equipment. The sensitivity of CAI results is investigated due to variation of certain parameters, including the mechanical properties of rocks, the effect of the water content of rock specimens, and the effect of scratch length. The relationship between CAI and mechanical parameters of rock specimens, both in dry and fully saturated conditions for 1 cm scratch lengths and its repeatability is investigated through statistical analyses of a series of CAI test results obtained from 9 selected rock specimens.

The performed analyses show that there is a linear relationship between the mechanical properties of rock specimens and CAI. As the strength of the rock material increases, CAI is also increasing and this leads to the wear of the tools. The relationships between UCS and BTS and CAI are depicted for 9 rock samples in Figure 6.1.

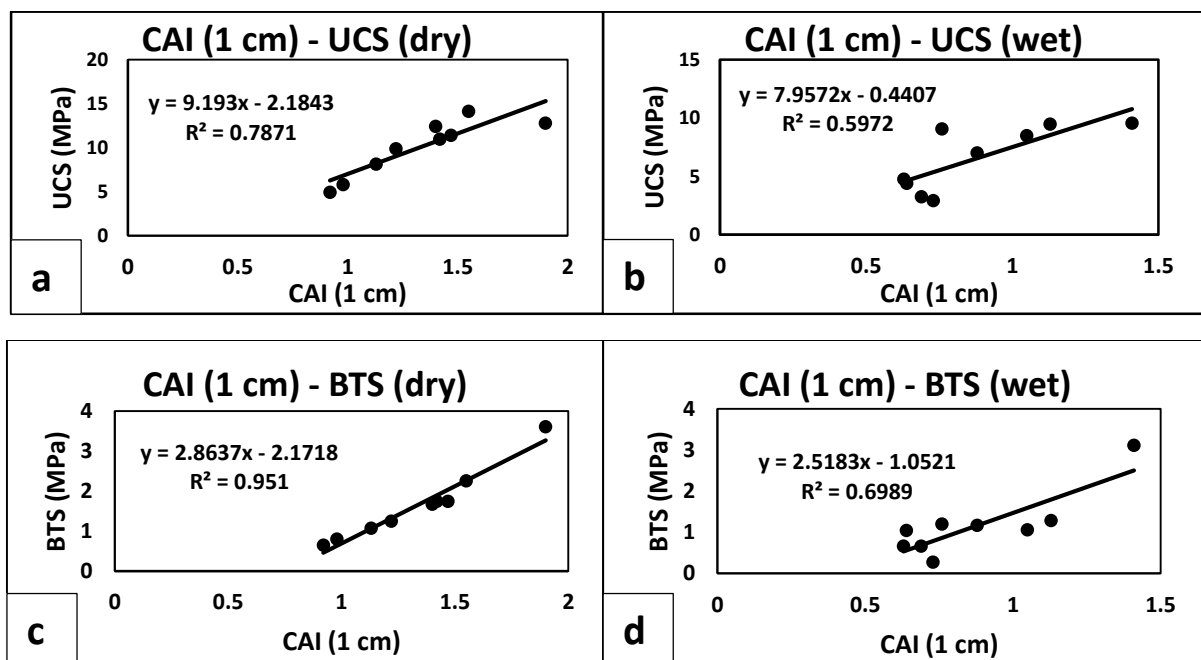


Figure 6.1. Relationship between UCS and BTS and CAI.

According to Figure 6.1, CAI is higher in dry samples (a and c) compared to the saturated samples (b and d). The reason is related to the effect of water content on the UCS and BTS of the rock samples. As the mechanical properties of the rock material decrease, it is easier to break them. It results in less tool wear and consumption. Many authors (Vutukri 1974, Van Eeckhout 1976, Dyke and Dobereiner 1991, Hawkins and McConnell 1992, Vasarhelyi 2003) have proved that, as the water content of the rock material increases, the

mechanical properties decrease.^{49, 50, 52, 53, 54} However, Brace and Martin (1968) report an increase in the rock strength with water saturation under increased strain rate.⁴⁸

Further, Figure 6.2 shows a relationship between CERCHAR abrasivity index values measured on wet and dry rock surfaces for 1 cm (a) and 5 cm (b) scratching lengths which are presented below:

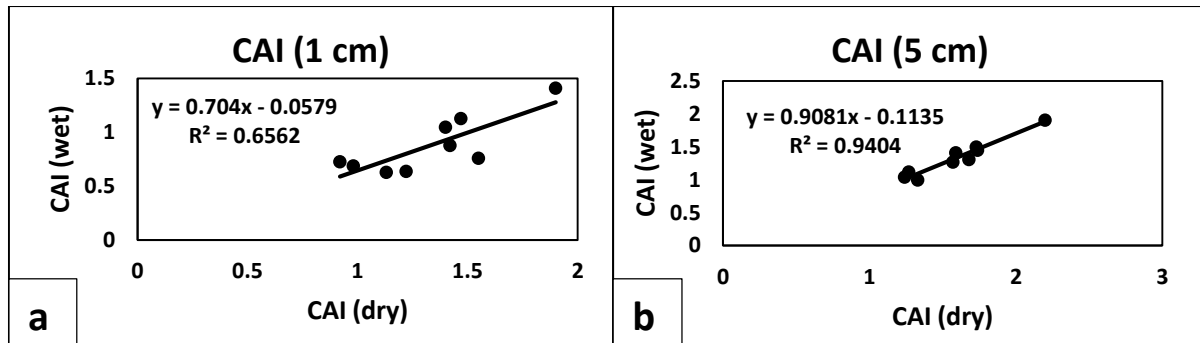


Figure 6.2. Relationship between dry and wet CAIs.

The proposed correlations (Equations 6.1 and 6.2) explain that CAI (wet) is about 65% and 80% of the CAI (dry) value for 1 cm and 5 cm scratching lengths, respectively.

$$CAI_{wet} = 0.704 * CAI_{dry} - 0.0579; (R^2 = 0.6562) \quad (6.1)$$

$$CAI_{wet} = 0.9081 * CAI_{dry} - 0.1135; (R^2 = 0.9404) \quad (6.2)$$

The reduction in CAI values upon saturation can be ascribed to the lubricating effect imparted by saturated water between the CERCHAR stylus and the rock surface thereby reducing the friction between the two surfaces. In other words, the lubrication provided by the rock water content significantly reduces wear by decreasing the temperature at the CERCHAR stylus tip. This phenomenon can also be seen in the study of Phillips and Roxborough (1981)⁶¹, where tool wear rate was significantly higher while cutting dry Bunter sandstone compared to the wear observed in cutting wet rock.

6.2.2. The Effect of Adhesion on CAI

As it can be noted in Figure 6.3, the difference of CAI values between dry and saturated samples is less in the case of 5 cm scratching length compared to the 1 cm of scratching length. The mean value for the difference in the 1 cm scratching length is 0.45 which is higher than the difference for the CAI (5 cm) which is equal to 0.26. This means, after a certain length, the wear of tip in saturated rocks will be closer to the wear in dry rocks. It is due to the adhered rock materials on the tip of the stylus that increase the deformation and shear failure at the stylus tip and this tempts the stylus to wear more easily in saturated rock samples as the scratching length increase. The extreme high difference when passing from dry to wet samples in CAI (1 cm) values for some samples such as sample 6 and sample 7 may be due to the petrographic characteristics as well as the intrinsic physical properties of the rock samples. These rock samples include some minerals (Kalait, Orthoclase, Alkali Feldspat, Plagioclase, Tridmit, Illite, Kaolin, and Quartz formations) that can affect the CAI values (see Appendix).

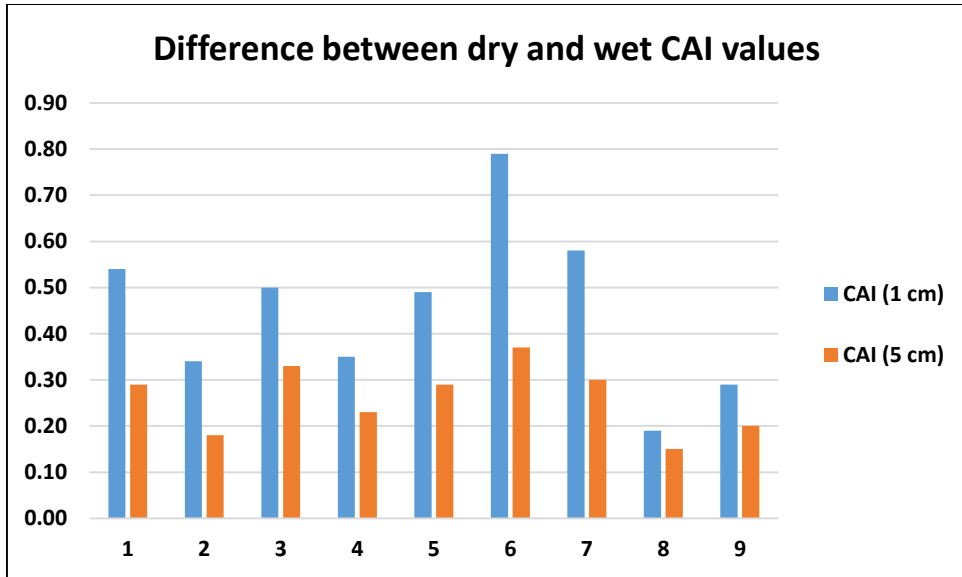


Figure 6.3. Difference between dry and wet CAI values.

The adhesion phenomena can also be proved by the difference between dry CAI (1 cm and 5 cm) values and the difference between wet CAI (1 cm and 5 cm) values (Figure 6.4).

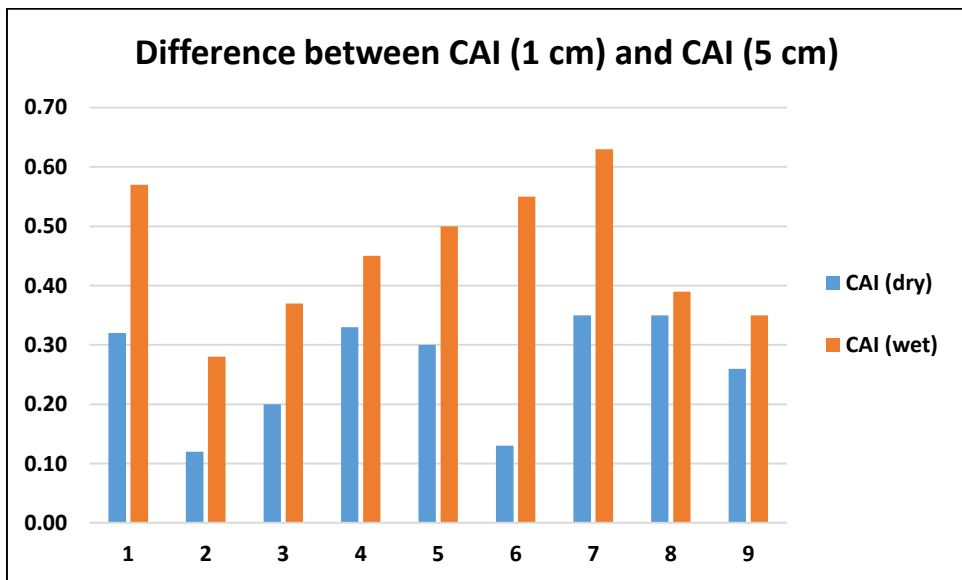


Figure 6.4. Difference between CAI (1 cm) and CAI (5 cm).

According to Figure 6.4, it can be noted that the difference between wet CAI values is higher than the difference between dry CAI values. As previously explained, the reason for the extreme increase of change in CAI (wet) values is due to the sticking of the rock material on the tip of the stylus as the 7 kg load acts on the rock surface along the scratching length. Therefore, the increase of CAI values when passing from 1 cm to 5 cm scratching length in wet samples is higher compared to the dry samples.

6.3. The Effect of Mechanical Properties and Adhesion on Field Performance Parameters of Roadheaders

6.3.1. The Effect of Mechanical Properties on Field Performance Parameters of Roadheaders

In general, UCS shows a strong correlation with the net cutting rate for most rock types; however, experience shows that sometimes UCS does not correlate well to NCR for particular ground conditions. For example, Figure 6.6 (a and b) shows that the measured field NCR (m^3/h) was rather insensitive to the UCS. This demonstrates that UCS measurements alone can be an insufficient representation of intact rock properties for NCR estimates. So, it is reasonable to accept that the NCR is mostly dependent on the mineralogical and petrographic properties of the rock formations. It can be seen that, for the most abrasive geological formation, the net cutting rate is the lowest. From the XRD analyses (see Appendix), it is found that this formation is rich with Plagioclase (Labradorite).

One of the intrinsic parameters that affect the NCR and CCR is the existence of water in the rock mass. It is clear that, as the water content in the rock formation increase, the strength properties of this rock mass decrease. Although UCS of the rock formations decreases with the water content, the NCR also decreases (Figure 6.4 (b)). This is because, in saturated rock formations, especially in pyroclastic rocks, the adhesion properties can affect the NCR. The sticking potential of these formations on the tools can result in clogging of the machine equipment.

In previous studies, strong positive correlations were found between UCS and rock abrasivity, and these studies reported that the CCR values of mechanical excavators would increase by increasing the UCS value of the rocks as the results of this study^{63,64,65,66}(Figure 6.5).

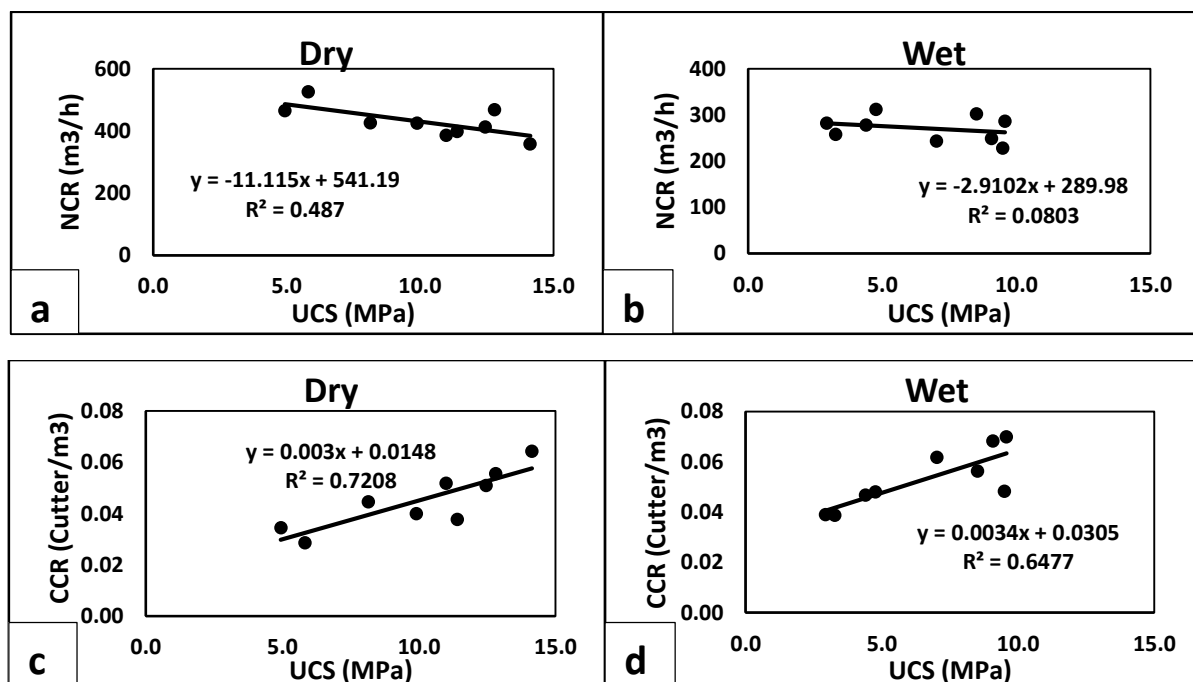


Figure 6.5. Correlation between UCS and field performance parameters of roadheaders.

However, the aforementioned researchers did not use the field CCR data of mechanical excavators such as roadheaders. They only used the CAI values of rocks with medium or high UCS values. Deliormanli⁶⁴ found a positive linear correlation between CAI and UCS for marbles with a variation of UCS values between 45.67 and 149.94 MPa. Similarly, Er and Tugrul⁶³ found linear correlations between CAI and UCS for granitic rocks. However, in this study, a reliable correlation was not found between the CAI and UCS values. However, the fit between NCR and UCS is not good enough. It is because, the UCS values do not change enough to be in a good linear trend with the NCR values. It is seen that CCR is high in the case of saturated rock formations. It can be explained by the effect of water on the sticking potential of material on the cutter head of the roadheaders. The material sticks on a metal surface as the adhesive shear strength increase. The adhesive shear strength is mainly dependent on the mineral type, the roughness of steel surface, contact time between rock material and steel, and applied normal stress. The sticking rock materials on the cutter head create the layers on the cutter head and after a certain period, the consolidation of these materials on the cutters occurs. As the machine applies normal stress, the friction between the cutters and material stick on cutters increases and it results in wear of the cutters.

The same considerations can also be found for the correlation between BTS and field performance parameters of roadheaders. As seen in Figure 6.6, the correlation coefficient is very low. It can be noted that the correlation coefficient is extremely low in saturated conditions. This can be explained by the similar BTS values that do not correlate well with the NCR values.

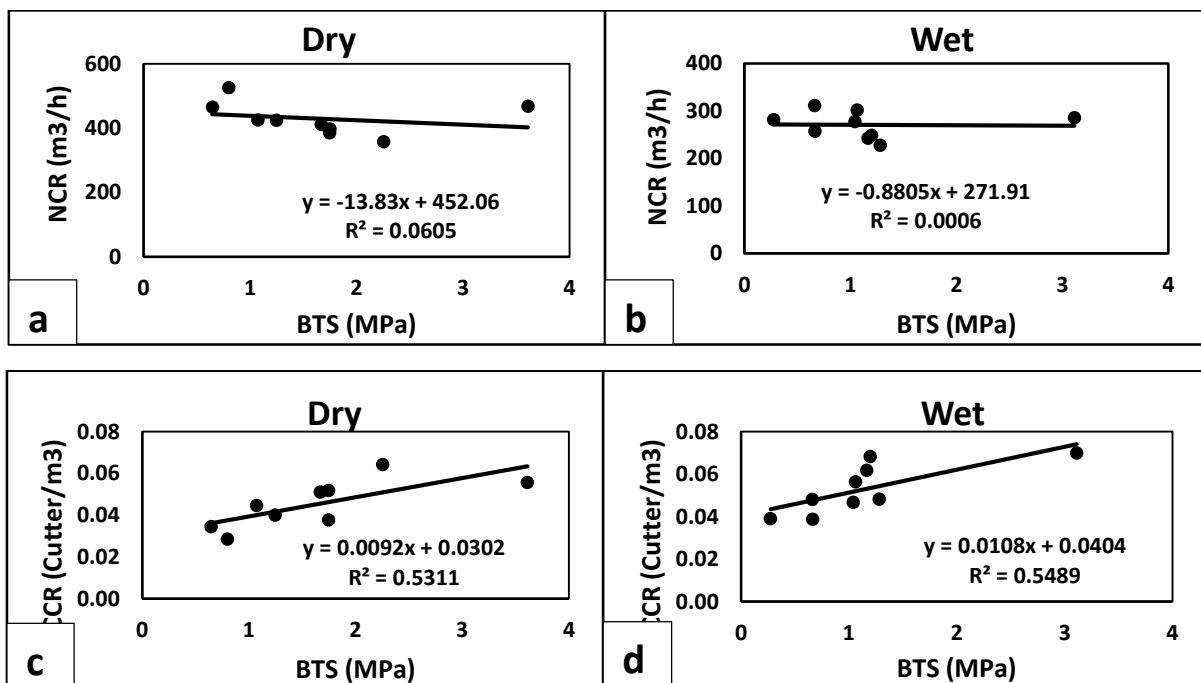


Figure 6.6. Correlation between BTS and field performance parameters of roadheaders.

6.3.2. The Effect of Adhesion on Field Performance Parameters of Roadheaders

In previous studies, some models for predicting the CCR of roadheaders, which are based on Cerchar abrasivity test results, were developed by researchers^{63,64,65}. In this study, a positive linear correlation was found between CCR and CAI, which was similar to the results of previously reported models (Figure 6.7). Previous models, on the other hand, yielded stronger correlation coefficient (R^2) values than the ones used in this study. The differences in rock types could explain this. All of the rock types in this investigation were low-strength tuffs, and the CAI values did not vary significantly.

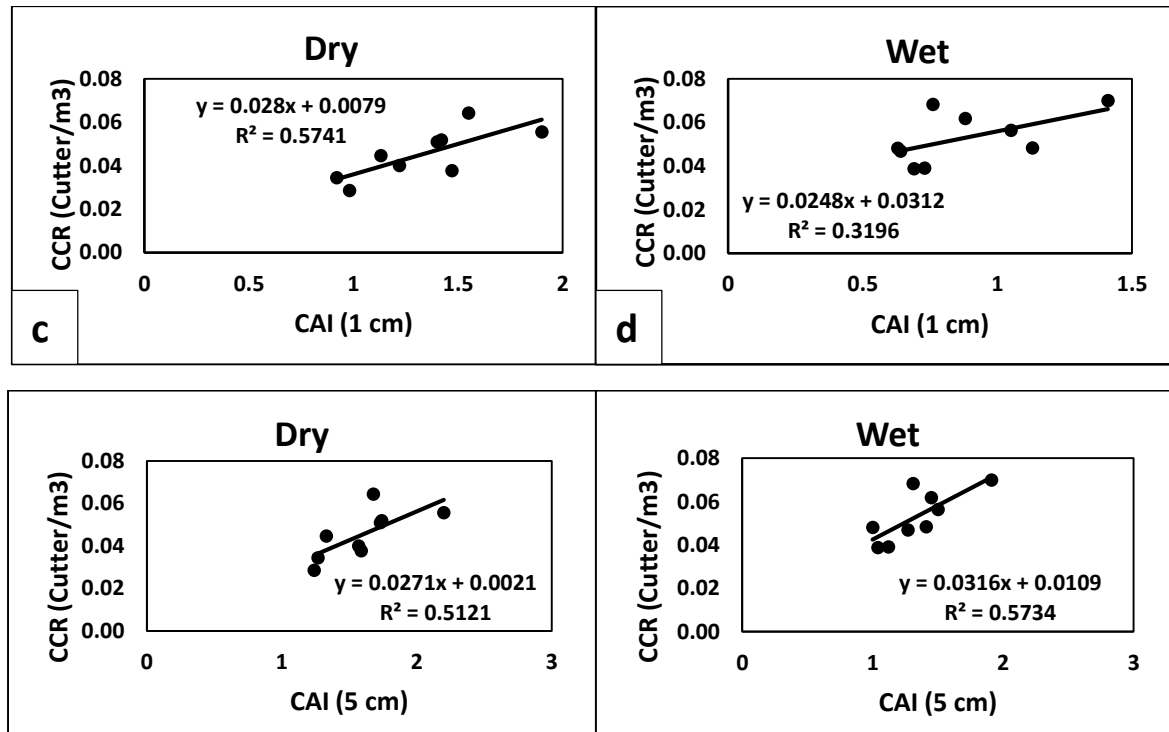


Figure 6.7. Correlation between CAI (1 cm, 5 cm) and field performance parameters of roadheaders.

The negative effect of adhesion on the field performance parameters can be proved by the relationship between field performance parameters and the weight of adhered material on the pin of the stylus in the Cerchar abrasivity test. As known from the results of Cerchar abrasivity test, adhesion of rock material on the pin of the stylus is shown only in the CAI (wet) with the scratching length of 5 cm. Therefore, the weight of the adhered material on the tip of the stylus obtained from the CAI (wet) is correlated with the real field data (CCR_{wet}). Figure 6.8 illustrates the relationship between the weight of adhered material obtained from CAI (wet) and CCR.

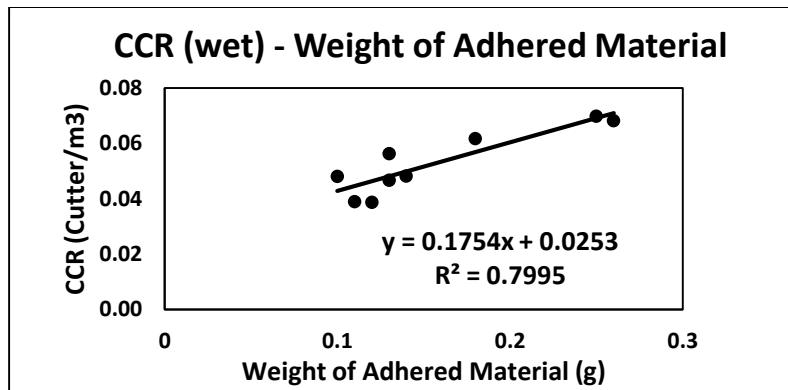


Figure 6.8. Correlation between CCR (wet) and Weight of Adhered Material on Pin of Stylus (CAI-5 cm).

It is seen that, as the weight of adhered material increases, the CCR also increases. The negative effect of adhesion can also be noticed in the NCR values which decrease as the weight of adhered material increases.

Another correlation is made to fulfill the adhesion effect on the CCR. The correlation is between the weight of adhered material on the rotating steel arm and CCR (Figure 6.9).

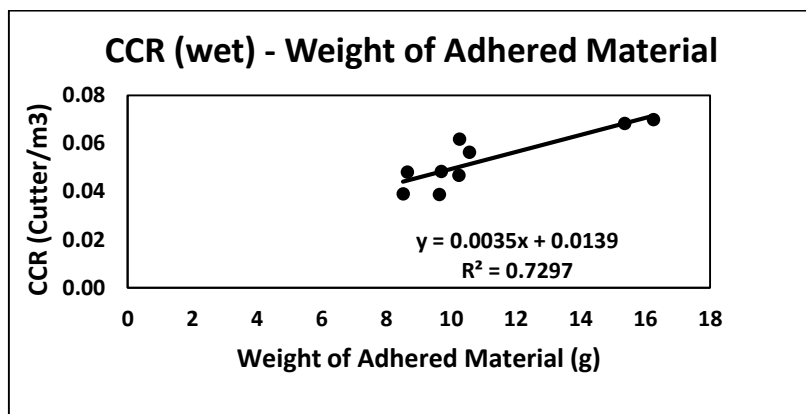


Figure 6.9. Correlation between CCR (wet) and Weight of Adhered Material on Rotating Steel Arm.

6.5. Conclusions

This study presents the sticking potential of the pyroclastic rocks on the cutterhead and tools of roadheaders and evaluates the effect of adhesion on the tools' wear. A set of 9 pyroclastic rocks were collected from different parts of the Cappadocia region and were subjected to a comprehensive laboratory testing program including CAI, petrographic analyses, thin section, and rock mechanics testing in both dry and wet conditions. Field studies were also carried out to measure the effect of mineralogical and mechanical properties of rock formations on the field performance parameters of roadheaders. Field studies were done in both dry and wet CSCs to compare the sticking behavior of the rock formations on the tools of roadheaders in wet conditions and to evaluate its effect on the field performance parameters of roadheaders.

The following conclusions have been achieved through this study:

- The results of rock mechanical experiments show that the strength properties of the rock formations are reduced through the influence of water in the wet rock samples.
- The wear of the stylus in Cerchar abrasivity test depends on the abrasive mineral content of the rock material as the stylus encounters along its path.
- CAI values are higher in the case of 5 cm scratching length compared to the CAI values in the case of 1 cm scratching length. According to previous findings by Al-Ameen and Waller (1994), the development of wear flat at the stylus tip at the start of the test (i.e. 1 mm scratch distance) is due to its initial burial into the rock surface, deformation, and shear failure under the applied static load of 7 kg, not the amount of abrasive mineral content of the rock. For the remaining (2–10 mm) scratch distance, the wear flat will increase in diameter depending on the inherent physical characteristics and mineralogy of rock samples.⁶² So, if the stylus is considered as the cutterhead of the roadheaders, it can be assumed that over time during the cutting performance of the roadheaders, as the contact time increase between the tools of roadheaders and the surface of the rock formations, the rock mass consolidates on the cutting tools and make them worn as the cutterhead applies constant pressure on it.
- According to the field studies, it is proved that the adhesion of the rock materials on the tools' of roadheaders is the highest in the Kavak CSCs which are composed of the ignimbrite with the highest volcanic mineral content (Volcanic clasts (21%), Quartz (17%), Plagioclase (14%)). This affects the field performance parameters of the roadheaders, thus the ICR is the lowest in Kavak CSCs and CCR is the highest (Appendix B).
- The effect of mechanical properties on the field performance parameters shows that the CCR increases with increasing the strength properties of rock formations. This effect is higher in wet conditions. It can be predicted by the fact that the presence of water in the pores of rock formation increases its adhesive shear strength, which means that sticking of the rock material on the tools of roadheaders increase. Over time, sticking of the material creates the layers on the tools of roadheaders. As the contact time increase, the rock material on the tools of roadheaders consolidates and consolidated material tempts the tools to wear more frequently. The consequences are low ICR and high CCR (Appendix B).
- Decreasing of the CAI values when passing from dry condition to wet condition is lower in the case of 5 cm scratching length compared to the CAI values in the case of 1 cm scratching length. The reason is that, as the scratching length increase, the adhered content of rock materials in wet condition increases and it results in wear of the tip of the stylus (Figure 6.4). The wear of the tip of the stylus can also be proved by comparing the difference between CAI (1 cm) and CAI (5 cm) in both dry and wet conditions. It can be noted that the difference is higher in the case of wet samples (Figure 6.5). This can be explained by the fact that the adhesion of rock materials on the tip of the stylus occurs in wet samples as the scratching length increase, and thus, the consolidation of this adhered material makes the tip of the stylus wear.
- Through the correlation between CCR and weight of adhered material on the tip of the stylus (CAI-5 cm) and the rotating steel arm, it is proved that, as the weight of adhered material increases, CCR also increases, and thus, NCR decreases.

References

Articles and Books

[1] - Jamal Rostami, Levent Ozdemir Earth Mechanics Institute, Colorado School of Mines, Golden, Colorado 80401, "Roadheaders Performance Optimization for Mining and Civil Construction".[Online].Available:

https://www.researchgate.net/publication/237470051_ROADHEADERS_PERFORMANCE_OPTIMIZATION_FOR_MINING_AND_CIVIL_CONSTRUCTION [Accessed 12 April 2021].

[2] - G. Spagnoli, M. Feinendegen, R. Ernst, M. Weh (2012) Manipulations of the sticky clays regarding EPB tunnel driving: 111.

[3] – Feng QL (2004) Soil conditioning for modern EPBM drives. Tunnel and Tunnelling International 36(12): 18-20.

[4] – Thewes, M. & Burger, W. 2005. Clogging of TBM drives in clay—identification and mitigation of risks. In Erdem & Solak (eds) Underground Space USE: Analysis of the Past and Lessons for the Future, 737–742.

[5] - Thewes, M. 1999. Adhäsion von Tonböden beim Tunnelvortrieb mit Flüssigkeitsinsschilden. PhD thesis, University of Wuppertal, Institute of Soil Mechanics and Foundation Engineering, 21.

[6] – Feng, Q.L. 2004. Soil conditioning for modern EPBM drives. Tunnels and Tunnelling International, 18–20.

- [7] - Weh, M., Ziegler, M. & Zwick, O. 2009. Verklebungen bei EPB-Vortrieben in wechselndem Baugrund: Eintrittsbedingungen und Gegenmaßnahmen. In Tunnel—Räume für zukunftssichere Mobilität. 185–189, STUVA-Tagung 2009, Hamburg. Gütersloh: Bauverlag.
- [8] - Bölükbaşı, N., “Yeraltı kömür ve ayak kazı mekanizasyonu”, TKİ Genel Müdürlüğü Seminerleri no.4, Mining Eng. Dept., ODTÜ, Ankara, August, 1986.
- [9] - Çopur, H., Özdemir, L., Rostami, J., “Roadheader applications in mining and tunneling industries”, The Mining Engineer, pp. 38-42, March, 1998.
- [10] - M. Neil, J.Rostami, L. Ozdemir, R.Gertsch, “ Production Estimating Techniques for Underground Mining using Roadheaders”.
- [Online].Available:https://www.researchgate.net/publication/237795297_Production_estimating_techniques_for_underground_mining_using_roadheaders [Accessed 12 April 2021].
- [11] - N. Bilgin, H. Copur, C.Balci, “Mechanical Excavation in Mining and Civil Industries”. 2014, pp. 138-139.
- [12] - N. Bilgin, H. Copur, C.Balci, “Mechanical Excavation in Mining and Civil Industries”. 2014, pp. 138-139.
- [13] – N. Bilgin, S. Yazic, and S. Eskikaya, “A model to predict the performance of roadheaders and impact hammers in tunnel drivages”. Proc. Eurock 96, Italy-Torino, Balkema, 1996, pp. 715–720.
- [14] - H. Copur, L. Ozdemir, and J. Rostami, “Roadheader applications in mining and tunneling”.
- [Online].Available:https://www.researchgate.net/publication/237780459_Roadheader_applications_in_mining_and_tunneling [accessed Apr 26 2021].
- [15] – J. Rostami, L. Ozdemir, D. Neil, “Roadheaders Performance Optimization for Minign and Civil Construction”.
- [16] - Copur, H., Ozdemir, L., and Rostami, J., 1998a. SME Annual Meeting, Preprint No: 98-185,p. 5; Copur, H., Ozdemir, L., and Rostami, J., 1998b. Mining Engineering, 50(3):38-42.

[17] – J. McPhie, M. Doyle, R.L. Allen, and R. Allen, “Volcanic Textures: A Guide to the Interpretation of Textures in Volcanic Rocks. Centre for Ore Deposits and Exploration Studies, University of Tasmania. 1933”.

[18] – R.V. Fisher, “Rocks composed of volcanic fragments and their classification”. [Online].Available:

<https://www.sciencedirect.com/science/article/abs/pii/0012825266900109?via%3Dihub>

[accessed Apr 30 2021].

[19] – P. Tomassi, L. Verrucci, T. Rotonda, “Mechanical properties of a weak pyroclastic rock and their relationship with microstructure”. [Online].Available:

https://www.researchgate.net/publication/271715299_Mechanical_properties_of_a_weak_pyroclastic_rock_and_their_relationship_with_microstructure[accessed Apr 30 2021].

[20] - Atterberg A (1911) Über die physikalische Bodenuntersuchung und über die Plastizität der Tone [On the investigation of the physical properties of soils and on the plasticity of clays]. Internationale Mitteilungen für Bodenkunde 1: 10-43. (In German).

[21] - ASTM D4318–17 (2017b), “Standart test methods for liquid limit, plastic limit, and plasticity index of soils”, ASTM International (2017).

[22] – A. Cassagrande, “Research on the Atterberg Limits of Soils”, Public Roads v.13 (1932), pp. 121-136.

[23] - K. Terzaghi, R.B. Peck, G. Mesri Soil Mechanics in Engineering Practice John Wiley & Sons (1996). [Online].Available:

<https://cequcest.files.wordpress.com/2015/09/terzaghi129883967-soil-mechanics-in-engineering-practice-3rd-edition-karl-terzaghi-ralph-b-peck-gholamreza-mesri-1996.pdf>

[accessed Apr 30 2021].

[24] – Michael J. Heap, Marie E.S. Violay, “The mechanical behaviour and failure modes of volcanic rocks: a review”. [Online].Available:

<https://link.springer.com/content/pdf/10.1007/s00445-021-01447-2.pdf> [accessed Apr 30 2021].

[25] - I. Sass, U. Burbaum (2007) A method for assessing adhesion of clays to tunneling machines.

[26] - Atterberg, A. (1911). Die Plastizität der Tone. Int. Mitt. Bodenkd. 1, 10 – 43 (in German).

[27]-[Online]. Available: <https://geotechpedia.com/Equipment/Show/218/Liquid-limit-devices--Casagrande-> [Accessed 12 April 2021].

[28] - R. Galindo-Aires, A. Lara-Galera, and G. Guillán-Llorente, "Contribution to the knowledge of early geotechnics during the twentieth century: Arthur Casagrande". [Online]. Available:

https://www.researchgate.net/publication/326996911_Contribution_to_the_knowledge_of_early_geotechnics_during_the_twentieth_century_Arthur_Casagrande [accessed Apr 14 2021].

[29] - Boisson, J.Y. (1981). "Etude de l'adhérence de sédiments argileux à des surfaces métalliques, application à l'étude de la traficabilité sous marine par vis d'Archimède", Université: Paul Sabatier de Toulouse.

[30] - Littleton, I. (1976). "An experimental study of the adhesion between clay and steel", Journal of Terramechanics, Vol. 13, No. 3, pp.141-152.

[31] - Daniela Garroux Gonçalves de Oliveira EPB EXCAVATION AND CONDITIONING OF COHESIVE MIXED SOILS: CLOGGING AND FLOW EVALUATION pp.42-43

[32] - F.S.Hollmann, M.Thewes, "Assessment method for clay clogging and disintegration of fines in mechanised tunneling". [Online]. Available:

<https://www.sciencedirect.com/science/article/pii/S0886779813000576>

[33] - Thewes, M. and Burger, W., 2005, Clogging of TBM drives in Clay- Identification and Mitigation of Risks. Underground Space Use, Vol 2, pp 737-742.

[34] - R. Zimnik, R. Baalen, N.W. Verhoef, J.M. Ngan-Tillard, "The Adherence of Clay to Steel Surfaces". [Online]. Available from:

https://www.researchgate.net/publication/265180190_THE_ADHERENCE_OF_CLAY_TO_STEEL_SURFACES [accessed Apr 15 2021].

[35] - [Online]. Available from: <https://www.semanticscholar.org/paper/The-Adherence-Of-Clay-To-Steel-Surfaces-Zimnik-Baalen/066211a1eee08750f65132142d8f518b68bd484d/figure/6>

[accessed Apr 15 2021].

- [36] - Weh, M., Ziegler, M. & Zwick, O. 2009. Verklebungen bei EPB-Vortrieben in wechselndem Baugrund: Eintrittsbedingungen und Gegenmaßnahmen. In Tunnel—Räume für zukunftssichere Mobilität. 185–189, STUVA-Tagung 2009, Hamburg. Gütersloh: Bauverlag.
- [37] - Feinendegen, M., 2010, A New Laboratory Test to evaluate the problem of clogging in mechanical tunnel driving with EPB-shields. In Rock Mechanics in Civil and Environmental Engineering, London, U.K. pp429-432.
- [38] - Feinendegen, M., Ziegler, M., Spagnoli, G., FernándezSteeger, T., Stanjek, H. 2010. A new laboratory test to evaluate the problem of clogging in mechanical tunnel driving with EPB-shields. In: Proc. EUROCK 2010, Lausanne, Switzerland, Taylor & Francis Group, London.
- [39] - Spagnoli, G., Fernández-Steeger, T., Azzam, R. Feinendegen, M., Neher, H.P. & Stanjek, H. 2010a. Investigation of adherence behaviour and related effects on different scales in mechanical tunnel driving. In: Proc. Underground Construction Prague 2010, Transport and City Tunnels, ITA-AITES, 14–16. June 2010, Prague, Czech Republic, 692–699.
- [40] – Temel, A., 1992. Kapadokya eksploziv volkanizmasının petrolojik ve jeokimyasal özellikleri. PhD Thesis, Dept. of Geological Engng., Hacettepe University (in Turkish).
- [41] - [Online]. Available from: <https://link.springer.com/article/10.1007/s12517-016-2727-9> [accessed May 11 2021].
- [42] - Toprak, V., Keller, J., Schumacher, R., 1994. Volcanotectonic features of the Cappadocian Volcanic Province. In: International Volcanological Congress-IAVCEI, Ankara, Excursion Guide.
- [43] - Aydar, E., Schmitt, A.K., Çubukçu, H.E., Akin L., Ersoy, O., Şen, E., Duncan, R.A., Atici G., 2012. Correlation of ignimbrites in the central Anatolian volcanic province using zircon and plagioclase ages and zircon compositions. Journal of Volcanology and Geothermal Research, 213–214, 83-97.
- [44] - R.H. Atkinson, 5 – hardness tests for rock characterization, in: J.A. Hudson (Ed.), Rock Test. Site Charact, 3rd ed., Pergamon, Oxford, 1993, pp. 105–117. [Online]. Available from: <https://doi.org/10.1016/B978-0-08-042066-0.50012-4> [accessed July 21 2021].

- [45] - M.Z. Abu Bakar, L.S. Gertsch, Evaluation of saturation effects on drag pick cutting of a brittle sandstone from full scale linear cutting tests, *Tunn. Undergr. Space Technol.* 34 (2013) 124–134. [Online] Available from: <https://www.sciencedirect.com/science/article/abs/pii/S0886779812001824> [accessed July 21 2021].
- [46] - P. Reh binder, V. Lichtman, Effect of surface active media on strains and rupture in solids, in: *Proceedings of the 2nd International Congress on Surface Activity, 1957*, pp. 563–582.
- [47] - P.S.B. Colback, B.L. Wiid, The influence of moisture content on the compressive strength of rocks, in: *Proceedings of the 3rd Rock Mechanics Symposium, Toronto, Canada, 1965*, pp. 65–83.
- [48] - W.F. Brace, R.J. Martin, A test of the law of effective stress for crystalline rocks of low porosity, *Int. J. Rock Mech. Min. Sci.* 5 (1968) 415–426. [Online] Available from: [A test of the law of effective stress for crystalline rocks of low porosity - ScienceDirect](#) [accessed July 26 2021].
- [49] - V.S. Vutukuri, The effect of liquids on the tensile strength of limestone, *Int. J. Rock Mech. Min. Sci. Geo-mech.* 11 (1974) 27–29. [Online] Available from: [The effect of liquids on the tensile strength of limestone - ScienceDirect](#) [accessed July 26 2021].
- [50] - E.M. Van Eeckhout, The mechanisms of strength reduction due to moisture in coal mine shales, *Int. J. Rock Mech. Min. Sci. Geomech.* 13 (1976) 61–67. [Online] Available from: [The mechanisms of strength reduction due to moisture in coal mine shales - ScienceDirect](#) [accessed July 26 2021].
- [51] - E. Broch, Changes in rock strength caused by water, in: *Proceedings of 4th Congress of International Society for Rock Mechanics, Montreux, Switzerland, 1, 1979*, pp. 71–75.
- [52] - C.G. Dyke, L. Dobereiner, Evaluating the strength and deformability of sandstones, *Q. J. Eng. Geol.* 24 (1991) 123–134. [Online] Available from: [Current Links for doi: 10.1144/GSL.QJEG.1991.024.01.13 \(crossref.org\)](#) [accessed July 26 2021].
- [53] - A.B. Hawkins, B.J. McConnell, Sensitivity of sandstone strength and deformability to changes in moisture content, *Q. J. Eng. Geol.* 25 (1992) 115–130.

- [54] - B. Vasarhelyi, Some observations regarding the strength and deformability of sandstones in dry and saturated conditions, *Bull. Eng. Geol. Environ.* 62 (2003) 245–249.
- [55] - Z.A. Erguler, R. Ulusay, Water induced variations in mechanical properties of clay bearing rocks, *Int. J. Rock Mech. Min. Sci.* 46 (2009) 355–370. [Online] Available from: [Water-induced variations in mechanical properties of clay-bearing rocks - ScienceDirect](#) [accessed July 26 2021].
- [56] - J. Mammen, S. Saydam, P. Hagan, A Study on the Effect of Moisture Content on Rock Cutting Performance, in Aziz, N (ed), *Coal 2009: Coal Operators' Conference*, University of Wollongong & the Australasian Institute of Mining and Metallurgy (2009) 340–347.
- [57] - I. Yilmaz, Influence of water content on the strength and deformability of gypsum, *Int. J. Rock Mech. Min. Sci.* 47 (2010) 342–347. [Online] Available from: [Influence of water content on the strength and deformability of gypsum - ScienceDirect](#) [accessed July 26 2021].
- [58] - M.S.A. Perera, P.G. Ranjith, M. Peter, Effects of saturation medium and pressure on strength parameters of Latrobe Valley brown coal: Carbon dioxide, water and nitrogen saturations, *Energy* 36 (2011) 6941–6947. [Online] Available from: [Effects of saturation medium and pressure on strength parameters of Latrobe Valley brown coal: Carbon dioxide, water and nitrogen saturations - ScienceDirect](#) [accessed July 26 2021].
- [59] - B.A. Poulsen, B. Shen, D.J. Williams, C. Huddleston-Holmes, N. Erarslan, J. Qin, Strength reduction on saturation of coal and coal measures rocks with implications for coal pillar strength, *Int. J. Rock Mech. Min. Sci.* 71 (2014) 41–52. [Online] Available from: [Strength reduction on saturation of coal and coal measures rocks with implications for coal pillar strength - ScienceDirect](#) [accessed July 26 2021].
- [60] - D.K. Soni, Effect of saturation and deformation rate on split tensile strength for various sedimentary rocks *International Conference Data Mining, Civil and Mechanical Engineering*, Bali, Indonesia (2015), p. 53–55.
- [61] - H.R. Phillips, F.F. Roxborough, The influence of tool material on the wear rate of rock cutting picks, in: *Proceedings of the 34th Annual Conference of Australian Institute of Metals*, Brisbane, 1981, pp. 52–56

[62] - S.I. Al-Ameen, M.D. Waller, The influence of rock strength and abrasive mineral content on the Cerchar Abrasivity Index, Eng. Geol. 36 (1994) 293-301. [Online] Available from: [The influence of rock strength and abrasive mineral content on the Cerchar Abrasive Index - ScienceDirect](#) [accessed October 6 2021].

[63] L. Ozdemir, Mechanical Tunneling, Raise Boring and Shaft Drilling, Short Course., Golden, Colorado., 98. [Online] Available from: [Ozdemir: Mechanical Tunneling, Raise Boring and Shaft... - Академия Google](#) [accessed October 6 2021].

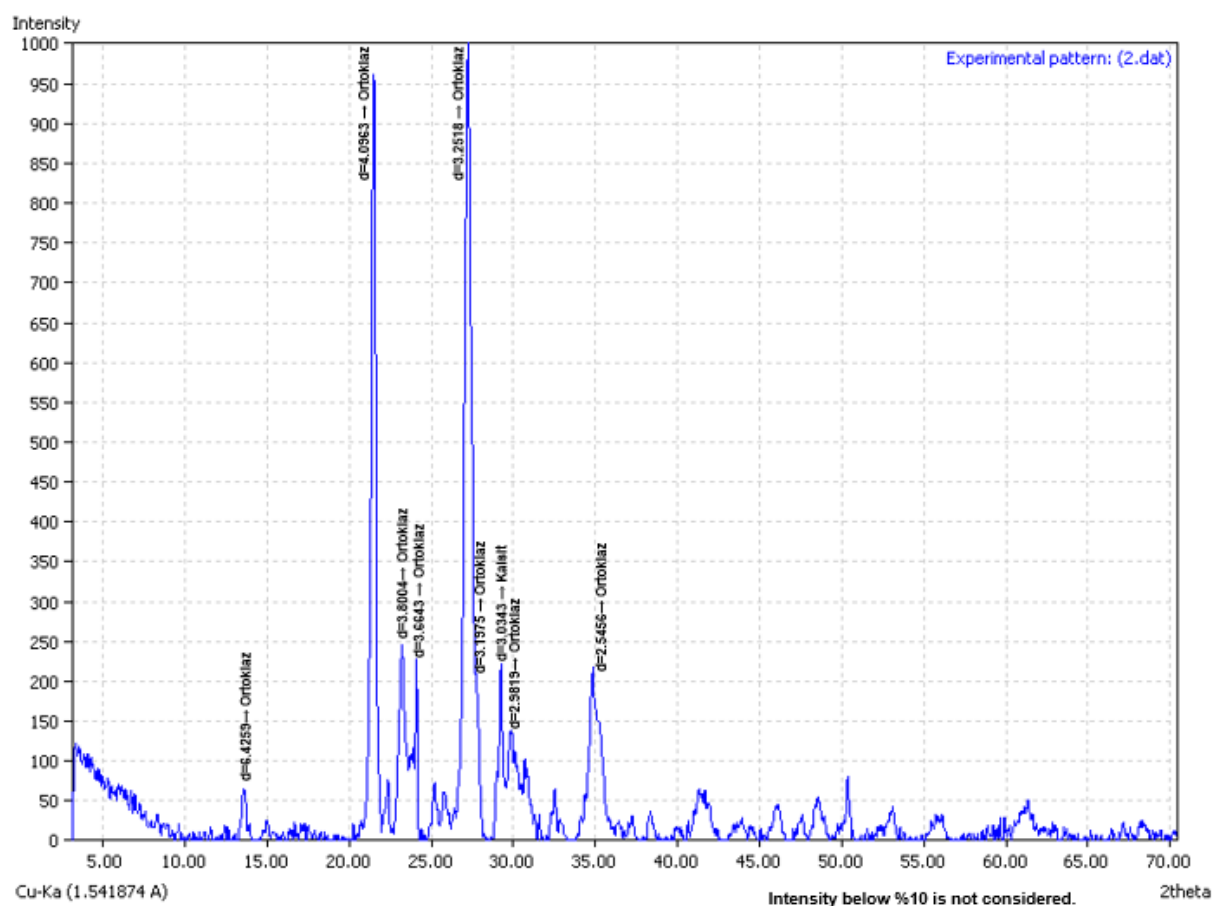
[64] Ramazan Comakli. Effects of the physico-mechanical properties of pyroclastic rocks on cutter wear of roadheaders.

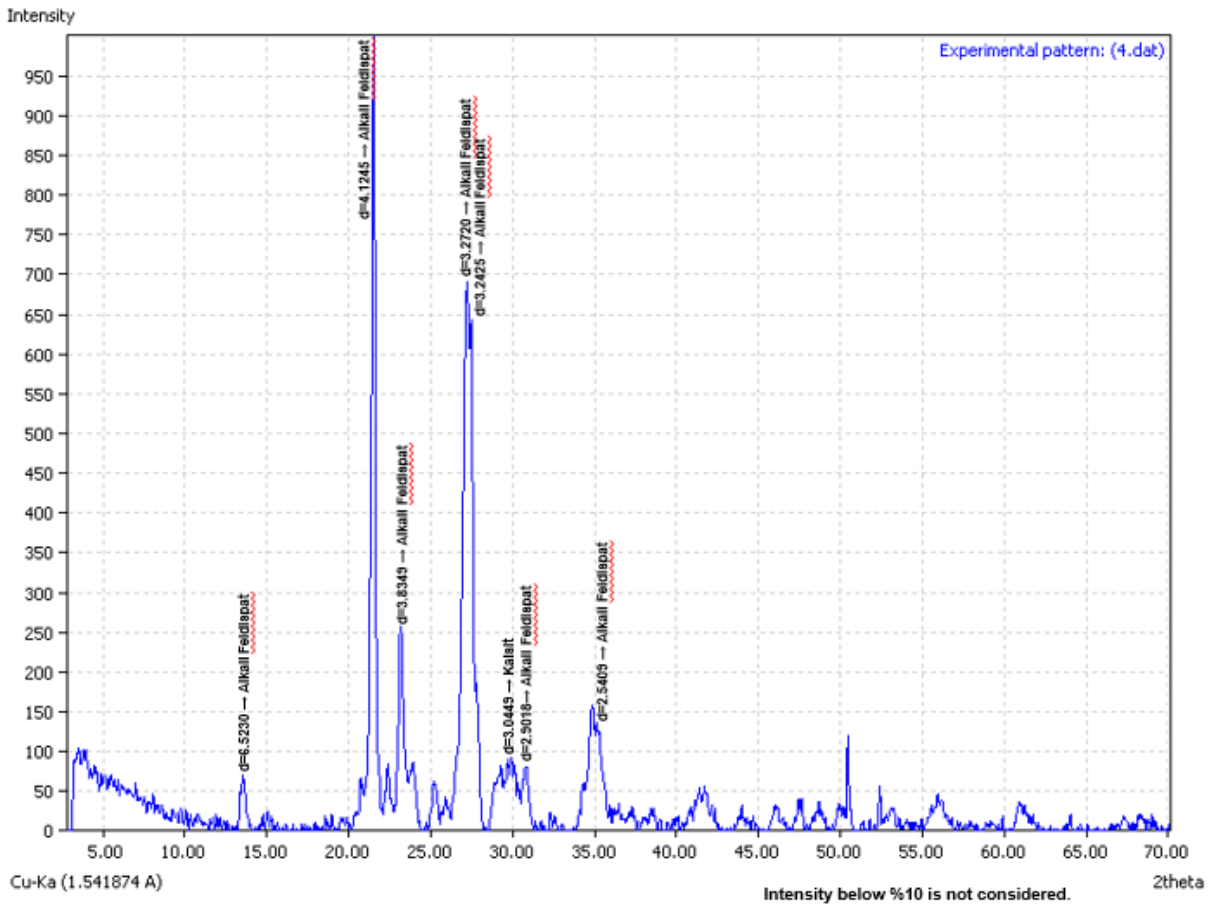
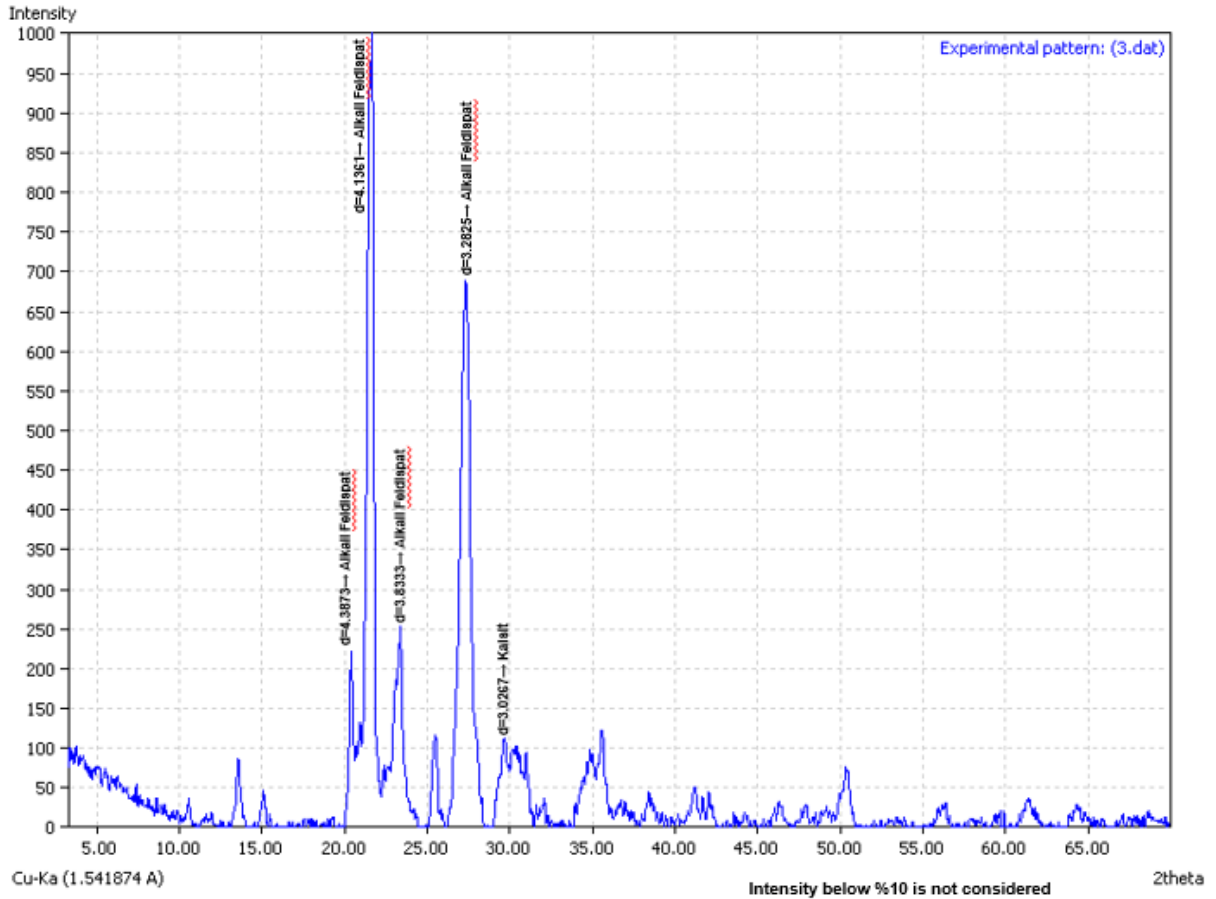
[Online] Available from: <https://www.researchgate.net/requests/attachment/91394701> [accessed October 9 2021].

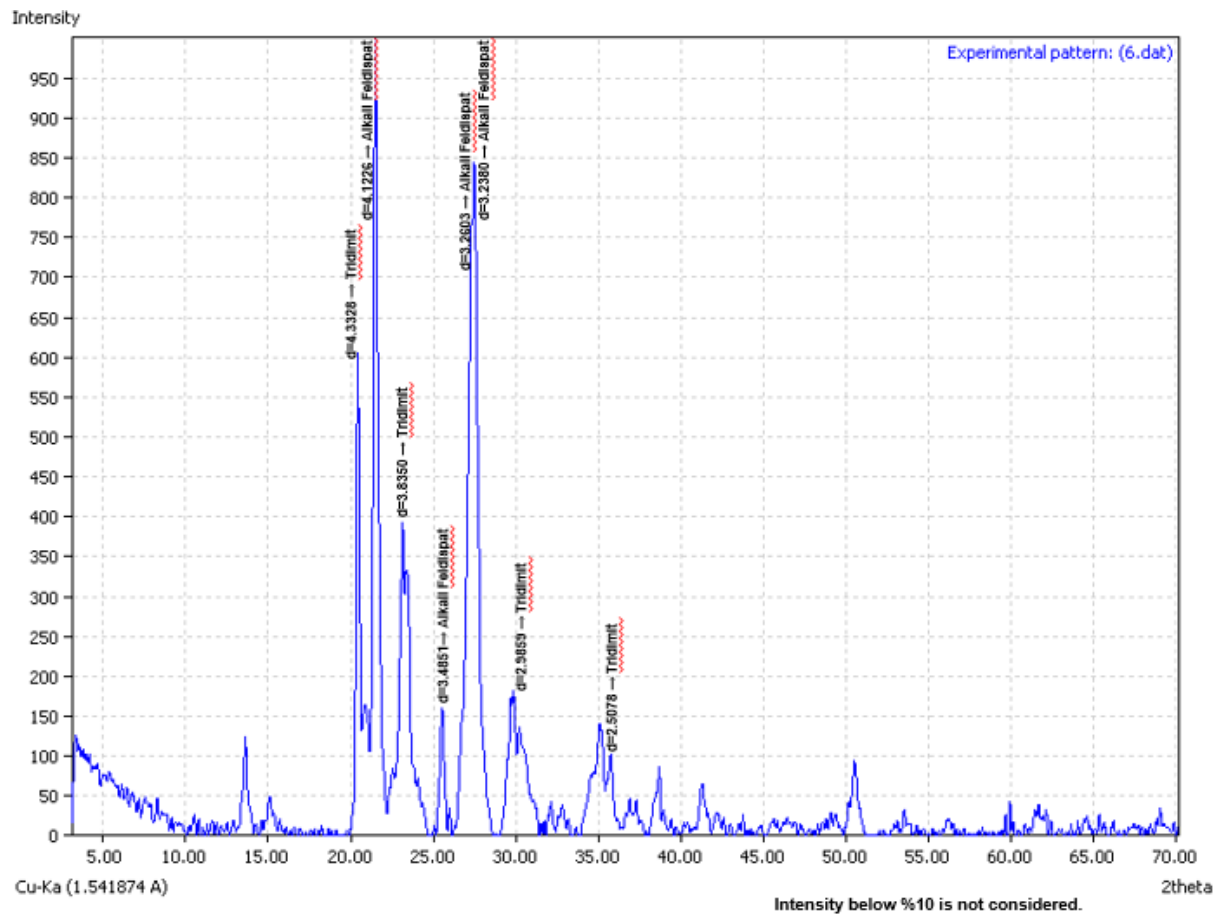
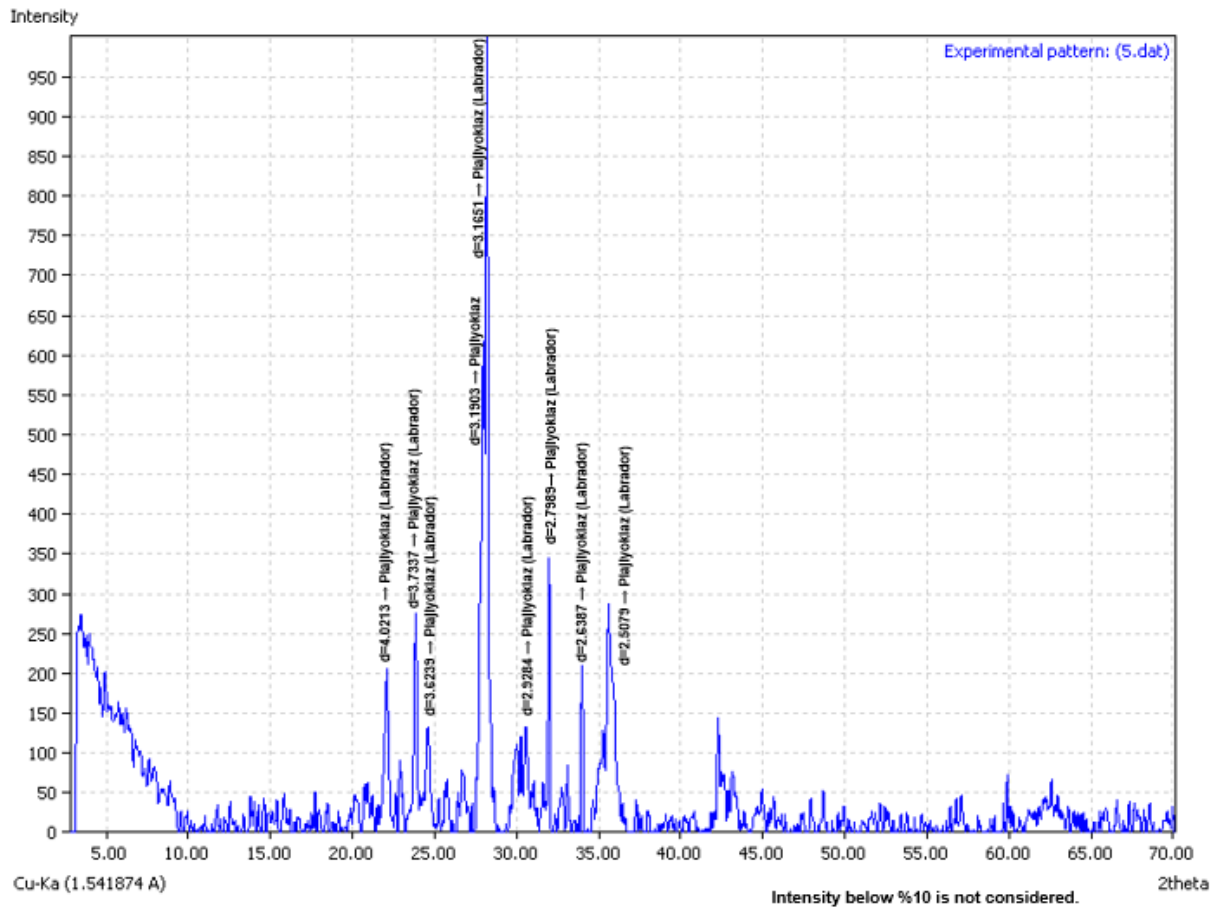
APPENDIX A

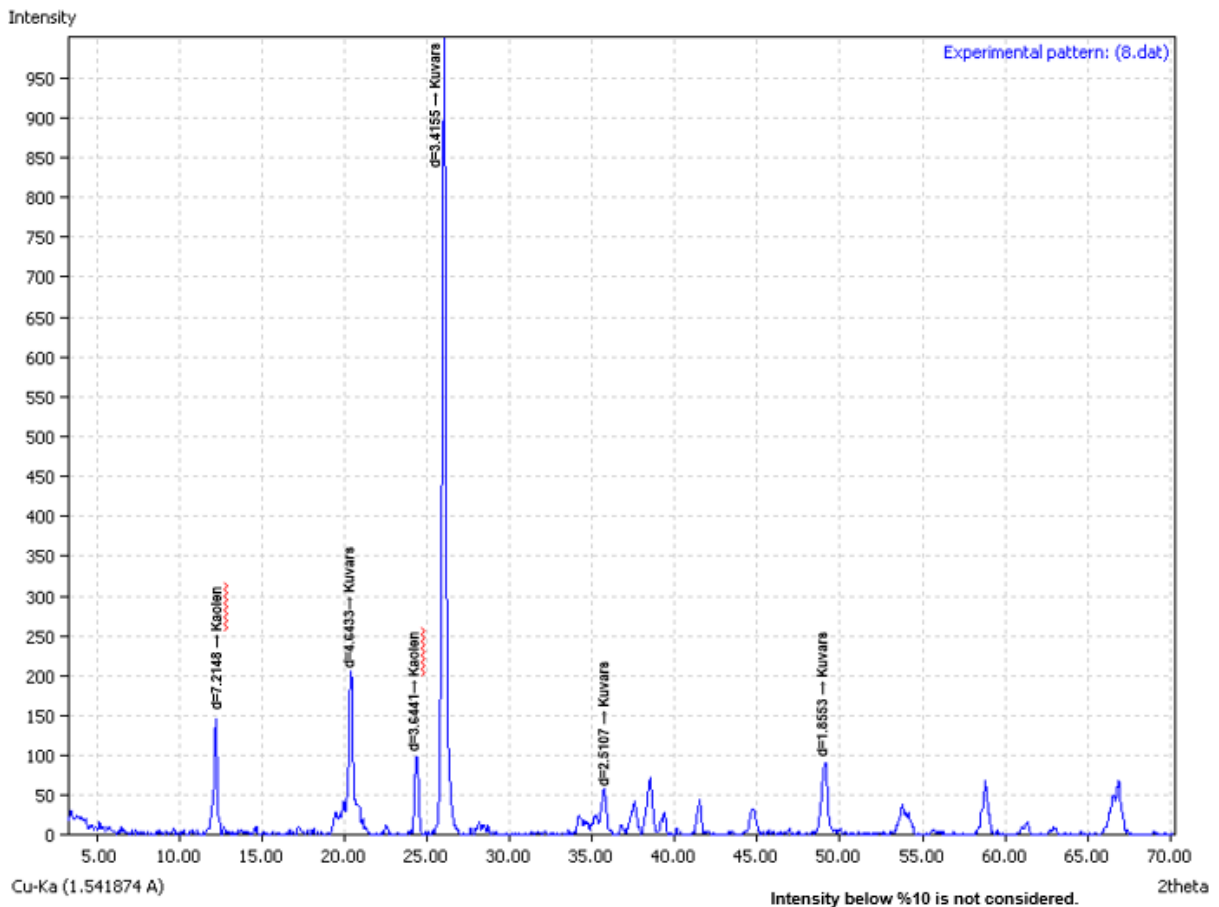
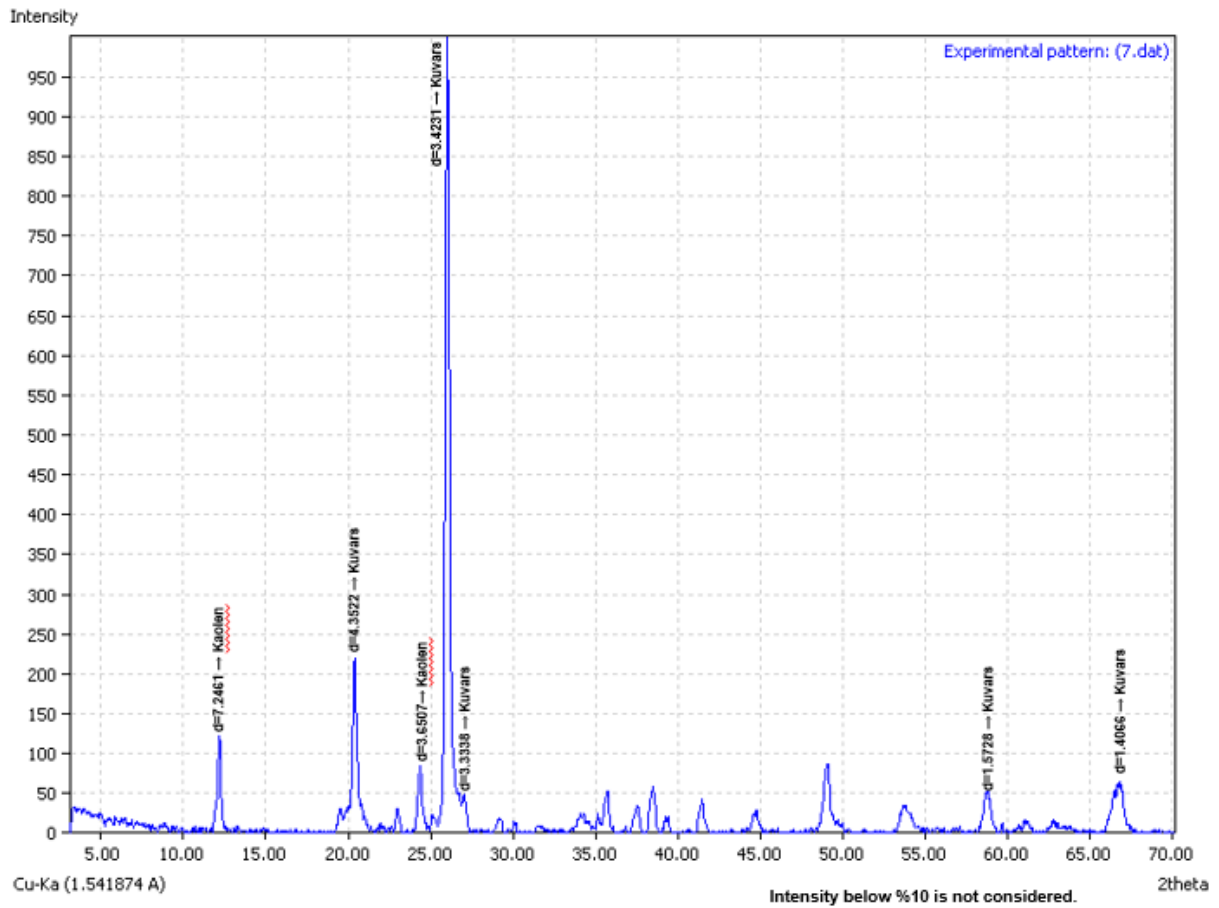
X-ray Diffraction

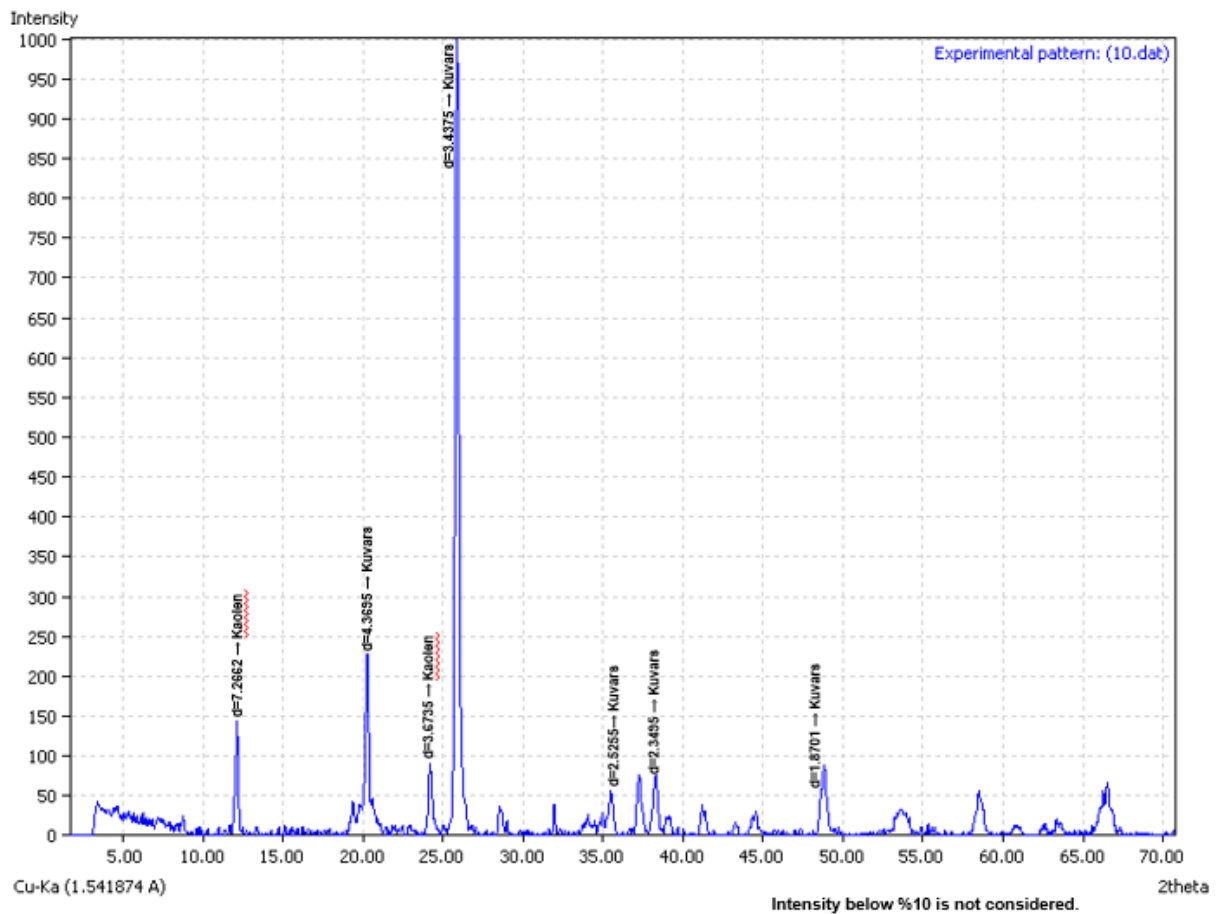
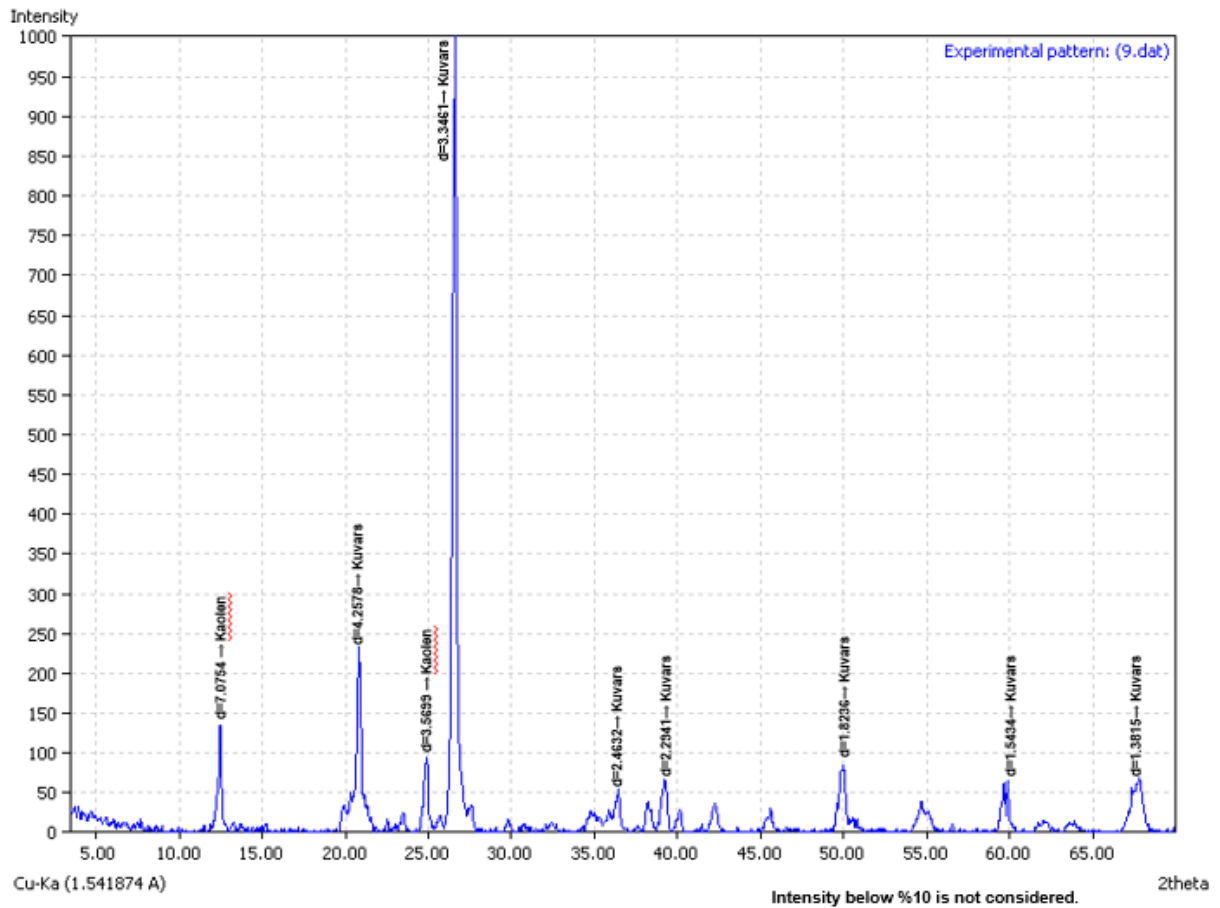
The following figures represent the results of X-ray Diffraction analyses for the specimens.

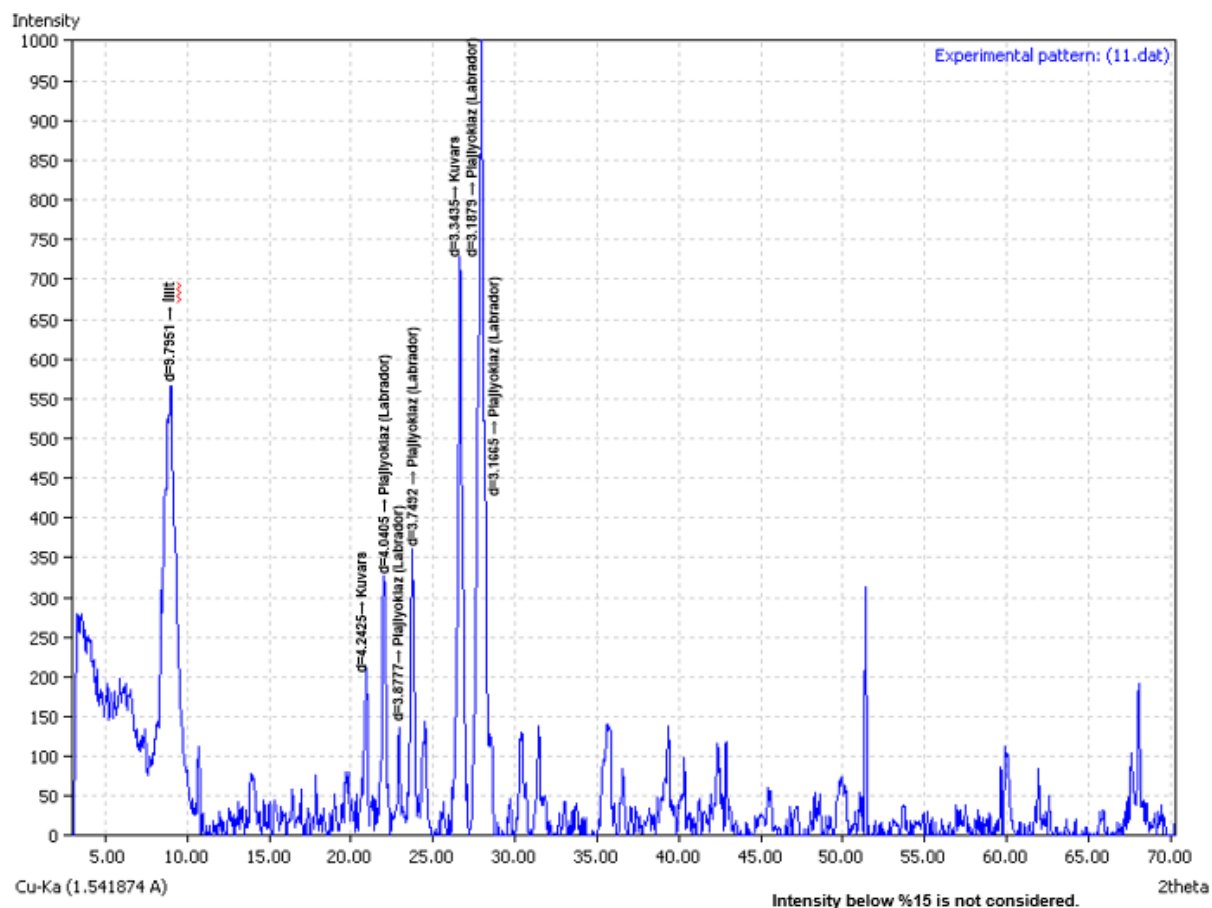












APPENDIX B

Field Performance Parameters of Roadheaders

Field performance parameters of the roadheaders for the different regions are given in the following tables.

Table B-1. Field performance parameters of roadheaders for the Kayhan-1.

Kayhan 1		Dry CSC	Wet CSC
Project Activity Dates	Starting		
	Ending		
Used Machine	Model / Weight (ton)	PAURAT E 134 55 TON	PAURAT E 134 55 TON
	Power (kW)	370	370
Daily Working Time (hour)		8	8
Daily Excavation Time (hour)		5.5	4.5
Machine Breakdown Maintenance (hour) per day		1.5	2.5
Lunch and Coffee Break (hour)		1	1
Daily Excavation Amount (m^3)		386	243
Number of Main Corridors		1	1
Main Corridors Dimensions (m) Length / Width / Height		140.00 * 6.50 * 7.20	140.00 * 6.50 * 7.20
Number of Lodges		60	60
Lodge Dimensions (m) Length / Width / Height		20.00 * 6.00 * 6.20	20.00 * 6.00 * 6.20
Daily Chisel Consumption		20	15
Net Cutting Rate (m^3/d)		386	243
Daily Advance Rate (m/d)		10.37	6.5
Machine Utilization (%)		62.5	56.25
Instantaneous Cutting Rate (m^3/h)		70.18	54
Cutter Consumption (picks/ m^3)		0.051813	0.061728

Table B-2. Field performance parameters of roadheaders for the Kayhan-2.

Kayhan 2		Dry CSC	Wet CSC
Project Activity Dates	Starting		
	Ending		
Used Machine	Model / Weight (ton)	PAURAT E 134 55 TON	PAURAT E 134 55 TON
	Power (kW)	370	370
Daily Working Time (hour)		8	8
Daily Excavation Time (hour)		5.5	4.5
Machine Breakdown Maintenance (hour) per day		1.5	2.5
Lunch and Coffee Break (hour)		1	1
Daily Excavation Amount (m^3)		398	228
Number of Main Corridors		1	1
Main Corridors Dimensions (m) Length / Width / Height		140.00 * 6.50 * 7.20	140.00 * 6.50 * 7.20
Number of Lodges		60	60
Lodge Dimensions (m) Length / Width / Height		20.00 * 6.00 * 6.20	20.00 * 6.00 * 6.20
Daily Chisel Consumption		15	11
Net Cutting Rate (m^3/d)		398	228
Daily Advance Rate (m/d)		10.69	6.13
Machine Utilization (%)		68.75	56.25
Instantaneous Cutting Rate (m^3/h)		72.36	50.66
Cutter Consumption (picks/ m^3)		0.037688	0.048246

Table B-3. Field performance parameters of roadheaders for the Aktas-1.

Aktas 1		Dry CSC	Wet CSC
Project Activity Dates	Starting		
	Ending		
Used Machine	Model / Weight (ton)	PAURAT E 134 55 TON	PAURAT E 134 55 TON
	Power (kW)	370	370
Daily Working Time (hour)		10	10
Daily Excavation Time (hour)		6	5
Machine Breakdown Maintenance (hour) per day		2	3
Lunch and Coffee Break (hour)		2	2
Daily Excavation Amount (m^3)		426	312
Number of Main Corridors		1	1
Main Corridors Dimensions (m) Length / Width / Height		100.00 * 6.00 * 6.00	100.00 * 6.00 * 6.00
Number of Lodges		44	44
Lodge Dimensions (m) Length / Width / Height		20.00 * 5.00 * 6.00	20.00 * 5.00 * 6.00
Daily Chisel Consumption		19	15
Net Cutting Rate (m^3/d)		426	312
Daily Advance Rate (m/d)		14.2	10.4
Machine Utilization (%)		60	50
Instantaneous Cutting Rate (m^3/h)		71	62.4
Cutter Consumption (picks/ m^3)		0.044601	0.048077

Table B-5. Field performance parameters of roadheaders for the Aktas-2.

Aktas 2		Dry CSC	Wet CSC
Project Activity Dates	Starting		
	Ending		
Used Machine	Model / Weight (ton)	PAURAT E 134 55 TON	PAURAT E 134 55 TON
	Power (kW)	370	370
Daily Working Time (hour)		10	10
Daily Excavation Time (hour)		6	5
Machine Breakdown Maintenance (hour) per day		2	3
Lunch and Coffee Break (hour)		2	2
Daily Excavation Amount (m^3)		412	302
Number of Main Corridors		1	1
Main Corridors Dimensions (m) Length / Width / Height		100.00 * 6.00 * 6.00	100.00 * 6.00 * 6.00
Number of Lodges		24	46
Lodge Dimensions (m) Length / Width / Height		24.00 * 6.00 * 6.40	25.00 * 6.00 * 4.30
Daily Chisel Consumption		15	10
Net Cutting Rate (m^3/d)		576	258
Daily Advance Rate (m/d)		15	10
Machine Utilization (%)		60	55
Instantaneous Cutting Rate (m^3/h)		96	46.90909
Cutter Consumption (picks/ m^3)		0.026042	0.03876

Table B-6. Field performance parameters of roadheaders for the Guvenal.

Guvenal		Dry CSC	Wet CSC
Project Activity Dates	Starting		
	Ending		
Used Machine	Model / Weight (ton)	PAURAT E 134 55 TON	PAURAT E 134 55 TON
	Power (kW)	370	370
Daily Working Time (hour)		10	10
Daily Excavation Time (hour)		6	4.5
Machine Breakdown Maintenance (hour) per day		2	3.5
Lunch and Coffee Break (hour)		2	2
Daily Excavation Amount (m ³)		468	286
Number of Main Corridors		1	1
Main Corridors Dimensions (m) Length / Width / Height		130.00 * 6.00 * 4.50	130.00 * 6.00 * 6.00
Number of Lodges		40	40
Lodge Dimensions (m) Length / Width / Height		20.00 * 5.00 * 4.50	20.00 * 5.00 * 4.50
Daily Chisel Consumption		26	20
Net Cutting Rate (m ³ /d)		468	286
Daily Advance Rate (m/d)		20.8	12.71
Machine Utilization (%)		60	45
Instantaneous Cutting Rate (m ³ /h)		78	63.25
Cutter Consumption (picks/m ³)		0.026042	0.03876

Table B-7. Field performance parameters of roadheaders for the Aksaray-2.

Kavak		Dry CSC	Wet CSC
Project Activity Dates	Starting		
	Ending		
Used Machine	Model / Weight (ton)	PAURAT E 134 55 TON	PAURAT E 134 55 TON
	Power (kW)	370	370
Daily Working Time (hour)		10	10
Daily Excavation Time (hour)		6	5
Machine Breakdown Maintenance (hour) per day		2	3
Lunch and Coffee Break (hour)		2	2
Daily Excavation Amount (m^3)		358	249
Number of Main Corridors		1	1
Main Corridors Dimensions (m) Length / Width / Height		130.00 * 6.00 * 4.50	130.00 * 6.00 * 6.00
Number of Lodges		40	40
Lodge Dimensions (m) Length / Width / Height		20.00 * 5.00 * 4.50	20.00 * 5.00 * 4.50
Daily Chisel Consumption		23	17
Net Cutting Rate (m^3/d)		358	249
Daily Advance Rate (m/d)		15.9	11
Machine Utilization (%)		60	45
Instantaneous Cutting Rate (m^3/h)		59.66	49.8
Cutter Consumption (picks/ m^3)		0.064246	0.068273

Table B-8. Field performance parameters of roadheaders for the Sulusaray.

Sulusaray		Dry CSC	Wet CSC
Project Activity Dates	Starting		
	Ending		
Used Machine	Model / Weight (ton)	PAURAT E 134 55 TON	PAURAT E 134 55 TON
	Power (kW)	370	370
Daily Working Time (hour)		8	8
Daily Excavation Time (hour)		5.5	5
Machine Breakdown Maintenance (hour) per day		1.5	2
Lunch and Coffee Break (hour)		1	1
Daily Excavation Amount (m^3)		425	278
Number of Main Corridors		1	1
Main Corridors Dimensions (m) Length / Width / Height		110.00 * 6.00 * 4.50	130.00 * 6.00 * 6.00
Number of Lodges		40	40
Lodge Dimensions (m) Length / Width / Height		20.00 * 5.00 * 4.50	20.00 * 5.00 * 4.50
Daily Chisel Consumption		17	13
Net Cutting Rate (m^3/d)		425	278
Daily Advance Rate (m/d)		15.9	11
Machine Utilization (%)		68.75	62.5
Instantaneous Cutting Rate (m^3/h)		77.27	55.6
Cutter Consumption (picks/ m^3)		0.04	0.046763

Table B-9. Field performance parameters of roadheaders for the Hoyuk.

Hoyuk		Dry CSC	Wet CSC
Project Activity Dates	Starting		
	Ending		
Used Machine	Model / Weight (ton)	PAURAT E 134 55 TON	PAURAT E 134 55 TON
	Power (kW)	370	370
Daily Working Time (hour)		10	10
Daily Excavation Time (hour)		6	5
Machine Breakdown Maintenance (hour) per day		2	3
Lunch and Coffee Break (hour)		2	2
Daily Excavation Amount (m^3)		465	282
Number of Main Corridors		1	1
Main Corridors Dimensions (m) Length / Width / Height		140.00 * 6.00 * 7.00	140.00 * 6.00 * 7.00
Number of Lodges		40	40
Lodge Dimensions (m) Length / Width / Height		20.00 * 5.00 * 4.50	20.00 * 5.00 * 4.50
Daily Chisel Consumption		16	11
Net Cutting Rate (m^3/d)		465	282
Daily Advance Rate (m/d)		11.07	6.71
Machine Utilization (%)		60	50
Instantaneous Cutting Rate (m^3/h)		77.5	56.4
Cutter Consumption (picks/ m^3)		0.034409	0.039007